ABSTRACT

PARK, JUNYEONG. Structural and Chemical Characterization of Thermally-Treated Woody Biomass. (Under the direction of Dr. Orlando J. Rojas and Dr. Sunkyu Park).

The objective of this research is to understand how chemistry and structure of thermally-treated woody biomass are changed as a function of process conditions. To achieve the goal, thermally-altered biomass was generated using different processes, at varying temperatures, and under different atmospheres (inert and oxidative), and then, was investigated using complementary analytical tools, including advanced techniques with solid-state ^{13}C NMR spectroscopy. It was found that the aromatic carbon fraction increases with elevated treatment temperature, which showed 53% for the sample generated at 300 °C and 75% for 700 °C biochar, and the estimated number of carbons per an aromatic cluster also increased up to 16 for the sample treated at 700 °C. Moreover, the presence of limited amount of oxygen during thermal treatment can increase aromaticity and cluster size at a higher rate, due to exothermal heat flow from oxidation of organic matters.

During the investigation for value-added application of biochar, it was found that the subsequent activation process can enhance the surface properties and the corresponding adsorption performance in activated biochars. From the studies about the correlation between the chemical and structural properties and the adsorption efficiency for a model aromatic contaminant, the adsorption kinetics of the activated biochar seems to be governed largely by the surface characteristics, such as BET surface area and pore volume. However, the aromatic carbon structure of biochars affects the binding strength between the activated

biochar and the target aromatic contaminant, which could be observed using solid-state ^{2}H NMR spectroscopy.

The series of works presented here can provide the insight for the details about thermal alteration of lignocellulosic biomass, and enlighten the potential of biochar as a promising adsorbent for removal of environmental contaminants. In addition, the possibility of designing the adsorbents for specific needs by manipulating process parameters in thermal treatment can be another big advantage for the value-added applications of biochar.

Structural and Chemical Characterization of Thermally-Treated Woody Biomass

by
Junyeong Park

A dissertation submitted to the Graduate Faculty of
North Carolina State University
in partial fulfillment of the
requirements for the degree of
Doctor of Philosophy

Forest Biomaterials

Raleigh, North Carolina

2013

APPROVED BY:

_____	_____
Dr. Orlando J. Rojas Co-Chair	Dr. Sunkyu Park Co-Chair
_____	_____
Dr. Martin A. Hubbe	Dr. Julie Willoughby
_____	
Dr. Kwang Hun Lim	

DEDICATION

To my beloved family.

BIOGRAPHY

Junyeong Park was born in Mokpo, South Korea, on Mar 16, 1979. He took a Bachelor of Science in Agriculture degree majored in Forest Products in 2005, and a Master of Science in Agriculture degree majored in Forest Science, Environmental Materials Science in 2007. He joined his Ph.D. course in August 2008 in the Department of Forest Biomaterials at North Carolina State University under the supervision of Dr. Sunkyu Park and Dr. Orlando J. Rojas.

ACKNOWLEDGMENTS

I would like to express my most sincere gratitude to Dr. Sunkyu Park and Dr. Orlando Rojas for their valuable advice and kind guidance on my research. I really appreciate Dr. Kwang Hun Lim for his great help and advice on NMR measurement and analysis, which helped me to break through a big difficulty in my works. And, I am also very grateful to Dr. Martin Hubbe and Dr. Julie Willoughby for their valuable comments and advice which enlightened me on expanding my works into new fields. Finally, I would like to thank all my friends in our department for their kind helps in the past five years.

TABLE OF CONTENTS

LIST OF TABLES

LIST OF FIGURES

CHAPTER 1

Thermal Treatment of Lignocellulosic Biomass: Chemical and Structural Changes and Their Characterizations

1. Introduction

Thermochemical processing, depending on its severity, can convert lignocellulosic biomass into dramatically different proportions of the three principles phases: solid, liquid, and gas. During the thermal decomposition of biomass, gaseous products, consisting of carbon monoxide and dioxide, hydrogen, water, and methane, as well as higher hydrocarbons, can be generated. Gasification is the thermochemical conversion process that mainly generates a gaseous mixture of hydrogen and carbon monoxide, which is generally referred to as syngas (or synthesis gas). This syngas can be used directly, or it can be converted into liquid fuels and useful precursors through the Fischer-Tropsch or other processes (Hu et al., 2005; Munasinghe & Khanal, 2010; Tijmensen et al., 2002). High-yield liquid fractions from the thermal treatment of biomass, known as pyrolysis oil or bio-oil, are usually produced via fast pyrolysis. Bio-oil has potential to be used as liquid fuel, but there are several limitations such as a lack of stability with respect to viscosity and oxidation (Czernik & Bridgwater, 2004). Solid products, among the three major fractions, have received less attention due to their relatively low value as produced, compared to the other two products. Solid products of thermochemical processing can be classified into three categories including torrefied biomass, biochar, and charcoal. During the torrefaction, several different reactions

including dehydration, depolymerization, and condensation take place, increasing energy-density, hydrophobicity, and homogeneity of biomass. As the severity of the thermal treatment is increased in a short processing time, however, extensive devolatilization and carbonization take place, generating highly condensed, char-like solids, which can be referred as biochar. When biomass is treated at high temperatures for an extended treatment time (slow pyrolysis), it remains as a highly carbonized residue, which is called charcoal. Recently, the solid products are receiving more attention because there are possibilities of utilizations in soil amendment, carbon sequestration, and environmental remediation. Biochar and charcoal are finding use as water/soil remediation agents or for soil amendment. There have been multiple efforts to investigate the mechanism of thermal conversion for the production of solid products, but the process details are not yet fully elucidated due to the complex native characteristics of biomass. In this review, existing studies concerning the changes of chemical and structural characteristics of lignocellulosic biomass during heating and various analytical tools for solid analysis are covered with the goal of providing comprehensive information about what has been revealed and where future research needs to proceed.

2. Thermal-induced alteration of lignocellulosic biomass

2.1. Carbohydrates during thermal treatment

Carbohydrate fractions consist of cellulose and various hemicelluloses. Compared to the lignin fraction, these saccharides, especially hemicellulose, are more susceptible to

hydrolysis and dehydration reactions during thermal treatment (Balat, 2008; Grønli et al., 2002; Peng & Wu, 2010; Soltes & Elder, 1981; Wikberg & Maunu, 2004). Based on thermogravimetric analysis, hemicellulose (xlyan as a reference material) starts its major weight loss at around 250°C and loses 70% of its initial mass by about 300°C (Williams & Besler, 1996). As for cellulose, the major weight loss starts above 300°C and the solid yield decreases until the temperature exceeds 450°C (Milosavljevic & Suuberg, 1995). It has been reported that 74% of the glucan in softwood (Loblolly pine) is lost after torrefaction at 330°C for 2.5 min, and most of hemicellulose was depleted under such conditions (Park et al., 2013).

2.1.1. Decomposition mechanisms

Although the mechanisms about the thermal degradation of carbohydrates have not been fully understood, several speculative pathways have been proposed. As for cellulose, the β-1,4-glucosidic bond is presumably cleaved, resulting in the formation of a hydroxyl radical from C-6. The hydroxyl radical can then make a linkage with C-4 to produce levoglucosan (1,6-anhydro-β-D-glucopyranose), a major intermediate product. Besides, direct ring opening and rearrangement reactions can generate other products, such as 5-HMF (5-hydroxy-methylfurfural) and furfural, which can also result from further thermal degradation of anhydrosugars (Shen & Gu, 2009). In addition, many thermally-induced chemical reactions, such as dehydration, decarbonylation, and decarboxylation, can result in the formation of different kinds of organic molecules, such as aldehydes, ketones, acids, and gaseous products (Lin et al., 2009; Piskorz et al., 1986; Tang & Bacon, 1964).

Hemicelluloses undergo thermal decomposition very readily. Similar to the thermal decomposition of cellulose, hemicelluloses are also subject to the cleavage of the glycosidic bonds during thermal treatment. In addition, due to their branched and heterogeneous structures, they undergo other reactions, such as deacetylation from the cleavage of acetyl groups, the decomposition of side-chain structures, and further fragmentation of depolymerized units. The products consist of furfural, furans, and acids (Hosoya et al., 2007; Pouwels et al., 1987; Shafizadeh & Bradbury, 1979).

These kinds of thermal products from carbohydrates can be observed in liquid and gaseous products, and the proportions of different chemical species give clues to elucidate the mechanisms for thermal degradation of cellulose via the techniques of chromatography and spectrophotometry. As for the solid products, hemicelluloses yields more chars, despite its lower thermal stability compared to that of cellulose. (Hirata et al., 1991; Ramiah, 1970; Yang et al., 2007), but their mechanisms and characteristics have not been fully elucidated yet.

2.2. Lignin during thermal treatment

Lignin is the second most abundant and the only biomass component based on aromatic units (Gosselink et al., 2004; Lora & Glasser, 2002). Due to the high heterogeneity and the yet undetermined chemical and structural details, however, the mechanism of thermal conversion of lignin is less elucidated, compared to the other two components. The detailed information for the thermal-induced changes of the lignin fraction is important in the characterization of solid residue after the thermal process, because the large portion of mass

in thermally-treated lignocellulosic biomass is from lignin, considering its fraction in feedstock and relatively low thermal reactivity. However, the elucidation of the complicated characteristics of the lignin has been considered to be quite challenging, due to the diversity of chemistry and their heterogeneous structures. Because of these reasons, existing studies have been mostly focused on the variety and the amount of different functional groups in model compounds, chemically-modified lignins, and partially-degraded or extracted lignins.

From the point of chemical aspects, it has been generally accepted that lignin has three types of monolignols that are cross-linked to make complicated three-dimensional network structures with various C-O and C-C linkages, as shown in Fig. 1 (Dence & Lin, 1992; Freudenb.K, 1965; Glasser et al., 1981; Nimz, 1974; Sarkanen & Ludwig, 1971; Sjöström, 1993). There are at least 20 different linkage types that have been identified (Whetten et al., 1998). Besides the diverse intermolecular linkages, the lignin macromolecule also contains a variety of functional groups that have an impact on its reactivity (Brebu & Vasile, 2010; Jakab et al., 1997), such as methoxyl groups, phenolic hydroxyl groups, and aldehyde groups. The methoxyl group is one of the main chemical groups in lignin, and dissociation of the methoxyl groups generates methyl radicals and phenoxy radicals, which can act as reactive sites for further thermal reactions, e.g. degradation and condensation. Phenolic hydroxyl groups play an important role affecting the characteristics of lignin (Adler, 1977) and depolymerization/degradation processes (Gierer, 1985; Olivares et al., 1988). Different ratios between the three lignin monomers, various linkages, and functional groups contribute to the diversity in these chemical moieties, and this leads to differences in the chemical reactivity of lignins. Consequently, it may possibly

affect the overall reaction mechanism and the corresponding products from different thermal treatments.

Due to the high heterogeneity in structural and chemical characteristics mentioned above, lignin shows different thermal reactions and behavior, compared to carbohydrate fractions. Existing studies about lignin cleavage and condensation have been mainly focused on pulping processes. The main purpose of pulping, especially alkaline pulping, is lignin fragmentation to allow individual fibers to be released from the lignocellulosic matrix with mild mechanical treatment. The major degradation reactions during kraft pulping include the cleavage of α- and β-aryl ether bonds, resulting the fragmentation of lignin. The degradation and fragmentation reactions are believed to be counter-balanced by condensation reactions during kraft pulping. Primary condensation reactions occur when quinone methide intermediates are formed by the elimination of an α-substituent, while secondary condensation reactions occur with quinone methide structures formed after an initial ether cleavage (Gierer, 1980).

This kind of lignin cleavage and condensation reaction can also happen in similar ways during thermal treatment. Thermal degradation of lignin takes place over a broad temperature range due to the fact that different functional groups have different thermal stabilities, and their scission occurs at the corresponding temperatures (Brebu & Vasile, 2010). The cleavage of the intermolecular linkages and the functional groups reduces high molecular weight polymers into low molecular weight products. Also, during thermal degradation, the backbone structure can be rearranged at a higher temperature, making solid char and releasing volatile products. The cleavage of the aryl-ether linkages will generate

highly reactive and unstable free radicals (Watanabe et al., 2009), which can react further through rearrangement, electron abstraction, or radical-radical interactions, to form more stable products (Afifi et al., 1989). The cleavage can lead to condensation reactions between intermediates to form polymerized products, too. During the reactions, the presence of phenol affects condensation due to its radical scavenging capabilities (Lin et al., 1997). The differences in wood species mainly result in different degradation rates for lignin. Coniferous lignin is thermally more stable than deciduous lignin, the latter producing smaller char yields (Muller-Hagedorn et al., 2003).

2.2.1. Depolymerization: Ether Bond Cleavage

As already mentioned in 2.2, there are several different linkages in the lignin structure (Freudenb.K, 1965; Nimz, 1974), and due to their respective bonding energy, the cleavage of the linkages is induced at different temperatures. The aryl-ether bonds (β-O-4 and α-O-4 linkages, which are major in the structure of lignin) are relatively easier to cleave and therefore are the predominant reactions in deplymerization of lignin (Fig. 2). It has been reported that a substantial amount of the β-O-4 aryl-ether linkages are cleaved during the heat treatment process with steam (Haw & Schultz, 1985; Sudo et al., 1985). Thermal modification and steam partially hydrolyze the aryl-ether linkages in syringyl and guaiacyl monomers, resulting in the formation of free phenolic hydroxyl groups and α/β carbonyl groups. This aryl-ether cleavage by thermal decomposition is supported by several different analytical methods. Windeisen and Wegener reported that the yield of degradation products by thioacidolysis was decreased in thermally-treated woods, which is indicating a reduction

of structural units bound by aryl-ether linkages (Windeisen & Wegener, 2008). NMR (nuclear magnetic resonance) spectroscopy could also measure the decrease in etherified C-4 in guaiacyl units and the increase in non-etherified C-4 in syringyl units of steam-treated spruce (Wikberg & Maunu, 2004).

2.2.2. Decomposition: Demethylation/demethoxylation

There are several characteristic functional groups of lignin molecules, and among them, methoxyl groups (-OCH_3) have been studied most extensively due to their role in the decomposition of biomass by microorganisms (Waksman & Smith, 1934). The methoxyl content in lignin varies with the type of biomass and even in the same plant, at different stages of growth. It may also depend on the position of the lignin in the plant tissues. The methoxyl content of the lignin in the middle lamella of wood have been found to be 11-13%, while that of the lignin in the cell wall was only 4.3-4.8% (Ritter, 1926). It has been reported that the methoxyl content decreases during thermal treatment of wood (Sivonen et al., 2002; Wikberg & Maunu, 2004), but it is generally considered that the methoxyl group is relatively difficult to be cleaved during thermal treatment. The methoxyl group is cleaved about four times slower compared to β-O-4 (Britt et al., 2000).

Funaoka and co-workers reported a slight decrease of methoxyl content below 200°C and increasing at 220°C when heating water-saturated wood mills of spruce. This is attributed to the modification of hemicellulose-containing methoxyl groups below 200°C, and the relative increase of the lignin proportion caused by the degradation of carbohydrates above that temperature (Funaoka et al., 1990), and it is expected that the demethoxylation of

lignin takes place at a higher temperature. Experiments with some lignin model compounds suggested that the primary hydrodeoxygenation for the chemicals is demethylation, followed by dehydroxylation and hydrogenation reactions to benzene and cyclohexane (Hurff & Klein, 1983). CH_4 is produced readily from a weakly bonded methoxyl group, -OCH (bond energy 60 kcal/mol), at lower temperatures, and additional CH_4 will be produced from methylene groups, $-CH_2-$ (bond energy 72 kcal/mol), in the bridges connecting the lignin subunits at higher temperatures. CO is produced from two types of ether groups. The first is the ether bridges joining the lignin subunits. Since this group has a low dissociation energy (60 ~ 75 kcal/mol), this is the main source of CO at low temperatures. Additionally, at high temperatures, dissociation of diaryl ether will also occur and act as the CO source (Sada et al., 1992). With a higher dissociation energy, demethoxylation also takes place, leaving the benzenediol structure and methanol from the guaiacol structure (Fig. 4).

2.2.3. Condensation

The ether bond cleavage results in a relative increase of the condensed structure in lignin because the carbon-carbon bonds, such as 5-5 linkages, have a higher bond dissociation energy (Luo, 2007), which requires a higher temperature to be cleaved. Along with this, it has also been reported that a condensed lignin structure is formed by thermal treatment (Kawamoto et al., 2007; Nakamura et al., 2007). Although lignin is the least reactive component of wood, compared to the other two, it is considered that the depolymerization of lignin complex results in a higher concentration of phenolic units, and this state increases the reactivity of lignin (Tjeerdsma & Militz, 2005). The free phenolic

hydroxyl group, released by thermal treatment, plays an important role for the lignin reaction, increasing the degree of condensation in the solid residue in general. This statement is supported by spectroscopic analyses, which have showed more condensed guaiacyl structure than etherified (uncondensed) structure in FTIR (Faix, 1992; Windeisen & Wegener, 2008), but the detailed mechanisms about condensation has not been elucidated yet. At low temperatures of heating, it seems that diphenylmethane type condensation is mainly observed in protolignin in spruce (Funaoka et al., 1990). In the same study, however, modified lignin (dioxane-extracted) also generated various types of modification, as well as diphenylmethane type condensation. Recently, there have been several attempts to explain the thermal condensation reaction of lignin. Kadla and co-workers reported that the mild thermal treatment for isolated lignin samples produced solids with higher molecular weight, up to 50% greater than that of untreated lignin. They also found a correlation between the difference in the MW of lignin and its phenolic hydroxyl content (Kadla et al., 2002). In another study, it was shown that coniferyl aldehyde and alcohol, which are abundant in softwood lignin, act as significant precursors for the condensation reactions at low temperatures due to their vinyl structure on the side-chain (Nakamura et al., 2007). Using ^{1}H NMR analysis for the products after pyrolysis of lignin model compounds at 250°C for 2 hrs, aryl-aryl, aryl-O-aryl, and diphenyl methane structures were observed. The formation of these structures strongly suggests the existence of various radical species derived from phenoxy and benzyl radicals. The vinyl structure is also generated by thermal reactions, which could result in more condensed quinone methide forms via nucleophilic reactions of creosol-C6 and hydroxyl group in creosol moiety.

2.2.4. Aromatic cluster formation

It has been reported that, during the thermal degradation of lignin, the concentration of aromatic carbons decreased by only about 10% relative to the starting Kraft lignin at the high heating temperature of 600°C (Sharma et al., 2004). This implies that most of the weight loss during thermal treatment of lignin is due to the volatilization of the non-aromatic carbons. These results show that the aromatic fraction of lignin is very resistant to thermal decomposition compared to the non-aromatic carbon structure, and that the resulting char is highly recalcitrant to thermal decomposition. Sharma and co-workers also proposed the condensation of smaller aromatic structure into larger aromatic carbon networks (Sharma et al., 2004). The methoxyl group was suggested as a key structure for lignin char formation, probably in vapor-phase after volatilization of the compounds. After pyrolysis at 600°C for 80 seconds under inert conditions (nitrogen), a substantial amount of char was formed only from the compounds with the guaiacyl-units, especially guaiacol and derivatives with the C=C or C=O side-chains (Hosoya et al., 2009).

3. Characterization of structure and chemistry in thermally-treated lignocellulosics

3.1. Quantification of carbohydrate

For the determination of structural carbohydrates in lignocellulosic biomass, there are several procedures available such as ASTM E1758-01 and a NREL (National Renewable Energy Laboratory) LAP (Laboratory Analytical Procedure), but the basic concept of all of these procedures is quite similar. The carbohydrate fraction is broken down into monomeric

sugars using dilute-acid hydrolysis, then the sugars in hydrolyzate can be quantified by appropriate methods, such as HPLC. This kind of dilute acid hydrolysis has been extensively used to quantify the carbohydrate fraction, as well as the acid-insoluble fraction, in the wood science and pulp & paper field. This quantification method is a quite straightforward analysis, but it is hard to apply to thermally-treated lignocellulsic biomass. As addressed earlier in this review, carbohydrate fractions in lignocellulosics are decomposed more easily than lignin fractions, and only in samples treated with relatively mild severity can some amount of this fraction be conserved, containing acid-soluble carbohydrates. Even under torrefaction conditions, treatment at 330°C for 2.5 min could decompose most of hemicellulose, and more than 70% of cellulose is also degraded (Park et al., 2013). Above certain degrees of thermal treatment conditions, therefore, carbohydrate analysis using dilute-acid hydrolysis might not be feasible. In addition, due to the lack of available isolation methods for solids from thermally-treated carbohydrates out of the whole residue, it is necessary to find other analysis tools that can be applied to whole solid residues from thermal treatment of biomass.

3.2. Lignin quantification/isolation

3.2.1. Klason lignin

There have been several different approaches for the determination of lignin, but most of them are not regarded as totally satisfactory, because that lignin has not been isolated or analyzed as its natural form. Despite these limitations, there are some methods that are widely accepted for the determination of lignin.

Acid-hydrolysis is one of the most widely used ways to quantify the lignin content in a lignocellulosic material. It consists of the hydrolysis and solubilization of the carbohydrates in lignocellulosics, as described above, leaving the lignin as a residue, which is determined gravimetrically. Hydrolysis of the carbohydrates can be catalyzed by different mineral acids, and detailed methods involving different acids have been studied (Browning, 1967; Pearl, 1967).

Klason lignin is the most widely used gravimetrical measurement of the lignin amount after acid hydrolysis by sulfuric acid, which was developed by a Swedish chemist, Johan Peter Klason. This method consists of two-step hydrolysis – pre-hydrolysis of lignocellulosic biomass with sulfuric acid of 72% concentration at low temperature, followed by dilution of the acid to 3% and heating at high temperature for complete hydrolysis of the carbohydrates. The acid-insoluble residue is gravimetrically measured and considered as Klason lignin content in the samples, and acid-soluble lignin and hydrolyzed carbohydrates can be determined using UV-Vis spectroscopy and HPLC, respectively (ASTM, 2009; TAPPI, 2002). There have been several modifications for this analysis method, to be used for small amounts of samples (Effland, 1977; Whiting et al., 1981), or to shorten the heating time after dilution (Yoshihara et al., 1984).

It is necessary to use caution when this analysis method is used for heat-treated biomass. As already indicated, the problem of applying acid-hydrolysis for removal of remaining carbohydrates in heat-treated biomass is that the lignin is not the only acid-insoluble portion in the sample. For example, a situation may be envisioned wherein the lignin has been modified to such a degree that its characteristic properties totally or partially

disappear and yet is still capable of yielding a acid-insoluble residue after being treated by the Klason lignin procedure. It might also be falsely to use the acid hydrolysis method due to condensing of degradation products from the carbohydrates, which can make the proportion of acid-insoluble structure increased after thermal treatment. In addition, the insoluble residue after this acid-hydrolysis method might not be suitable for further analyses, because it causes considerable condensation reaction to the lignin structure (Sarkanen & Ludwig, 1971).

3.2.2. Lignin isolation from solid residues

There are two methods that are widely used for isolation of lignin from biomass – milled wood lignin (MWL) and cellulolytic enzyme lignin (CEL). MWL was introduced by Björkman and involves the use of a preliminary, extensive grinding, followed by solvent extraction (Björkman, 1956; Björkman, 1957; Björkman & Person, 1957). The latter, CEL, involves an enzymatic hydrolysis for the removal of associated polysaccharides before solvent extraction to increase the amount of solubilized lignin (Chang et al., 1975; Pew, 1957; Pew & Weyna, 1962). These methods are generally used for the isolation of lignin from raw or biologically/chemically processed biomass. However, they are not suitable for thermal-treated lignocellulosics. As discussed above, the thermal process removes the uncondensed fraction easily and substantially increases the degree of condensation, making it hard to achieve a sufficient yield for the soluble fraction and losing the representability of the extracted products toward the whole thermally-modified lignin. Considering the enzymatic hydrolysis, it might be less effective due to the fact that the carbohydrates are already

degraded substantially. In addition, it has been reported that the thermal treatment for biomass increases the resistance against the biological activities (Militz & Tjeerdsma, 2001; Tjeerdsma et al., 2000). Hence, it is necessary to find methods to characterize solid products after thermal treatment as a whole, due to the lack of practical and proper ways for isolation.

3.3. Functional group in lignin

3.3.1. Methoxyl group

The Ziesel procedure is a treatment to cleave the methoxyl or ethoxyl groups in a sample using concentrated hydriodic acid, releasing the functional groups as methyl or ethyl iodide forms. These volatile iodide products are readily reacted with silver nitrate in a solution, and yield a precipitated silver iodide that can be measured to quantify the methoxyl or ethoxyl content in the sample. The problem with the original Ziesel method is that sulfur in the compound can be converted to hydrogen sulfide during the hydriodic acid treatment, and this chemical can react with silver nitrate. Due to the interference of the sulfur in the reaction, the original Zeisel method is not appropriate for sulfur-containing samples, such as technical lignins. To solve this, different methods of detection for methyl or ethyl iodide have been introduced, namely, absorbing onto different chemicals, extracting with organic solvents, and measurements by titration or gas chromatography (Dence & Lin, 1992; TAPPI, 1972). NMR spectroscopy was also employed to measure methoxyl/aryl carbon atom ratios (Obst & Landucci, 1986).

In 1996, Baker introduced a rapid and safe analytical method for methoxyl groups using gas chromatography (Baker, 1996). Briefly, wood mill is reacted with hydriodic acid

with heat, and then the mixture is extracted with pentane to dissolve methyl iodide into the organic phase. The pentane layer is collected and analyzed using gas chromatography for the quantification of methoxyl groups in the compound. However, it has been suggested that the hydriodic acid treatment can be interfered with by glucose and the other carbohydrates, which give rise to "apparent" methoxyl content (Gran, 1953). Goto and co-workers confirmed this scenario using methoxyl-free compounds and gas chromatography (Goto et al., 2001; Goto et al., 2005).

3.3.2. Hydroxyl group

Hydroxyl content in lignin can be classified into two fractions – the aliphatic hydroxyl and the phenolic hydroxyl content. The total hydroxyl content can be determined by acetylation with a mixture of acetic anhydride and pyridine, followed by saponification of the acetate and titration of the resulting acetic acid with a basic solution, or HPLC analysis (Gosselink et al., 1995).

The phenolic hydroxyl group content provides pertinent information about the lignin, because it affects the physical/chemical properties and reactivity of lignin in various applications and processes (Adler, 1977; Gierer, 1986; Gierer, 1985; Olivares et al., 1988). The UV method, based on the difference in absorption of phenolic units in neutral and in alkaline solution, is suitable for soluble lignin preparations (Goldschmid, 1954). However, it needs to use model compounds for calibration, and can be difficult for interpretation in the case of wood species (Adler, 1977).

Direct measurements of the free-phenolic units have been reported, including ultraviolet absorption (UV) (Boutelje & Eriksson, 1984; Yang & Goring, 1980), titration (Butler & Czepiel, 1956), pyrolysis (Whiting & Goring, 1982), aminolysis (Gellerstedt & Lindfors, 1984), and periodate oxidation (Lai et al., 1990). Among these methods, periodate oxidation was reported to be a convenient and suitable method for both softwood and hardwood. It is also not interfered with by the reducing end groups of the carbohydrates, which happens in the aminolysis method. The method is based on the finding that phenols carrying a methoxyl group in the o-position are oxidized by periodate, releasing on a molecule of methanol, and the methanol can be analyzed using gas chromatography (Gierer et al., 1964).

In spite of its several advantages, some limitations have been also reported. Because the periodate oxidation method is based on methanol formation from methoxyl groups, it cannot be applied to methoxyl-free phenolic units, which are present in a large quantity in non-wood lignins and in compression wood lignin (Adler, 1977). Also, the milling process can affect the phenolic hydroxyl content. Fragmentation of the lignin macromolecules is induced by extensive milling, decreasing the average molecular weights from the original lignins (Chang et al., 1975). This will result in certain chemical changes, such as an increase in the free phenolic hydroxyl and α-carbonyl groups, during the milling (Chang et al., 1975; Pew, 1957).

3.3.3. Other functional groups

Carbonyl groups, especially ring-conjugated ones, are known to exhibit a large influence on the rate of delignification reaction and the quality of the products in the pulping process (Gierer & Noren, 1982). It is also known that the ring-conjugated carbonyl groups in lignin cause the colorization of wood or the products, when exposed to heat or UV light (Gierer & Lin, 1972). The increase of the content of the carbonyl groups in proportion to the level of wood decay has been reported in the early stage of wood decay by fungi (Higuchi, 1971). Carbonyl content can be determined by reaction with hydroxylamine, followed by a titration method (Gierer & Lenz, 1965), or by UV spectroscopy in alkaline solution (Goldschmid, 1953).

3.4. Structural characterization

The fundamental structure of woody biomass has been intensively investigated, but the detailed information about the complex lignocellulosic matrix and the individual unit components has not been fully elucidated yet; especially for the highly-heterogeneous polymeric structure of lignin. There have been statistical attempts to construct the higher order structure of lignin by linking each possible unit compound using a computational approach (Glasser & Glasser, 1974a; Glasser & Glasser, 1974b; Glasser et al., 1976). However, this computational method has certain limitations, due to the fact that the results are based on several assumptions, such as a statistical polymer model that is randomly formed with less than three p-coumaryl alcohol-type phenols, the model lignins with limited functional groups, and their proposed conversion mechanisms. To investigate the practical

structure of lignin polymers, there have been diverse approaches, involving wet chemistry, physical analysis, mass spectrometry, spectroscopy, and many others. Among them, several kinds of effective and commonly used methods are reviewed below.

3.4.1. Nitrobenzene oxidation

Nitrobenzene oxidation yields oxidation products from uncondensed lignin structures (Chang & Allan, 1971; Dence & Lin, 1992). Hence, the yield of nitrobenzene oxidation products can indicate not only the compositions of lignin types (p-hydroxyphenyl, guaiacyl-, and syringyl-type), but can also be a relative indicator of the condensation degree, by providing information on the minimal quantities and the relative amounts of the uncondensed lignin units present in lignin. During the oxidation, base-catalyzed cleavage of α- and β-aryl ether bonds takes place, producing the corresponding phenolate anions. The oxidative cleavage between C_α-C_β bonds then follows. Nitrobenzene oxidation is performed under alkaline conditions, and 5-iodovanillin is usually used as the internal standard because it is not present in the oxidation products (Katahira & Nakatsubo, 2001). After the reaction, the products are extracted with an organic solvent, and can be analyzed by gas chromatography.

As mentioned above, the nitrobenzene oxidation products can provide information about the composition of lignin types. The ratio between different lignin units, such as the S/V ratio, can be used for classification of plants or the characterization of lignin (Creighton et al., 1944; Meshitsuka & Nakano, 1985; Obst et al., 1988). In addition, the results provide a relative measure of the extent of condensation in the aromatic moieties of lignins. In nitrobenzene oxidation, the total yield of product from each monomeric lignin unit

corresponds to the minimum quantities of uncondensed structures. Therefore, a decrease in the total yield of nitrobenzene oxidation products resulting from a particular treatment of lignin constitutes a sensitive measure of secondary condensation reactions.

3.4.2. Thioacidolysis

Thioacidolysis is also one of the most widely utilized and effective diagnostic methods in the study of lignin structure. It is routinely used to estimate the amount and composition of uncondensed aryl-ether structures. Thioacidolysis is an acid-catalyzed solvolysis reaction, which leads to the depolymerization of lignins. It proceeds by either cleavage of α-ethers or substitution of α-hydroxyl groups by the thioethyl group, followed by β-aryl ether cleavage and the formation of trithioethyl monomeric products (Holtman et al., 2003).

Briefly, extractive-free samples are mixed with thioacidolysis reagent, which is a mixture of boron trifluoride and ethanethiol in dioxane (Fuji et al., 1979; Node et al., 1976), and heated under inert atmosphere. The mixture is then extracted with organic solvents after pH adjustment. GC analyzes the obtained product after derivatization.

Compared with thioacidolysis, nitrobenzene oxidation leads to higher product yields, due to the fact that the oxidation method can degrade structures other than alkyl-aryl ether, such as diarylpropane units (Chang & Allan, 1971). However, thioacidolysis can provide additional information in certain samples (e.g. grass lignin), compared to oxidation methods, because oxidation of the p-coumaric and ferulic acid ester substituents leads to the same compounds as do p-hydrolyphenyl and guaiacyl lignin-building units, respectively.

3.5. Thermal analysis

From the structural point of view, lignin is considered to have a highly heterogeneous polymeric network. Due to its intrinsic characteristics and the difficulty in extraction as a native form, many limitations exist in understanding the structure of lignin. There are several different techniques for analyzing the changes of lignin during thermal treatment. Among them, the thermogravimetric technique (TGA) is a useful and powerful tool for determining the thermal degradation of lignocellulosic materials as a function of temperature and/or time. Lignin is usually considered to be the most thermally stable constituent of the biomass compounds. However, lignin undergoes a slight decomposition at very low temperatures, and during the initial stages of decomposition it is less stable than cellulose (Ramiah, 1970). Another characteristic of lignin during heat treatment is its glass transition at low heating temperatures. Based on several studies, it was proposed that temperatures above 100°C cause lignocellulosics to be softened, which results from the glass transition of the lignin (Hatakeyama et al., 1982; Irvine, 1984). Recently, however, it has been reported that the glass transition temperature of lignin might be close to 70~90°C, based on analyses by DSC (differential scanning calorimetry) (Irvine, 1984) or DMA (dynamic mechanical analysis) (Laborie et al., 2004) methods. The existing studies about thermal analysis for lignin propose that the thermal decomposition of lignin generally starts between 150 and 200°C, and the maximum rate of weight loss is reached between a wide range of temperatures (250~500°C) (Ferdous et al., 2002; Jiang et al., 2010) depending on the feedstock origin, extraction method, and the thermal history.

3.6. Spectroscopy

Thermal analysis is a good tool for monitoring the thermal degradation as a function of time and temperature, and for investigating the overall thermal behavior of lignin. However, it is hard to obtain information about structural insights on the lignin transformation solely with thermogravimetric data. To get more details about the structural and chemical changes during thermal decomposition, some spectrometric tools have been employed. Avni et al. (1985) used an FTIR spectrophotometer connected with a flash pyrolysis unit to analyze the gas from lignin samples pyrolyzed at 150~900°C. This procedure showed that the substituted groups and aliphatic structures in lignin are degraded, releasing CO_2 from the carboxyl groups, H_2O from the hydroxyl groups, hydrocarbon gases from the aliphatic and methoxy groups, and CO from weakly bound oxygen groups, such as aldehyde groups. Further reactions at higher temperatures involve breakage and rearrangement of the aromatic rings, generating hydrogen and CO from oxygen functional groups, such as diaryl ethers and phenols. Another research group did the structural analysis for the solid residue after lignin pyrolysis using several different techniques – FTIR and NMR (Sharma et al., 2004). In FTIR spectra, peak areas of hydroxyl, methoxyl, and aliphatic CH are decreased as the pyrolysis temperature increased, but the aromatic CH showed an opposite trend. Most of the electron donor substituents including OH and OCH_3 were removed at 400°C. Similar observations on the pyrolysis of cellulose at temperatures of up to 450°C were also reported by a different research group (Mok et al., 1992). The major step of pyrolysis of biomass might consist of dehydration, carbonyl group formation and elimination, decomposition of aliphatics, and the formation of aromatics.

Raman spectroscopy, which can be considered as a complementary method with conventional IR spectroscopy, is another tool for structural analysis for solids. It can measure the shift in frequency by an amount corresponding to the energy of the particular vibrational transition (Atalla et al., 1992). Due to its inherent characteristics dependent on polar band systems, conventional IR spectra are easily interfered with by water in samples. By contrast, Raman spectra represent adsorptions by highly covalent, non-polar bonds, so the method is relatively free from the effect of water. In Raman spectra, aromatic ring stretching vibrations in lignin are distinguishable against the bands from the other two main components of lignocellulose. However, in other band regions, all the components interfere with each other, and this makes the interpretation complicated. The early Raman spectroscopy studies were focused on the orientation of cellulose and lignin in the cell walls (Agarwal & Atalla, 1986; Atalla & Agarwal, 1985). Many subsequent studies have been carried out to interpret Raman spectra of lignin, and the important band positions and assignments have been identified (Agarwal & Ralph, 1997; Agarwal et al., 1997; Atalla, 1987; Ehrhardt, 1984). The method also has been applied to investigate carbon structures in biochar. By calculating the fraction of band areas for assigned Raman peaks, it is possible to figure out the fraction of large aromatic carbon clusters, as well as amorphous carbon with small aromatic ring systems. With this technique, structural characterization of biochar can be achieved (Chang et al., 1975; Cheng et al., 2008; Wu et al., 2012).

3.7. NMR spectroscopy

After the isolation and dissolution of lignin in certain solvents, such as DMSO-d_6, several different analytical techniques of liquid-state NMR spectroscopy have been employed and contributed to a better understanding of detailed lignin structure (Gellerstedt & Robert, 1987; Lundquist, 1992; Robert, 1992). In a similar manner, the solid-state NMR has also been used for the characterization of lignocellulosic biomass and its thermal products, including torrefied biomass and biochars from different thermal processes (Baldock & Smernik, 2002; Brewer et al., 2009; Gil & Neto, 1999; Park et al., 2013). The solid-state ^{13}C NMR spectroscopy is a powerful tool for the structural analysis of carbonaceous materials *in situ*. For the characterization of thermally-treated biomass, it can provide valuable complementary information about structural alterations during thermal processes, because specific resonance peaks can be estimated based on the total resonance intensity, giving the relative abundance of certain molecular structures. In conventional solid-state ^{13}C NMR, such an approach has been considered less useful because of its weak and broad signals. However, the weak signal problem can be overcome by using cross polarization pulse sequences (Pines et al., 1973), and the broad widths problem by spinning samples at a certain angle relative to the magnetic field, which is referred as "magic angle" (Schaefer & Stejskal, 1976).

This advanced solid-state NMR technique has been applied to characterize the thermal treatment on lignocellulosic biomass. Thermally modified woody samples at relatively low temperatures (< 200°C) were analyzed by ^{13}C CP/MAS (cross polarization/magic angle spinning) NMR spectroscopy (Wikberg & Maunu, 2004). In their

study, it was reported that the crystalline indices for all the samples were increased, which might be due to the thermal degradation of less ordered carbohydrates, such as hemicellulose and amorphous cellulose. In the case of lignin, it was possible to calculate the degree of cleavage for β-O-4 linkages during thermal treatment, based on the spectra from lignin monomeric units with/without etherification. Furthermore, it was detected that there are more condensed linkages, such as biphenyl (5-5) or diphenylmethane, existing after treatment. It was also suggested that demethoxylation of lignin generates more reactive sites on lignin, resulting in the condensation of lignin structure.

Sharma and co-workers demonstrated using ^{13}C CP/MAS NMR that there is a loss of lignin substructure and increasing aromaticity in pyrolyzed lignin as the heating temperature increases. The decrease of the resonance from methoxyl groups is also observed under 400°C, and the spectra for the lignin pyrolyzed at 600°C is similar to that of the pure char structure (Sharma et al., 2004). When thoroughly carbonized charcoal is analyzed using solid-state NMR, the symmetricity of the peak presents structural information about the sample. Bourke et al. applied ^{13}C CP/MAS NMR spectroscopy to analyze the carbonized charcoal from corncob. The NMR peak spectra they obtained was not completely symmetrical, which might indicate the existence of small peaks associated with carboxyl and phenolic carbons. Also, it was observed that the higher carbonization temperature resulted in a more intense symmetrical aromatic peak. The authors interpreted this as a loss of oxygen with increasing carbonization temperature via dehydration, decarbonylation, and decarboxylation reactions, which lead to condensation and aromatic growth (Bourke et al., 2007).

Recent solid-state NMR applications to the study of biomass char have provided more detailed information about the pyrolyzed biomass structure. The CP (cross polarization) NMR technique tends to underestimate the nonprotonated carbons because of the slow transfer of hydrogen magnetization to carbons in the large aromatic structure. Also, it is sensitive to signal loss induced by the interaction with unpaired electrons (Simpson & Hatcher, 2004; Smernik & Oades, 2000). To overcome the semiquantitative nature of the CP NMR technique, caused by the inherent problems mentioned above, a combination of several different NMR techniques have been applied to make it possible to measure the aromaticity and the non-protonated aromatic carbon fraction in solid biomass samples (Mao & Schmidt-Rohr, 2004). Using these techniques (DP/MAS, DP/MAS with dipolar dephasing, CP/TOSS, and DP/TOSS with recoupled ^{1}H-^{13}C dipolar dephasing), the quantitative analysis for the carbon structure in biomass char can be achieved (Brewer et al., 2009). The approach is also applicable to get further structural information about the transformation of lignocellulosic biomass during thermal treatment, such as the putative structures of the aromatic cluster for pyrolysis char, presented in Fig. 5.

3.8. Limitations of analytical methods for solid biomass residues

Several different research groups (Bridgwater, 1984; Evans et al., 1986; Mcdermott et al., 1986; Vanderhage et al., 1993) have studied the thermal treatment of isolated biomass components and their model compounds. Due to the difficulty of isolation for lignin without significantly altering its structure, however, the thermal behavior of lignins isolated by different methods, such as ball milling and solvent extraction, is significantly different

(Evans et al., 1986; Vanderhage et al., 1993). In addition, chemical analysis via hydrolysis, oxidation reaction, and functional group analysis are not feasible for characterization of thermally-treated lignocellulosics due to the evolution of significantly altered and condensed structures beyond a certain point of treatment conditions. Consequently, the simple model compounds have been used to elucidate detailed kinetic and mechanistic insights into the degradation of the basic building blocks of lignocellulosic biomass (Evans et al., 1986; Lin et al., 2009; Mcdermott et al., 1986; Munasinghe & Khanal, 2010; Piskorz et al., 1986; Tijmensen et al., 2002; Vanderhage et al., 1993). However, using model compounds may have to limit the results to *in vitro* characterization. To address this issue, many current studies are focused on attempts at *in situ* solid characterization, employing complementary tools, such as vibrational spectroscopy and solid-state NMR analysis of thermally treated lignocellulosics.

4. Summary

Characteristics of thermally treated lignocellulosic biomass and analytical methods for solid characterization have been reviewed, focusing on chemical/structural properties. Due to relatively higher susceptibility to thermal decomposition of carbohydrate fractions, solid analyses have been more concentrated on the characterization of the lignin fraction and some kind of spectroscopic analyses that can observe the overall structures of solids. As the severity of thermal treatment increases, the cleavage of inter-unit bonds and functional groups occur, reducing the MW of lignin polymer and releasing corresponding degradation

products. Meanwhile, the condensation reaction take place, which is initiated by various radical formed during thermal degradation or conversion. Aromatic clusters are also formed during the process, resulting in increased aromaticity in the thermal-treated biomass. These changes can be observed using different wet chemistry and spectroscopic analyses. However, due to the structural characteristics of thermally treated lignocellulosics and the limitations of analysis tools, understanding the importance of chemistry and structure for target materials and appropriate application of complementary tools for characterization should be considered.

References

Adler, E. 1977. Lignin Chemistry - Past, Present and Future. *Wood Science and Technology*, **11**(3), 169-218.

Afifi, A.I., Hindermann, J.P., Chornet, E., Overend, R.P. 1989. The Cleavage of the Aryl-O-Ch3 Bond Using Anisole as a Model-Compound. *Fuel*, **68**(4), 498-504.

Agarwal, U.P., Atalla, R.H. 1986. Insitu Raman Microprobe Studies of Plant-Cell Walls - Macromolecular Organization and Compositional Variability in the Secondary Wall of Picea-Mariana (Mill) Bsp. *Planta*, **169**(3), 325-332.

Agarwal, U.P., Ralph, S.A. 1997. FT-Raman spectroscopy of wood: Identifying contributions of lignin and carbohydrate polymers in the spectrum of black spruce (Picea mariana). *Applied Spectroscopy*, **51**(11), 1648-1655.

Agarwal, U.P., Ralph, S.A., Atalla, R.H. 1997. FT Raman spectroscopic study of softwood lignin. *Iswpc - 9th International Symposium on Wood and Pulping Chemistry - Poster Presentations*, 81-84.

ASTM. 2009. E1721-01(2009): Standard Test Method for Determination of Acid-Insoluble Residue in Biomass.

Atalla, R.H. 1987. Raman-Spectroscopy and the Raman Microprobe - Valuable New Tools for Characterizing Wood and Wood Pulp Fibers. *Journal of Wood Chemistry and Technology*, **7**(1), 115-131.

Atalla, R.H., Agarwal, U.P. 1985. Raman Microprobe Evidence for Lignin Orientation in the Cell-Walls of Native Woody Tissue. *Science*, **227**(4687), 636-638.

Atalla, R.H., Agarwal, U.P., Bond, J.S. 1992. Raman Spectroscopy. in: *Methods in lignin chemistry*, (Eds.) S.Y. Lin, C.W. Dence, Springer-Verlag. Berlin ; New York, pp. xxx, 578 p.

Baker, S.M. 1996. Rapid methoxyl analysis of lignins using gas chromatography. *Holzforschung*, **50**(6), 573-574.

Balat, M. 2008. Mechanisms of thermochemical biomass conversion processes. Part 1: Reactions of pyrolysis. *Energy Sources Part a-Recovery Utilization and Environmental Effects*, **30**(7), 620-635.

Baldock, J.A., Smernik, R.J. 2002. Chemical composition and bioavailability of thermally, altered Pinus resinosa (Red Pine) wood. *Organic Geochemistry*, **33**(9), 1093-1109.

Björkman, A. 1956. Studies on Finely Divided Wood .1. Extraction of Lignin with Neutral Solvents (Reprinted from Svensk Papperstidning, Vol 59, Pg 477-485, 1956) Is a Citation-Classic. *Svensk Papperstidning-Nordisk Cellulosa*, **95**(12), 38-&.

Björkman, A. 1957. Studies on finely divided wood. Part 3. Extraction of lignin-carbohydrate complexes with neutral solvents. *Svensk Papperstidn*, **60**, 243-251.

Björkman, A., Person, B. 1957. Studies on finely divided wood Part 2. The properties of lignins extracted with neutral solvents from softwoods and hardwoods. *Svensk Papperstidn*, **60**, 158-169.

Bourke, J., Manley-Harris, M., Fushimi, C., Dowaki, K., Nunoura, T., Antal, M.J. 2007. Do all carbonized charcoals have the same chemical structure? 2. A model of the chemical structure of carbonized Charcoal. *Industrial & Engineering Chemistry Research*, **46**(18), 5954-5967.

Boutelje, J., Eriksson, I. 1984. Analysis of Lignin in Fragments from Thermomechanical Spruce Pulp by Ultraviolet Microscopy. *Holzforschung*, **38**(5), 249-252.

Brebu, M., Vasile, C. 2010. Thermal Degradation of Lignin - a Review. *Cellulose Chemistry and Technology*, **44**(9), 353-363.

Brewer, C.E., Schmidt-Rohr, K., Satrio, J.A., Brown, R.C. 2009. Characterization of Biochar from Fast Pyrolysis and Gasification Systems. *Environmental Progress & Sustainable Energy*, **28**(3), 386-396.

Bridgwater, A.V. 1984. *Thermochemical processing of biomass*. Butterworths, London ; Boston.

Britt, P.F., Buchanan, A.C., Cooney, M.J., Martineau, D.R. 2000. Flash vacuum pyrolysis of methoxy-substituted lignin model compounds. *Journal of Organic Chemistry*, **65**(5), 1376-1389.

Browning, B.L. 1967. *Methods of wood chemistry*. Interscience Publishers, New York,.

Butler, J.P., Czepiel, T.P. 1956. Determination of Phenolic Groups in Lignin Preparations - Titration with Potassium Methoxide Using Dimethylformamide as a Solvent. *Analytical Chemistry*, **28**(9), 1468-1472.

Chang, H.M., Allan, G.G. 1971. Oxidation. in: *Lignins: occurrence, formation, structure and reactions*, (Eds.) K.V. Sarkanen, C.H. Ludwig, John Wiley & Sons, Inc. New York.

Chang, H.M., Cowling, E.B., Brown, W., Adler, E., Miksche, G. 1975. Comparative Studies on Cellulolytic Enzyme Lignin and Milled Wood Lignin of Sweetgum and Spruce. *Holzforschung*, **29**(5), 153-159.

Cheng, C.H., Lehmann, J., Engelhard, M.H. 2008. Natural oxidation of black carbon in soils: Changes in molecular form and surface charge along a climosequence. *Geochimica Et Cosmochimica Acta*, **72**(6), 1598-1610.

Creighton, R.H.J., Gibbs, R.D., Hibbert, H. 1944. Studies on lignin and related compounds LXXV Alkaline nitrobenzene oxidation of plant materials and application to taxonomic classification. *J Am Chem Soc*, **66**, 32-37.

Czernik, S., Bridgwater, A.V. 2004. Overview of applications of biomass fast pyrolysis oil. *Energy & Fuels*, **18**(2), 590-598.

Dence, C.W., Lin, S.Y. 1992. *General structural features of lignin*. Springer-Verlag, Berlin.

Effland, M.J. 1977. Modified Procedure to Determine Acid-Insoluble Lignin in Wood and Pulp. *Tappi*, **60**(10), 143-144.

Ehrhardt, S.M. 1984. An investigation of the vibrational spectra of lignin model compounds, Vol. Ph. D., The Institute of Paper Chemistry. Appleton, Wisconsin.

Evans, R.J., Milne, T.A., Soltys, M.N. 1986. Direct Mass-Spectrometric Studies of the Pyrolysis of Carbonaceous Fuels .3. Primary Pyrolysis of Lignin. *Journal of Analytical and Applied Pyrolysis*, **9**(3), 207-236.

Faix, O. 1992. Fourier Transform Infrared Spectroscopy. in: *Methods in lignin chemistry*, (Eds.) S.Y. Lin, C.W. Dence, Springer-Verlag. Berlin ; New York, pp. 83-109.

Ferdous, D., Dalai, A.K., Bej, S.K., Thring, R.W. 2002. Pyrolysis of lignins: Experimental and kinetics studies. *Energy & Fuels*, **16**(6), 1405-1412.

Freudenb.K. 1965. Lignin - Its Constitution and Formation from P-Hydroxycinnamyl Alcohols. *Science*, **148**(3670), 595-&.

Fuji, K., Ichikawa, K., Node, M., Fujita, E. 1979. Hard Acid and Soft Nucleophile System - New Efficient Method for Removal of Benzyl Protecting Group. *Journal of Organic Chemistry*, **44**(10), 1661-1664.

Funaoka, M., Kako, T., Abe, I. 1990. Condensation of Lignin during Heating of Wood. *Wood Science and Technology*, **24**(3), 277-288.

Gellerstedt, G., Lindfors, E. 1984. Structural changes in lignins during kraft cooking. Part 4. Phenolic hydroxyl groups in wood and kraft pulps. *Svensk Papperstidn*, **87**, R115-R118.

Gellerstedt, G., Robert, D. 1987. Structural-Changes in Lignin during Kraft Cooking .7. Quantitative C-13 Nmr Analysis of Kraft Lignins. *Acta Chemica Scandinavica Series B-Organic Chemistry and Biochemistry*, **41**(7), 541-546.

Gierer, J. 1980. Chemical aspects of kraft pulping. *Wood Science and Technology*, **14**(4), 241-266.

Gierer, J. 1986. Chemistry of delignification. *Wood Science and Technology*, **20**(1), 1-33.

Gierer, J. 1985. Chemistry of delignification. *Wood Science and Technology*, **19**(4), 289-312.

Gierer, J., Lenz, B. 1965. Reaction of lignin during sulphate cooking. *Svensk Papperstidn*, **68**, 334-338.

Gierer, J., Lenz, G., Norrn, I., Srderberg, S. 1964. Reactions of lignin during sulfate cook. III. The splitting of aryl-alkyl ether bonds in milled wood lignin by alkali. *TAPPI*, **47**, 233-239.

Gierer, J., Lin, S.Y. 1972. Photodegradation of lignin. A contribution to the mechanism of chromophore formation. *Svensk Papperstidn*, **75**, 233-239.

Gierer, J., Noren, I. 1982. Oxidative Pretreatment of Pine Wood to Facilitate Delignification during Kraft Pulping. *Holzforschung*, **36**(3), 123-130.

Gil, A.M., Neto, C.P. 1999. Solid-state NMR studies of wood and other lignocellulosic materials. *Annual Reports on Nmr Spectroscopy, Vol 37*, **37**, 75-117.

Glasser, W.G., Glasser, H.R. 1974a. Simulation of Reactions with Lignin by Computer (Simrel) .1. Polymerization of Coniferyl Alcohol Monomers. *Macromolecules*, **7**(1), 17-27.

Glasser, W.G., Glasser, H.R. 1974b. Simulation of Reactions with Lignin by Computer (Simrel) .2. Model for Softwood Lignin. *Holzforschung*, **28**(1), 5-11.

Glasser, W.G., Glasser, H.R., Morohoshi, N. 1981. Simulation of Reactions with Lignin by Computer (Simrel) .6. Interpretation of Primary Experimental-Analysis Data (Analysis Program). *Macromolecules*, **14**(2), 253-262.

Glasser, W.G., Glasser, H.R., Nimz, H.H.H. 1976. Simulation of Reactions with Lignin by Computer (Simrel) .5. Non-Dehydrogenative Polymerization in Lignin Formation. *Macromolecules*, **9**(5), 866-867.

Goldschmid, O. 1954. Determination of Phenolic Hydroxyl Content of Lignin Preparations by Ultraviolet Spectrophotometry. *Analytical Chemistry*, **26**(9), 1421-1423.

Goldschmid, O. 1953. The Effect of Alkali and Strong Acid on the Ultraviolet Absorption Spectrum of Lignin and Related Compounds. *J Am Chem Soc*, **75**(15), 3780-3783.

Gosselink, R.J.A., de Jong, E., Guran, B., Abacherli, A. 2004. Co-ordination network for lignin - standardisation, production and applications adapted to market requirements (EUROLIGNIN). *Industrial Crops and Products*, **20**(2), 121-129.

Gosselink, R.J.A., Vandam, J.E.G., Zomers, F.H.A. 1995. Combined Hplc Analysis of Organic-Acids and Furans Formed during Organosolv Pulping of Fiber Hemp. *Journal of Wood Chemistry and Technology*, **15**(1), 1-25.

Goto, H., Koda, K., Matsumoto, Y., Meshitsuka, G. 2001. Precise determination of methoxyl content as an important indication of the extent of lignin oxidation remaining in bleached pulp. *Proceedings of 11th International Symposium on Wood and Pulping Chemistry*, **III**, 417-420.

Goto, H., Koda, K., Tong, G.L., Matsumoto, Y., Meshitsuka, G. 2005. Formation of methyl iodide from methoxyl-free compounds by hydriodic acid treatment. *Journal of Wood Science*, **51**(3), 312-314.

Gran, G. 1953. *An Investigation on the Determination of Methoxyl in Carbohydrate-containing Substances*. Haeggström.

Grønli, M.G., Varhegyi, G., Di Blasi, C. 2002. Thermogravimetric analysis and devolatilization kinetics of wood. *Industrial & Engineering Chemistry Research*, **41**(17), 4201-4208.

Hatakeyama, T., Nakamura, K., Hatakeyama, H. 1982. Studies on Heat-Capacity of Cellulose and Lignin by Differential Scanning Calorimetry. *Polymer*, **23**(12), 1801-1804.

Haw, J.F., Schultz, T.P. 1985. Carbon-13 CP/MAS NMR and FT-IR Study of Low-Temperature Lignin Pyrolysis. in: *Holzforschung - International Journal of the Biology, Chemistry, Physics and Technology of Wood*, Vol. 39, pp. 289.

Higuchi, T. 1971. Formation and Biological Degradation of Lignins. *Advances in Enzymology and Related Areas of Molecular Biology*, **34**, 207-&.

Hirata, T., Kawamoto, S., Nishimoto, T. 1991. Thermogravimetry of wood treated with water-insoluble retardants and a proposal for development of fire-retardant wood materials. *Fire and Materials*, **15**(1), 27-36.

Holtman, K.M., Chang, H.M., Jameel, H., Kadla, J.F. 2003. Elucidation of lignin structure through degradative methods: Comparison of modified DFRC and thioacidolysis. *Journal of Agricultural and Food Chemistry*, **51**(12), 3535-3540.

Hosoya, T., Kawamoto, H., Saka, S. 2007. Pyrolysis behaviors of wood and its constituent polymers at gasification temperature. *Journal of Analytical and Applied Pyrolysis*, **78**(2), 328-336.

Hosoya, T., Kawamoto, H., Saka, S. 2009. Role of methoxyl group in char formation from lignin-related compounds. *Journal of Analytical and Applied Pyrolysis*, **84**(1), 79-83.

Hu, J.L., Wang, Y., Cao, C.S., Elliott, D.C., Stevens, D.J., White, J.F. 2005. Conversion of Biomass syngas to DME using a microchannel reactor. *Industrial & Engineering Chemistry Research*, **44**(6), 1722-1727.

Hurff, S.J., Klein, M.T. 1983. Reaction Pathway Analysis of Thermal and Catalytic Lignin Fragmentation by Use of Model Compounds. *Industrial & Engineering Chemistry Fundamentals*, **22**(4), 426-430.

Irvine, G.M. 1984. The Glass Transitions of Lignin and Hemicellulose and Their Measurement by Differential Thermal-Analysis. *Tappi Journal*, **67**(5), 118-121.

Jakab, E., Faix, O., Till, F. 1997. Thermal decomposition of milled wood lignins studied by thermogravimetry mass spectrometry. *Journal of Analytical and Applied Pyrolysis*, **40-1**, 171-186.

Jiang, G.Z., Nowakowski, D.J., Bridgwater, A.V. 2010. A systematic study of the kinetics of lignin pyrolysis. *Thermochimica Acta*, **498**(1-2), 61-66.

Kadla, J.F., Kubo, S., Venditti, R.A., Gilbert, R.D., Compere, A.L., Griffith, W. 2002. Lignin-based carbon fibers for composite fiber applications. *Carbon*, **40**(15), 2913-2920.

Katahira, R., Nakatsubo, F. 2001. Determination of nitrobenzene oxidation products by GC and H-1-NMR spectroscopy using 5-iodovanillin as a new internal standard. *Journal of Wood Science*, **47**(5), 378-382.

Kawamoto, H., Horigoshi, S., Saka, S. 2007. Pyrolysis reactions of various lignin model dimers. *Journal of Wood Science*, **53**(2), 168-174.

Laborie, M.P.G., Salmen, L., Frazier, C.E. 2004. Cooperativity analysis of the in situ lignin glass transition. *Holzforschung*, **58**(2), 129-133.

Lai, Y.Z., Guo, X.P., Situ, W. 1990. Estimation of Phenolic Hydroxyl-Groups in Wood by a Periodate-Oxidation Method. *Journal of Wood Chemistry and Technology*, **10**(3), 365-377.

Lin, L.Z., Yoshioka, M., Yao, Y.G., Shiraishi, N. 1997. Liquefaction mechanism of lignin in the presence of phenol at elevated temperature without catalysts - Studies on beta-O-4 lignin model compound .2. Reaction pathway. *Holzforschung*, **51**(4), 325-332.

Lin, Y.C., Cho, J., Tompsett, G.A., Westmoreland, P.R., Huber, G.W. 2009. Kinetics and Mechanism of Cellulose Pyrolysis. *Journal of Physical Chemistry C*, **113**(46), 20097-20107.

Lora, J.H., Glasser, W.G. 2002. Recent industrial applications of lignin: A sustainable alternative to nonrenewable materials. *Journal of Polymers and the Environment*, **10**(1-2), 39-48.

Lundquist, K. 1992. Proton (^{1}H) NMR Spectroscopy. in: *Methods in lignin chemistry*, (Eds.) S.Y. Lin, C.W. Dence, Springer-Verlag. Berlin ; New York, pp. 242.

Luo, Y.-R. 2007. *Comprehensive handbook of chemical bond energies*. CRC Press, Boca Raton.

Mao, J.D., Schmidt-Rohr, K. 2004. Accurate quantification of aromaticity and nonprotonated aromatic carbon fraction in natural organic matter by C-13 solid-state nuclear magnetic resonance. *Environmental Science & Technology*, **38**(9), 2680-2684.

Mcdermott, J.B., Klein, M.T., Obst, J.R. 1986. Chemical Modeling in the Deduction of Process Concepts - a Proposed Novel Process for Lignin Liquefaction. *Industrial & Engineering Chemistry Process Design and Development*, **25**(4), 885-889.

Meshitsuka, G., Nakano, J. 1985. Structural Characteristics of Compound Middle Lamella Lignin. *Journal of Wood Chemistry and Technology*, **5**(3), 391-404.

Militz, H., Tjeerdsma, B.F. 2001. Heat treatment of wood by the PLATO-process. *COST ACTION E22-Environmental optimisation of wood protection*, Proceedings of Special Seminar in Antibes, France.

Milosavljevic, I., Suuberg, E.M. 1995. Cellulose Thermal-Decomposition Kinetics - Global Mass-Loss Kinetics. *Industrial & Engineering Chemistry Research*, **34**(4), 1081-1091.

Mok, W.S.L., Antal, M.J., Szabo, P., Varhegyi, G., Zelei, B. 1992. Formation of Charcoal from Biomass in a Sealed Reactor. *Industrial & Engineering Chemistry Research*, **31**(4), 1162-1166.

Muller-Hagedorn, M., Bockhorn, H., Krebs, L., Muller, U. 2003. A comparative kinetic study on the pyrolysis of three different wood species. *Journal of Analytical and Applied Pyrolysis*, **68-9**, 231-249.

Munasinghe, P.C., Khanal, S.K. 2010. Biomass-derived syngas fermentation into biofuels: Opportunities and challenges. *Bioresource Technology*, **101**(13), 5013-5022.

Nakamura, T., Kawamoto, H., Saka, S. 2007. Condensation reactions of some lignin related compounds at relatively low pyrolysis temperature. *Journal of Wood Chemistry and Technology*, **27**(2), 121-133.

Nimz, H. 1974. Beech Lignin - Proposal of a Constitutional Scheme. *Angewandte Chemie-International Edition in English*, **13**(5), 313-321.

Node, M., Hori, H., Fujita, E. 1976. Demethylation of Aliphatic Methyl Ethers with a Thiol and Boron-Trifluoride. *Journal of the Chemical Society-Perkin Transactions 1*(20), 2237-2240.

Obst, J.R., Landucci, L.L. 1986. Quantitative C-13 Nmr of Lignins - Methoxyl-Aryl Ratio. *Holzforschung*, **40**, 87-92.

Obst, J.R., Sachs, I.B., Kuster, T.A. 1988. The Quantity and Type of Lignin in Tyloses of Bur Oak (Quercus-Macrocarpa). *Holzforschung*, **42**(4), 229-231.

Olivares, M., Guzman, J.A., Natho, A., Saavedra, A. 1988. Kraft Lignin Utilization in Adhesives. *Wood Science and Technology*, **22**(2), 157-165.

Park, J., Meng, J., Lim, K.H., Rojas, O.J., Park, S. 2013. Transformation of lignocellulosic biomass during torrefaction. *Journal of Analytical and Applied Pyrolysis*, **100**(0), 199-206.

Pearl, I.A. 1967. *The chemistry of lignin*. Dekker, New York.

Peng, Y.Y., Wu, S.B. 2010. The structural and thermal characteristics of wheat straw hemicellulose. *Journal of Analytical and Applied Pyrolysis*, **88**(2), 134-139.

Pew, J.C. 1957. Properties of powdered wood and isolation of lignin by cellulytic enzymes. *TAPPI*, **40**, 553-558.

Pew, J.C., Weyna, P. 1962. Fine grinding, enzyme digestion, and the lignin-cellulose bond in wood. *Tappi Journal*, **45**, 247-256.

Piskorz, J., Radlein, D., Scott, D.S. 1986. On the Mechanism of the Rapid Pyrolysis of Cellulose. *Journal of Analytical and Applied Pyrolysis*, **9**(2), 121-137.

Pouwels, A.D., Tom, A., Eijkel, G.B., Boon, J.J. 1987. Characterization of Beech Wood and Its Holocellulose and Xylan Fractions by Pyrolysis-Gas Chromatography-Mass Spectrometry. *Journal of Analytical and Applied Pyrolysis*, **11**, 417-436.

Ramiah, M.V. 1970. Thermogravimetric and Differential Thermal Analysis of Cellulose, Hemicellulose, and Lignin. *Journal of Applied Polymer Science*, **14**(5), 1323-&.

Robert, D. 1992. Carbon-13 Nuclear Magnetic Resonance Spectroscopy. in: *Methods in lignin chemistry*, (Eds.) S.Y. Lin, C.W. Dence, Springer-Verlag. Berlin ; New York, pp. 250 p.

Sada, E., Kumazawa, H., Kudsy, M. 1992. Pyrolysis of Lignins in Molten-Salt Media. *Industrial & Engineering Chemistry Research*, **31**(2), 612-616.

Sarkanen, K.V., Ludwig, C.H. 1971. *Lignins: occurrence, formation, structure and reactions*. John Wiley & Sons, Inc., New York.

Schaefer, J., Stejskal, E.O. 1976. Carbon-13 nuclear magnetic resonance of polymers spinning at the magic angle. *J Am Chem Soc*, **98**(4), 1031-1032.

Shafizadeh, F., Bradbury, A.G.W. 1979. Thermal-Degradation of Cellulose in Air and Nitrogen at Low-Temperatures. *Journal of Applied Polymer Science*, **23**(5), 1431-1442.

Sharma, R.K., Wooten, J.B., Baliga, V.L., Lin, X.H., Chan, W.G., Hajaligol, M.R. 2004. Characterization of chars from pyrolysis of lignin. *Fuel*, **83**(11-12), 1469-1482.

Shen, D.K., Gu, S. 2009. The mechanism for thermal decomposition of cellulose and its main products. *Bioresource Technology*, **100**(24), 6496-6504.

Simpson, M.J., Hatcher, P.G. 2004. Determination of black carbon in natural organic matter by chemical oxidation and solid-state C-13 Nuclear Magnetic Resonance spectroscopy. *Organic Geochemistry*, **35**(8), 923-935.

Sivonen, H., Maunu, S.L., Sundholm, F., Jamsa, S., Viitaniemi, P. 2002. Magnetic resonance studies of thermally modified wood. *Holzforschung*, **56**(6), 648-654.

Sjöström, E. 1993. *Wood Chemistry: Fundamentals and Applications (2nd edition)*. Academic Press, Inc., San Diego, CA.

Smernik, R.J., Oades, J.M. 2000. The use of spin counting for determining quantitation in solid state C-13 NMR spectra of natural organic matter 2. HF-treated soil fractions. *Geoderma*, **96**(3), 159-171.

Soltes, E.J., Elder, T.J. 1981. Pyrolysis. in: *Organic Chemicals from Biomass*, (Ed.) I.S. Goldstein, CRC Press. Boca Raton, FL, pp. 63.

Sudo, K., Shimizu, K., Sakurai, K. 1985. Characterization of Steamed Wood Lignin from Beech Wood. *Holzforschung*, **39**(5), 281-288.

Tang, M.M., Bacon, R. 1964. Carbonization of Cellulose Fibers .1. Low Temperature Pyrolysis. *Carbon*, **2**(3), 211-&.

TAPPI. 1972. TAPPI Test Method T 209 su-72: Methoxyl content of pulp and wood.

TAPPI. 2002. TAPPI Test Method T 222 om-02: Acid-insoluble lignin in wood and pulp.

Tijmensen, M.J.A., Faaij, A.P.C., Hamelinck, C.N., van Hardeveld, M.R.M. 2002. Exploration of the possibilities for production of Fischer Tropsch liquids and power via biomass gasification. *Biomass & Bioenergy*, **23**(2), 129-152.

Tjeerdsma, B.F., Militz, H. 2005. Chemical changes in hydrothermal treated wood: FTIR analysis of combined hydrothermal and dry heat-treated wood. *Holz Als Roh-Und Werkstoff*, **63**(2), 102-111.

Tjeerdsma, B.F., Stevens, M., Militz, H. 2000. Durability aspects of hydrothermal treated wood. International Research Group on Wood Preservation.

Vanderhage, E.R.E., Mulder, M.M., Boon, J.J. 1993. Structural Characterization of Lignin Polymers by Temperature-Resolved in-Source Pyrolysis Mass-Spectrometry and

Curie-Point Pyrolysis-Gas Chromatography Mass-Spectrometry. *Journal of Analytical and Applied Pyrolysis*, **25**, 149-183.

Waksman, S.A., Smith, H.W. 1934. Transformation of the methoxyl group in lignin in the process of decomposition of organic residues by microorganisms. *J Am Chem Soc*, **56**, 1225-1229.

Watanabe, T., Kawamoto, H., Saka, S. 2009. Radical chain reactions in pyrolytic cleavage of the ether linkages of lignin model dimers and a trimer. *Holzforschung*, **63**(4), 424-430.

Whetten, R.W., MacKay, J.J., Sederoff, R.R. 1998. Recent advances in understanding lignin biosynthesis. *Annual Review of Plant Physiology and Plant Molecular Biology*, **49**, 585-609.

Whiting, P., Favis, B.D., St-germain, F.G.T., Goring, D.A.I. 1981. Fractional Separation of Middle Lamella and Secondary Wall Tissue From Spruce Wood. *Journal of Wood Chemistry and Technology*, **1**(1), 29-42.

Whiting, P., Goring, D.A. 1982. Phenolic hydroxyl analysis of lignin by pyrolytic gas chromatography. *Paper, PUU*, **64**, 592-599.

Wikberg, H., Maunu, S.L. 2004. Characterisation of thermally modified hard- and softwoods by C-13 CPMAS NMR. *Carbohydrate Polymers*, **58**(4), 461-466.

Williams, P.T., Besler, S. 1996. The influence of temperature and heating rate on the slow pyrolysis of biomass. *Renewable Energy*, **7**(3), 233-250.

Windeisen, E., Wegener, G. 2008. Behaviour of lignin during thermal treatments of wood. *Industrial Crops and Products*, **27**(2), 157-162.

Wu, W.X., Yang, M., Feng, Q.B., McGrouther, K., Wang, H.L., Lu, H.H., Chen, Y.X. 2012. Chemical characterization of rice straw-derived biochar for soil amendment. *Biomass & Bioenergy*, **47**, 268-276.

Yang, H.P., Yan, R., Chen, H.P., Lee, D.H., Zheng, C.G. 2007. Characteristics of hemicellulose, cellulose and lignin pyrolysis. *Fuel*, **86**(12-13), 1781-1788.

Yang, J.M., Goring, D.A.I. 1980. The Phenolic Hydroxyl Content of Lignin in Spruce Wood. *Canadian Journal of Chemistry-Revue Canadienne De Chimie*, **58**(23), 2411-2414.

Yoshihara, K., Kobayashi, T., Akamatsu, I. 1984. A novel modification of Klason lignin quantitative method. *JAPAN TAPPI JOURNAL*, **38**, 86-95.

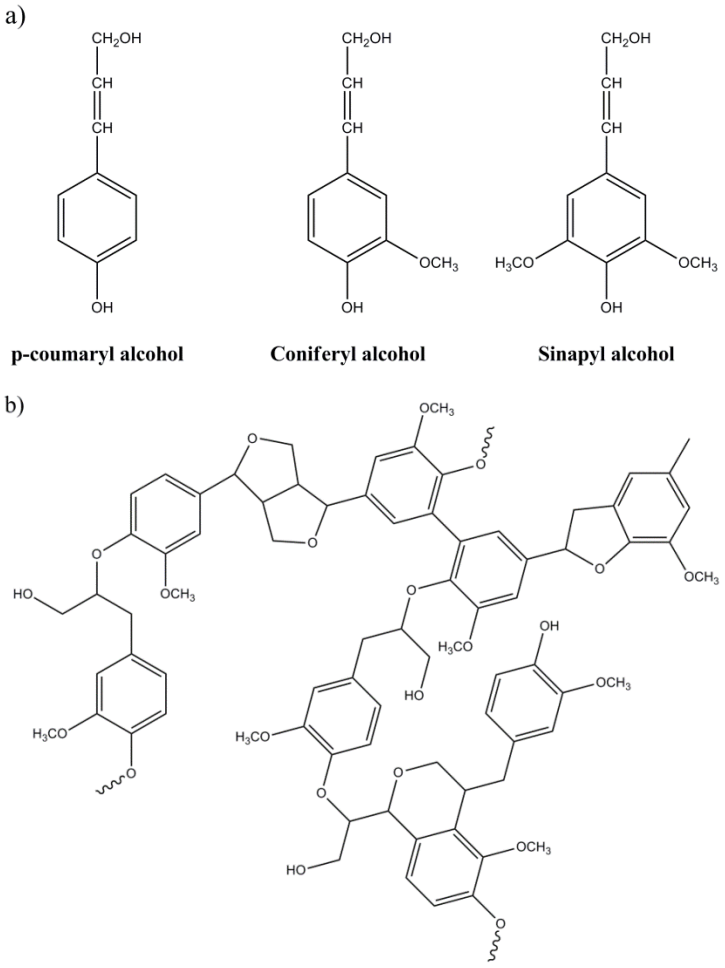

Figure 1. (a) Three monolignols : p-coumaryl, coniferyl, sinapyl alcohols; (b) A partial structural model for lignin.

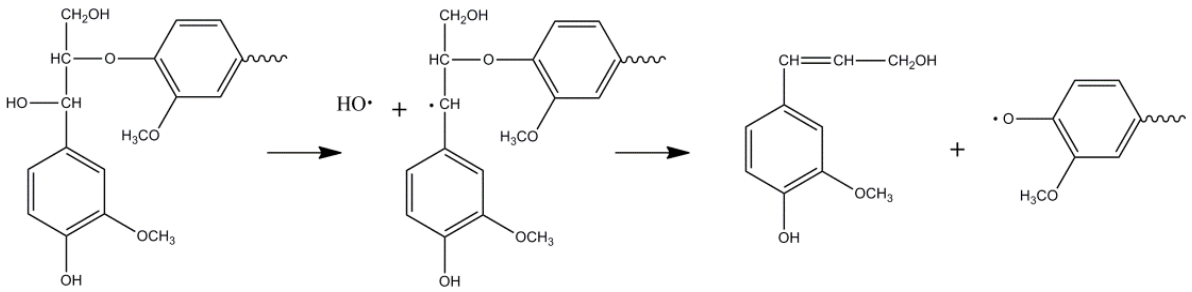

Figure 2. Proposed model for the cleavage of aryl-ether (β-O-4) linkages in lignin model compound (Evans et al., 1986).

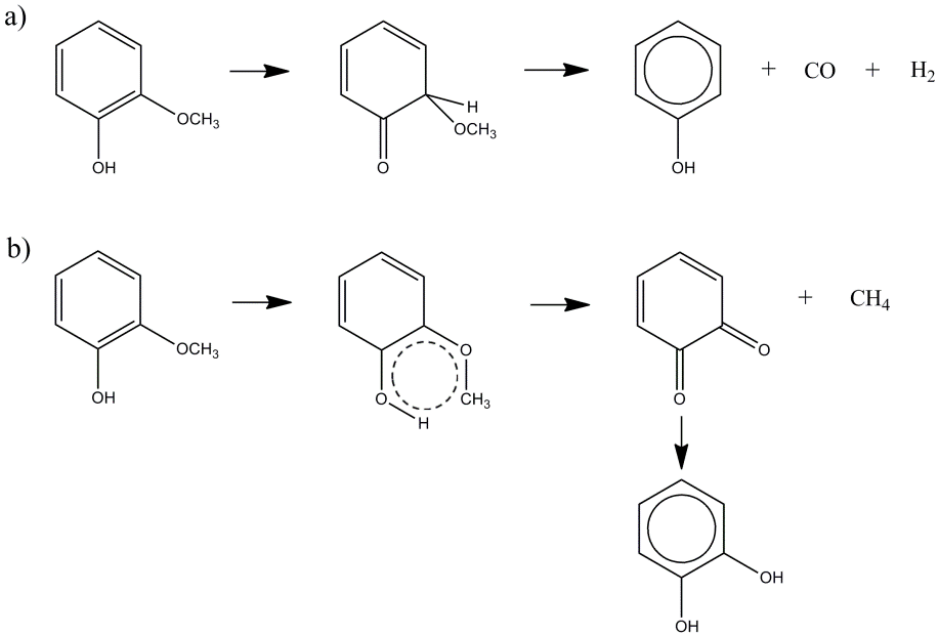

Figure 3. Proposed model for (a) demethoxylation and (b) demethylation of a model compound, guaiacol (Klein, 1981).

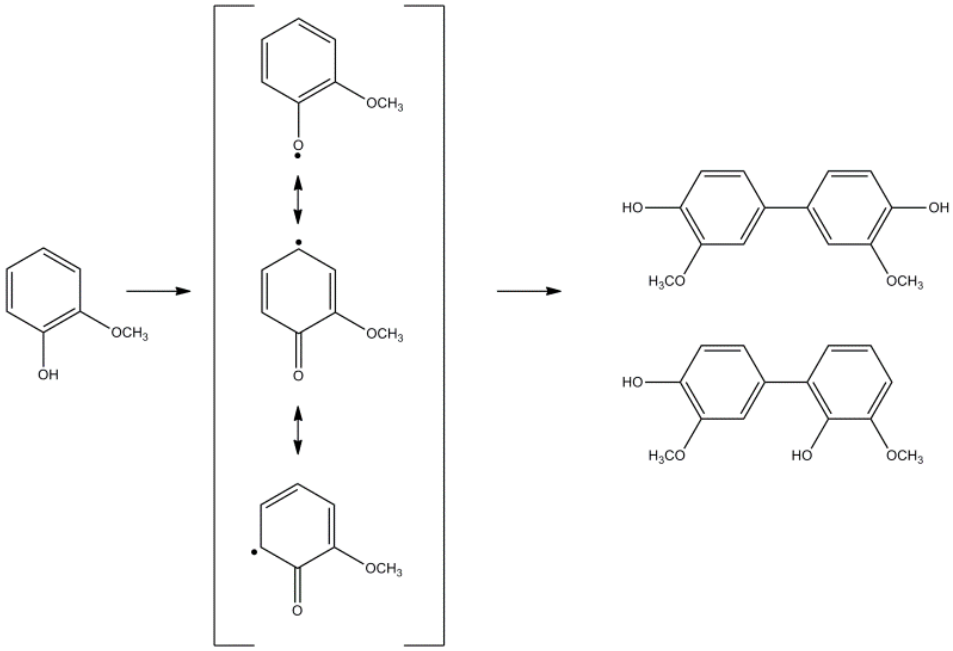

Figure 4. Thermal condensation (dimerization) of a model compound, guaiacol (Nakamura et al, 2007).

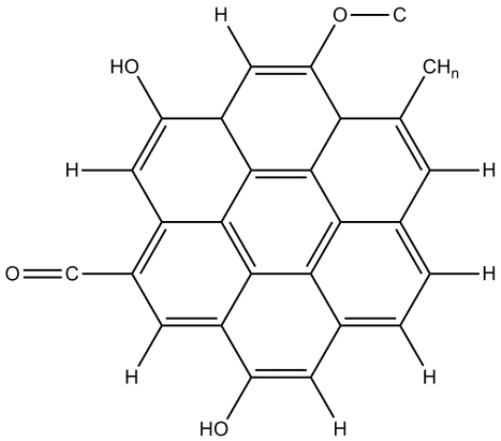

Figure 5. Aromatic cluster in pyrolysis char from switchgrass, derived from NMR (Brewer et al., 2009).

CHAPTER 2

Transformation of Lignocellulosic Biomass during Torrefaction

1. Introduction

Torrefaction is a relatively mild thermochemical process that uses low temperature (200 ~ 300 °C) and inert gas atmosphere to produce homogeneous solid fuels with higher hydrophobicity and lower oxygen content relative to the feed biomass. The main fiber cell-wall components (cellulose, hemicelluloses, and lignin) present in the biomass undergo different chemical transformations because of their distinct chemical and thermal reactivity during torrefaction (Shafizadeh, 1985). It has been reported that compared to cellulose and lignin fractions, most of the hemicelluloses degrade into volatile components at low torrefaction temperatures (Peng & Wu, 2010; Soltes & Elder, 1981). Due to the fuel value of torrefied biomass, it has been used as replacement of coal, in co-combustion with other fuels, and in the production of pellets or briquettes (Lipinsky et al., 2002; Pach, 2002). Recently, torrefaction has received renewed interest as thermochemical processes are further investigated for the production of solid fuels from different raw materials and under optimized conditions.

The evaluation of torrefied biomass as an enhanced solid fuel is mandatory prior to any application and therefore several methods have been applied within the fields of wood and fuel sciences and industries. Common analyses include wet-chemistry methods for

identifying wood composition (cellulose, hemicelluloses, and lignin) in lignocellulosic biomass (Bridgeman et al., 2008; Phanphanich & Mani, 2011; Sluiter et al., 2008), and proximate/ultimate analyses (volatile matter, fixed carbon, ash content, and elemental CHN). These methods have also been generally applied in coal assays (Deng et al., 2009; Pentananunt et al., 1990). In addition, the amount of energy required for grinding (Arias et al., 2008; Repellin et al., 2010), mass/energy balances (Deng et al., 2009; Prins et al., 2006; Yan et al., 2010), hydrophobicity (Acharjee et al., 2011; Yan et al., 2010), and combustion analyses (Bridgeman et al., 2008; Pimchuai et al., 2010) have been used to evaluate processability as solid fuels.

Furthermore, there have been multiple efforts to investigate the fundamental mechanism of the thermal alteration of lignocellulosic biomass. Spectroscopic analyses such as FTIR or NMR are usually employed for analyzing chars from biomass. For example, FTIR can indicate relative changes in spectrum and assess changes in functional groups and chemical bonding in solid samples (Cheng et al., 2006; Sharma et al., 2004). Solid-state NMR spectroscopy is a powerful tool for structural analysis of solid biomass. For example, ^{13}C CP/MAS (cross polarization/magic angle spinning) NMR spectroscopy has been applied to thermally modified biomass (Wikberg & Maunu, 2004) to indicate the increased crystallinity of treated samples. This observation has been ascribed to the thermal degradation of less ordered domains rich in hemicelluloses and amorphous cellulose.

The cleavage of β-O-4 linkages and condensation of lignin structures have been suggested after comparison of the spectra from untreated and thermally-treated spruce samples. Sharma and co-workers used ^{13}C CP/MAS NMR to show the loss of lignin

substructure and increased aromaticity of pyrolized lignin, which was transformed to char-like structures from biomass (Sharma et al., 2004). Recently, it was shown that more quantitative analyses of biochar are possible by using direct polarization and magic angle spinning (DP/MAS) ^{13}C NMR (Brewer et al., 2009; Brewer et al., 2011); as a consequence, biomass models for fused aromatic ring cluster have been proposed. The techniques discussed above have been generally used for studying biochar, which is highly homogeneous, but rarely applied to torrefied biomass which is a more complex and heterogeneous material in its composition. In fact, despite its reported use since early 1980's, details about the thermal and chemical transformations that occur during torrefaction are still not well understood.

In this study, we characterized torrefied biomass by combining different chemical and structural approaches. Conventional methods were used to quantify the compositional changes of biomass fractions undergoing thermal transformation. In addition, we applied complementary methods to gain information on structural alteration. This included changes in methoxyl functional groups and spectroscopic fingerprints obtained by solid-state DP/MAS NMR spectroscopy. To the best of our knowledge, these methods have not been applied to torrefied biomass. From these observations, it was possible to reveal the principal chemical changes that occurred in lignocellulosic biomass during torrefaction and to shed new light to further related applications.

2. Material and Methods

2.1. *Sample production*

Loblolly pine chips (about 15 mm × 6 mm) containing bark were obtained from a local wood product industry and were torrefied using a pilot-scale torrefaction unit (about 1 ton/day capacity), which was installed in North Carolina State University (Lake Wheeler Road Field Laboratory, Raleigh, NC). Three torrefied samples with different treatment temperatures (270, 300, and 330 °C) and residence time of 2.5 minutes were prepared and named as lightly (TA), moderately (TB), and severely (TC) torrefied biomass. Untorrefied biomass is indicated as "Raw" biomass for short. The weight loss of biomass during torrefaction was estimated using a linear correlation (R^2=0.997) between the weight loss and the atomic O/C ratio, developed from lab-scale experiments with a tube furnace. The correlation was measured within the temperature range of 200 ~ 500 °C with seven data points. All samples were milled to 40 ~ 60 mesh using a Willey mill, and stored in an air-tightened plastic bag at 4 °C before further analyses.

2.2. *Ultimate and proximate analysis, heating value measurement*

Carbon, hydrogen, and nitrogen content in the samples were analyzed by using PerkinElmer 2400 Series II Elemental Analyzer (PerkinElmer, Waltham, MA). Oxygen content was calculated by subtraction of the ash and the CHN content from the total. Proximate analysis was conducted according to ASTM standard method D5142-09 (ASTM, 2009) with the following adaptations. For ash determination, the leftover solid after volatile matter determination from the standard method was heated to 750 °C for 6 hrs without cover

under atmospheric condition, then cooled in a desiccator to minimize moisture absorption, and weighed to determine the ash content. Both ultimate and proximate analyses were performed at least by duplicate. Heating values were measured using 1341 Oxygen Bomb Calorimeter (Parr Instrument Company, Moline, IL). About 10 mg of sample was loaded into the apparatus and combusted under oxygen atmosphere and the temperature rise recorded at 1-min intervals to calculate the higher heating value (HHV) for each sample.

2.3. *Compositional Analysis*

Structural carbohydrates – cellulose and hemicelluloses – were measured by HPLC sugar analysis after two-step acid hydrolysis (Sluiter et al., 2008). Acid soluble/insoluble lignin content was measured using a modified Klason lignin analysis (Yeh et al., 2004). Based on the calculated weight loss and compositional analysis of the torrefied biomass, the extent of mass reduction for glucan, other polysaccharides, and acid-insoluble residue from the Klason lignin method was determined.

2.4. *Thermogravimetric Analysis (TGA)*

The thermal behaviors of the samples (about 10 mg of milled wood per run) were investigated using a TGA Q500 (TA Instruments, New Castle, DE). The heating program consisted on a 5-min hold at 30°C, ramp up to 900°C at a heating rate of 10 °C/min, and then the weight difference was recorded as a function of temperature profile. Nitrogen was used as purging gas at a flow rate of 100 ml/min.

2.5. *FTIR Spectroscopy*

FTIR analyses were performed with a Nexus 470 instrument (Thermo Scientific, Waltham, MA) using potassium bromide (KBr) pellets with 1 % (w/w) dried samples. Each spectrum was recorded after 64 scans in the wavenumber range from 4000 to 650 cm^{-1}. Background spectra were collected before every measurement. KBr was oven-dried before making the pellets to reduce interferences from water.

2.6. *Quantification of Methoxyl Groups*

Methoxyl group content was measured by the GC quantification method (Baker, 1996). Briefly, 20 mg of milled and dried samples were dispersed in 5 mL 57 % hydriodic acid at 130 °C for 30 min with frequent agitation. Following, 10 mL of n-pentane was added with a known concentration of an internal standard, ethyl iodide. After dissolution of the generated methyl iodide in the pentane solvent, the liquid was analyzed in a gas chromatograph instrument (Hewlett Packard HP 5890, Agilent Technologies) equipped with a flame ionization detector, using with DB-WAX column (40 m x 0.18 mm i.d. x 0.3 μm; Agilent Technologies Inc., CA, USA).Temperature for injector and detector was set to 110 and 150 °C, respectively. Oven temperature was isothermal at 80 °C, and total run time was 7 min.

2.7. *Solid-state NMR*

The solid-state magic angle spinning (MAS) NMR spectra were acquired with a Varian 3.2 mm MAS probe, on a Varian Inova 500 spectrometer. A spinning speed of 7 kHz

and a contact time of 1 ms were used for cross-polarization (CP) MAS NMR experiments. In order to remove spinning sidebands, the four-pulse total suppression of sidebands (TOSS) was applied before detection, and 1,000 – 2,000 FID (free induction decay) signals were accumulated with an acquisition delay of 2 s. For the direct-polarization (DP) MAS experiments, the sample was spun at a higher frequency of 14 kHz and the TOSS pulse sequence was not used. A dephasing time of 68 μs was used for dipolar dephasing experiments to determine the non-protonated aromatic carbon fraction (Brewer et al., 2009; Brewer et al., 2011). For the quantitative DP NMR experiments, 1,000 – 2,000 FIDs were collected with a long acquisition delay of 60 s. The 90° pulse-lengths for ^{1}H and ^{13}C were 3.0 μs and 2.7 μs, respectively. The two-pulse phase-modulated (TPPM) decoupling scheme was employed with radio-frequency field strength of 80 kHz. Quantitative spectral analysis was performed by integrating the assigned area of DP NMR spectra and fractionating into three major categories – carbonyl, aromatic, and alkyl carbon fractions (Brewer et al., 2009). Quantification for corresponding non-protonated aromatic carbon fraction was carried out in the same manner using DP NMR spectra with dipolar dephasing.

3. Results and Discussion

3.1. *Proximate and ultimate analysis*

The basic compositional analysis of the feedstock material and the torrefied biomass is presented in Table 1. Thermal breakdown and release of volatile matter is expected to be mainly from the carbohydrate fractions, especially hemicelluloses, the content of which

decreased from approximately 85 to 60% after the most severe torrefaction condition at 330 °C (TC). Due to the degradation of volatilized matter, residual ash was accumulated after torrefaction at increased levels (from TA to TC). In addition, the content of fixed carbon increased with the severity of the torrefaction conditions. Ultimate analysis data showed large reductions in oxygen content after torrefaction. High oxygen content is a distinctive characteristic of biomass compared to that of other fuels. The significant decrease of oxygen content can be explained by dehydration reaction, which generates water vapor as a product. Furthermore, the loss of volatile organic products and their release as gases (mostly of CO and CO_2) were also responsible for the decrease of oxygen in the solid phase. The amount of hydrogen also decreased along with the loss of volatile/gaseous products and water. Due to the loss of oxygen and hydrogen, the carbon content experienced a relatively important increase, from approximately 51 to 66%, equivalent to a change in atomic O/C ratio from 0.63 to 0.31 after torrefaction. This substantial changes in elemental analysis showed that the torrefied biomass is getting close to lignite on the Van Krevelen diagram (Bridgeman et al., 2008; Rousset et al., 2011), and its HHV is also comparable with that of lignite (Pimchuai et al., 2010).

3.2. *Compositional analysis*

In this study, the compositional changes were monitored by quantification of each component, as indicated in Table 2. The fraction of each component in the untorrefied as well as the torrefied samples are presented based on 100 g of the initial biomass. Compared to the untorrefied biomass (Raw), the content of glucans and other carbohydrates in the

highly-torrefied sample (TC) were reduced by approximately 74 and 97%, respectively. It has been widely accepted that the carbohydrate fraction, especially hemicelluloses, are more easily degraded by thermal treatment. By comparing the untorrefied biomass with that after a light torrefaction (TA), there is evidence that hemicelluloses degraded more rapidly than cellulose.

The amount of the solid residues after acid hydrolysis, expressed as Klason lignin, increased with torrefaction. In the Klason lignin analysis, highly-concentrated sulfuric acid (72 %) swells the carbohydrate structure, and the dilute acid hydrolysis at high temperature that follows degrades glycosidic bonds of the carbohydrates, converting them into monomeric sugars and leaving an acid-insoluble fraction as Klason lignin. If the solid residue after the acid hydrolysis represents the actual lignin content in the biomass, the amount of residues in the torrefied samples should decrease or become close to the initial amount, compared to that from untorrefied material. It was observed that the amount of acid-insoluble residue increased from approximately 30 to 38 g for the Raw and TC samples, respectively (Table 2). This observation might indicate the formation of condensed structures into thermally degraded/modified products. As the severity of torrefaction increases, the heat energy may induce the formation of acid-resistant linkages between products, e.g. carbon-carbon bonds, resulting in an increased amount of acid-insoluble residue. For example, Pastorova and coworkers reported that, when a microcrystalline cellulose (Avicel) was pretreated under inert atmosphere for 2.5 hours at 270 °C, it showed 40 % of weight loss, and only 13% of glucose can be recovered from the char by sulfuric acid hydrolysis. And, over 290 °C, glucose recovery was below 3% (Pastorova et al., 1993). This implies that the loss

of glycosidic bonds in cellulose structure and the formation of acid-resistant condensed solid products, induced by thermal treatment. Hence, it is expected that a close correlation exists between the amount of residue and the formation of condensed structures during torrefaction.

3.3. *Thermogravimetric analysis*

Figure 1 shows the thermograms of torrefied woods. One distinct difference from the weight loss curves is that the char amount, which is defined as the % residue left in the TGA pan after analysis, was substantially increased with the severity of torrefaction, from Raw to TC samples. The opposite trend was observed for the volatile matters released during the heating process, consistent with the proximate data discussed previously. No significant differences in peak temperatures were observed from the derivative thermogravimetry (DTG) curves. Thermal degradation of cellulose generally occurred between 300 ~ 400 °C in TGA (Yang et al., 2007). It was reported that the DTG peak of cellulose can be shifted by structural changes of cellulose quantifiable by the crystallinity index, crystallite size, and degree of polymerization (Kim et al., 2010). Hence, the almost identical peak position between the samples might indicate that the structural characteristic of cellulose fraction was preserved even after the torrefaction condition for TC sample that resulted in a degraded material with half its original weight. Other features observed in the DTG curves are the small and wide bumps placed around at 200 °C ("a" in Fig. 1) just before the major DTG peak, and the shoulder at 340 ~ 350 °C ("b" in Fig. 1) on the major DTG peak. The former might be ascribed to thermal degradation of low-molecular weight, volatile products. These products were likely to be released as gases during treatment, but considerable amounts are

expected to be remained in the residual solid by re-condensation and/or entrapment. The shoulder at 340 ~ 350 °C ("b") observed in the DTG of the untorrefied sample has been reported from the degradation of hemicelluloses in lignocellulosic biomass (Carrier et al., 2011; Grønli et al., 2002). Hemicelluloses are less thermally stable than cellulose, since they are more susceptible to hydrolysis and dehydration reactions (Balat, 2008). Due to the degradation of hemicelluloses, DTG curves of TA and TB samples showed shoulders smaller than those of the Raw sample. In the thermogram for TC, identification is less clear, which is ascribed to the more limited presence of hemicelluloses in this fraction, as indicated in the compositional analyses (Table 2). In addition, the relative difference between the DTG peak area reflects the changes of the carbohydrates fractions in the torrefied wood – smaller peaks as the severity of torrefaction is increased.

3.4. *FTIR (Fourier Transform Infrared) Spectroscopy*

FTIR spectroscopy was used to investigate the changes in chemical structure after torrefaction (Figure 2). The spectra of Raw, TA, and TB samples were similar, but the spectrum collected for TC sample was distinguishable. The peak around 1740 cm^{-1} ("a" in Fig. 2) corresponds to carbonyl group in samples (Faix, 1992; Pandey & Theagarajan, 1997), and that for TC might be due to the removal of ester group in hemicelluloses which is caused by deacetylation during thermal treatment (Carrasco & Roy, 1992). It has been also reported that the reduction of the intensity of the peak at 1740 cm^{-1} was observed during the hydrothermal treatment of wood samples (Tjeerdsma & Militz, 2005). The peak at 1700 cm^{-1} ("b"), together with the peak at 1600 (left peak of "C"), were for C=O and C=C stretching

vibrations, which can be from ketones, aldehydes, esters, carboxyl groups, and aromatic structures (Chen et al., 2008; Guo & Bustin, 1998; Keiluweit et al., 2010). The increased intensity of this peak indicates that the degradation of carbohydrates and the relative increase of lignin result in more intense C=O absorptions (1700 cm^{-1}) as the severity of torrefaction increases (from Raw to TC). The substantial intensity increase at 1600 and 1511 cm^{-1} ("c"), as well as at 1268 cm^{-1} ("d"), can be ascribed to aromatic skeletal vibrations and guaiacyl ring with C–O stretch, and it implies an increase of aromatic fraction by thermal modification. In addition, the peak at 1600 cm^{-1} ("c") could also indicate that in torrefied biomass more condensed guaiacyl units are present relative to etherified ones (Faix, 1992). This supports the assumption that thermal treatment induces the cleavage of ether bond in lignin (mainly, β-O-4 structure) and the condensation of lignin by linking carbons directly (*e.g.*, 5-5 coupling). The increasing peak shoulder at about 1221 cm^{-1} ("e") corresponds to more condensed guaiacyl units. The increased intensity of FTIR signal from aromatic and condensed structure is in good agreement with the compositional data presented before, which showed larger amounts of acid-insoluble residues in TC sample. The assigned bands around 1030 ~ 1060 cm^{-1} ("f") with highest intensities correspond to aliphatic C-O-C and C-OH in alcohol, which is mainly from cellulose in the samples (Chen et al., 2008; Guo & Bustin, 1998). In this range, TC sample showed lower absorbance, indicating the loss of the carbohydrate fractions.

3.5. *Quantification of methoxyl group content by gas chromatography*

From the previous discussion, it can be suggested that the lignin fraction is thermally modified during the torrefaction process by way of cleavage of aryl ether linkages (*e.g.*, β-O-4) and condensation-like reactions. The β-O-4 linkage has an important role in the polymeric lignin structure. Compared to softwoods, hardwoods have a higher β-O-4 content, and lower condensed structures. This is due to the fact that hardwood lignin contains more syringyl units, carrying two methoxyl groups. This implies that the free C5 position is important in the production of condensed lignin structures. In this study, it was assumed that thermal condensation of lignin is accompanied by the loss of methoxyl groups, and thus it is possible to quantify the extent of lignin modification by measuring the extent of demethoxylation. Lignin in softwood, such as loblolly pine, contains primarily guaiacyl (3-methoxy-4-hydroxyphenyl) structures. Thermal modification of lignocellulosic biomass can induce the cleavage of aryl-ether bond, such as the linkage between phenylpropane unit and methoxyl group. Demethoxylation of lignin can generate additional reactive sites and lead to more condensed lignin during the thermal modification process (Tjeerdsma et al., 1998).

It is observed that the methoxyl content in torrefied biomass decreased with the severity of torrefaction, based on the mass of feedstock (Table 3). Consequently, the amount of unmodified lignin – lignin with one methoxyl group, which was calculated based on the decrement of methoxyl content in samples compared to the initial amount in the Raw – also decreased. By subtracting the unmodified lignin fraction from the total residue after acid hydrolysis, the amount of thermally-modified compounds can be determined. Some fraction of the total mass of the thermally-modified solids is from residual lignin. This fraction of

residual lignin can be referred to as “modified lignin”, in which the demethoxylated lignin units are interlinked by more condensed bonding, such as 5-5 biphenyl linkages.

However, the changes of condensed structure of lignin might not be enough to explain the substantial increase (by 27 % in weight) of acid-insoluble residues after torrefaction, from 30.1 to 38.2 g in TC sample. It is expected that a considerable portion of the acid-insoluble residue could originate from the carbohydrate fractions in the lignocellulosic biomass. For example, acid-resistant condensed structure of carbohydrates and their complexes with reactive lignin as well as degraded carbohydrates are likely.

3.6. *NMR spectroscopy*

Combined with the indirect methods to estimate the degree of thermal transformation of lignin using functional group analysis, solid-state NMR spectroscopy was employed to obtain more detailed structural information from samples of torrefied biomass. First, the solid-state ^{13}C CP/MAS NMR spectra were obtained from the untorrefied (Raw) and torrefied biomass (Figure 3). The NMR spectrum of a pyrolysis char, which is from fast pyrolysis of loblolly pine at 500 °C (Meng et al., 2012), was also acquired as a reference for highly aromatic solids after thermal treatment. One large and wide peak at 125 ppm (“a” in Fig. 3) is apparent, corresponding to aryl carbons. In contrast to the sharp peak for carbohydrates at 105 ppm (“b”) (Figure 3, Raw to TC) present in all samples, it is noticeable that the broad peak at around 125 ppm (“a”) for aromatic carbon and the small peak at 140 ~ 150 ppm (“c”) from lignin (Hawkes et al., 1993; Shafizadeh, 1984) were substantially increased upon torrefaction. The decrease in the NMR signal intensity for aliphatic carbons

in the carbohydrates – 72 ~ 75 ppm (“d”) for C2/C3/C5 and 105 ppm (“b”) for C1 in cellulose (Wikberg & Maunu, 2004) – clearly suggests relatively high decomposition of the carbohydrates after the heat treatment. In addition, a small shoulder at 102 ppm (“e”) from hemicellulose (Wikberg & Maunu, 2004) diminishes in TC sample (in Figure 3). One interesting observation is the presence of the peaks for C4 and C6 of ordered (crystalline) cellulose at 89 and 65 ppm (“f”), and disordered (amorphous) cellulose at 84 and 62 ppm (“g”) (Atalla & VanderHart, 1999; Gilardi et al., 1995; Wikberg & Maunu, 2004). For the Raw sample, the sharp peak corresponding to ordered cellulose is less intense than that of disordered cellulose. In the NMR spectra of TA and TB (Figure 3d and e), the signal for disordered fraction (“g”) becomes smaller, compared to that from ordered structure (“f”). This observation might be explained by the selective degradation of disordered cellulose fractions during low-severity torrefaction. In TC sample, however, there is a small sharp peak at 84 ppm without corresponding peak for less-crystalline cellulose at 62 ppm, which might indicate unidentified structural changes in the carbohydrate fraction. The peak at 56 ppm (“h”) corresponds to methoxyl groups in lignin, indicating the relative increase in signal due to the degradation of the carbohydrates fraction. In methoxyl group content analysis, it was observed that the amount of methoxyl group was decreasing, because the content is calculated based on the mass of feedstock, with consideration of weight loss during torrefaction process. From the NMR spectra, however, it is necessary to note that the signal from methoxyl group at 56 ppm was increased, because that the consideration of thermal degradation is not included. After torrefaction, carbohydrates were depleted and lignin

fraction became dominant, resulting in higher signal for methoxyl group, based on total carbons inside torrefied biomass.

The CP/MAS NMR technique has been widely used to measure carbon functionality and aromaticity in chars and other aromatic materials. However, it has been shown that the non-protonated carbon fraction in the aromatic structures is underestimated by CP/MAS due to the slow magnetization transfer from proton to remote carbon (Brewer et al., 2009; Czimczik et al., 2002; Kelemen et al., 2007). To overcome this limitation, solid-state ^{13}C DP/MAS NMR technique was employed for quantitative structural analyses of the thermally-treated biomass. Spectra from this technique showed some different aspects (Figure 4), compared to those of CP/MAS NMR. The intensity assigned to aromatic fractions increased substantially with the increased torrefaction severity from Raw to TC, which might be not apparent from the CP/MAS NMR spectra. The corresponding dipolar dephasing NMR spectra is also presented in Figure 4 to allow selectively detection of non-protonated aromatic carbons in the total aromatic structures (Brewer et al., 2009; Mao & Schmidt-Rohr, 2004). With this dipolar dephasing technique, it is possible to attenuate the signal from protonated carbons, resulting in the identification of non-protonated carbons. Based on this protocol, aromatic carbon fraction can be quantified as the total aromatic carbon fraction consists of aromatic C-O, aromatic C-H, and non-protonated aromatic carbon. Thus, the combined DP/MAS and dephasing NMR spectra were used to quantify total carbon fractions in the torrefied biomass (Table 4).

The amount of calculated total aromatic carbon is found to be very close to that obtained from compositional data after acid-insoluble residue content, except for sample TC

(30.1, 41.0, 48.1, and 74.2 % for untorrefied, TA, TB, and TC, respectively). This might imply that (1) the aromatic carbon fraction in woody biomass as measured by ^{13}C DP/MAS NMR indicates the acid-insoluble residue content in thermally-treated samples to a certain severity of treatment, and (2) formation of non-aromatic acid-insoluble carbon structures takes place in TC sample. The presence of complex condensed aromatic structure in torrefied loblolly pine has been recently reported (Ben & Ragauskas, 2012). Based on these quantitative analyses, it might be possible that the condensed solid products, which were generated at the early stage of torrefaction (TA and TB), were mainly aromatic in their structure; however, beyond some point of treatment, the formation of non-aromatic condensed structure became dominant. High aromaticity of extensively treated biomass, such as biochar, is likely achieved by rearrangement of non-aromatic products and/or selective degradation of the non-aromatic fractions, as well as the remaining carbohydrates at the temperature range beyond typical torrefaction processes. In addition, the increased aromaticity of torrefied biomass might correspond to observations about their higher hydrophobicity (Acharjee et al., 2011; Yan et al., 2010).

The DP/MAS NMR with recoupled dipolar dephasing also presents important characteristics of torrefied biomass. In Table 4, it was observed that the fraction of total aromatics and non-protonated carbon increases, while the protonated carbon/aromatic C-O fraction decreased. This corresponds with the ^{13}C DP/MAS NMR works on pyrolysis/gasification biochars (Brewer et al., 2009; Brewer et al., 2011). As the aromatic ring cluster increases, the portion for non-protonated carbons inside the cluster increases on a relative basis, compared to that of the protonated carbons/aromatic C-O along the edge of

cluster ring. Therefore, the fraction of non-protonated carbon can be used to assess the size of aromatic cluster. In summary, the solid-state NMR studies suggest that during torrefaction of lignocellulosic biomass not only the amount of aromatic carbons rises, but also the size of the aromatic ring clusters.

4. Conclusions

The chemical and structural changes that take place during torrefaction of biomass were elucidated by using a series of complementary methods. Torrefaction induced the formation of acid-insoluble residues by the formation of condensed aromatic structures. The increased aromaticity and amount of non-protonated aromatic carbon were quantified by solid-state NMR experiments, indicating larger aromatic clusters in TC. This study on the chemical and structural changes in biomass during torrefaction present a unique opportunity to reveal the complex and heterogeneous thermal transformation of torrefied biomass using complementary tools, including recently introduced ^{13}C DP/MAS NMR analysis.

References

Acharjee, T.C., Coronella, C.J., Vasquez, V.R. 2011. Effect of thermal pretreatment on equilibrium moisture content of lignocellulosic biomass. *Bioresource Technology*, **102**(7), 4849-4854.

Arias, B., Pevida, C., Fermoso, J., Plaza, M.G., Rubiera, F., Pis, J.J. 2008. Influence of torrefaction on the grindability and reactivity of woody biomass. *Fuel Processing Technology*, **89**(2), 169-175.

ASTM. 2009. D5142 - 09 : Standard Test Methods for Proximate Analysis of the Analysis Sample of Coal and Coke by Instrumental Procedures.

Atalla, R.H., VanderHart, D.L. 1999. The role of solid state C-13 NMR spectroscopy in studies of the nature of native celluloses. *Solid State Nuclear Magnetic Resonance*, **15**(1), 1-19.

Baker, S.M. 1996. Rapid methoxyl analysis of lignins using gas chromatography. *Holzforschung*, **50**(6), 573-574.

Balat, M. 2008. Mechanisms of thermochemical biomass conversion processes. Part 1: Reactions of pyrolysis. *Energy Sources Part a-Recovery Utilization and Environmental Effects*, **30**(7), 620-635.

Ben, H.X., Ragauskas, A.J. 2012. Torrefaction of Loblolly pine. *Green Chemistry*, **14**(1), 72-76.

Brewer, C.E., Schmidt-Rohr, K., Satrio, J.A., Brown, R.C. 2009. Characterization of Biochar from Fast Pyrolysis and Gasification Systems. *Environmental Progress & Sustainable Energy*, **28**(3), 386-396.

Brewer, C.E., Unger, R., Schmidt-Rohr, K., Brown, R.C. 2011. Criteria to Select Biochars for Field Studies based on Biochar Chemical Properties. *BioEnergy Research*, 1-12.

Bridgeman, T.G., Jones, J.M., Shield, I., Williams, P.T. 2008. Torrefaction of reed canary grass, wheat straw and willow to enhance solid fuel qualities and combustion properties. *Fuel*, **87**(6), 844-856.

Carrasco, F., Roy, C. 1992. Kinetic study of dilute-acid prehydrolysis of xylan-containing biomass. *Wood Science and Technology*, **26**(3), 189-208.

Carrier, M., Loppinet-Serani, A., Denux, D., Lasnier, J.M., Ham-Pichavant, F., Cansell, F., Aymonier, C. 2011. Thermogravimetric analysis as a new method to determine the lignocellulosic composition of biomass. *Biomass & Bioenergy*, **35**(1), 298-307.

Chen, B.L., Zhou, D.D., Zhu, L.Z. 2008. Transitional adsorption and partition of nonpolar and polar aromatic contaminants by biochars of pine needles with different pyrolytic temperatures. *Environmental Science & Technology*, **42**(14), 5137-5143.

Cheng, C.H., Lehmann, J., Thies, J.E., Burton, S.D., Engelhard, M.H. 2006. Oxidation of black carbon by biotic and abiotic processes. *Organic Geochemistry*, **37**(11), 1477-1488.

Czimczik, C.I., Preston, C.M., Schmidt, M.W.I., Werner, R.A., Schulze, E.D. 2002. Effects of charring on mass, organic carbon, and stable carbon isotope composition of wood. *Organic Geochemistry*, **33**(11), 1207-1223.

Deng, J., Wang, G.J., Kuang, J.H., Zhang, Y.L., Luo, Y.H. 2009. Pretreatment of agricultural residues for co-gasification via torrefaction. *Journal of Analytical and Applied Pyrolysis*, **86**(2), 331-337.

Faix, O. 1992. Fourier Transform Infrared Spectroscopy. in: *Methods in lignin chemistry*, (Eds.) S.Y. Lin, C.W. Dence, Springer-Verlag. Berlin ; New York, pp. 83-109.

Gilardi, G., Abis, L., Cass, A.E.G. 1995. C-13 Cp/Mas Solid-State Nmr and Ft-Ir Spectroscopy of Wood Cell-Wall Biodegradation. *Enzyme and Microbial Technology*, **17**(3), 268-275.

Grønli, M.G., Varhegyi, G., Di Blasi, C. 2002. Thermogravimetric analysis and devolatilization kinetics of wood. *Industrial & Engineering Chemistry Research*, **41**(17), 4201-4208.

Guo, Y., Bustin, R.M. 1998. FTIR spectroscopy and reflectance of modern charcoals and fungal decayed woods: implications for studies of inertinite in coals. *International Journal of Coal Geology*, **37**(1-2), 29-53.

Hawkes, G.E., Smith, C.Z., Utley, J.H.P., Vargas, R.R., Viertler, H. 1993. A COMPARISON OF SOLUTION AND SOLID-STATE C-13 NMR-SPECTRA OF LIGNINS AND LIGNIN MODEL COMPOUNDS. *Holzforschung*, **47**(4), 302-312.

Keiluweit, M., Nico, P.S., Johnson, M.G., Kleber, M. 2010. Dynamic Molecular Structure of Plant Biomass-Derived Black Carbon (Biochar). *Environmental Science & Technology*, **44**(4), 1247-1253.

Kelemen, S.R., Afeworki, M., Gorbaty, M.L., Sansone, M., Kwiatek, P.J., Walters, C.C., Freund, H., Siskin, M., Bence, A.E., Curry, D.J., Solum, M., Pugmire, R.J.,

Vandenbroucke, M., Leblond, M., Behar, F. 2007. Direct characterization of kerogen by x-ray and solid-state C-13 nuclear magnetic resonance methods. *Energy & Fuels*, **21**(3), 1548-1561.

Kim, U.J., Eom, S.H., Wada, M. 2010. Thermal decomposition of native cellulose: Influence on crystallite size. *Polymer Degradation and Stability*, **95**(5), 778-781.

Lipinsky, E.S., Arcate, J.R., Reed, T.B. 2002. Enhanced wood fuels via torrefaction. *Fuel Chemistry Division Preprints*, **47**(1), 408-410.

Mao, J.D., Schmidt-Rohr, K. 2004. Accurate quantification of aromaticity and nonprotonated aromatic carbon fraction in natural organic matter by C-13 solid-state nuclear magnetic resonance. *Environmental Science & Technology*, **38**(9), 2680-2684.

Meng, J.J., Park, J., Tilotta, D., Park, S. 2012. The effect of torrefaction on the chemistry of fast-pyrolysis bio-oil. *Bioresource Technology*, **111**, 439-446.

NETL. 2011. Cost and Performance baseline for Fossil energy Plants - Volume 3: Low Rank Coal and Natural Gas to Electricity: Combustion Cases. National Energy Technology Laboratory. DOE/NETL-2011/1463.

Pach, M.Z., R.; Björnbom, E. 2002. Torrefied Biomass a Substitute for Wood and Charcoal. in: *6th Asia-Pacific International Symposium on Combustion and Energy Utilization*. Kuala Lumpur, Malaysia.

Pandey, K.K., Theagarajan, K.S. 1997. Analysis of wood surfaces and ground wood by diffuse reflectance (DRIFT) and photoacoustic (PAS) Fourier transform infrared spectroscopic techniques. *Holz Als Roh-Und Werkstoff*, **55**(6), 383-390.

Pastorova, I., Arisz, P.W., Boon, J.J. 1993. Preservation of D-Glucose-Oligosaccharides in Cellulose Chars. *Carbohydrate Research*, **248**, 151-165.

Peng, Y.Y., Wu, S.B. 2010. The structural and thermal characteristics of wheat straw hemicellulose. *Journal of Analytical and Applied Pyrolysis*, **88**(2), 134-139.

Pentananunt, R., Rahman, A.N.M.M., Bhattacharya, S.C. 1990. Upgrading of Biomass by Means of Torrefaction. *Energy,* **15**(12), 1175-1179.

Phanphanich, M., Mani, S. 2011. Impact of torrefaction on the grindability and fuel characteristics of forest biomass. *Bioresource Technology*, **102**(2), 1246-1253.

Pimchuai, A., Dutta, A., Basu, P. 2010. Torrefaction of Agriculture Residue To Enhance Combustible Properties. *Energy & Fuels,* **24**, 4638-4645.

Prins, M.J., Ptasinski, K.J., Janssen, F.J.J.G. 2006. More efficient biomass gasification via torrefaction. *Energy*, **31**(15), 3458-3470.

Repellin, V., Govin, A., Rolland, M., Guyonnet, R. 2010. Energy requirement for fine grinding of torrefied wood. *Biomass & Bioenergy*, **34**(7), 923-930.

Rousset, P., Aguiar, C., Labbe, N., Commandre, J.M. 2011. Enhancing the combustible properties of bamboo by torrefaction. *Bioresource Technology*, **102**(17), 8225-8231.

Shafizadeh, F. 1984. The chemistry of pyrolysis and combustion. in: *Advances in chemistry series*, (Ed.) R.M. Rowell, American Chemical Society. Washington, DC, pp. 489-529.

Shafizadeh, F. 1985. Pyrolytic reactions and products of biomass. in: *Fundamentals of Biomass Thermochemical Conversion*, (Ed.) R.P.M. Overend, T. A.; Mudge, L. K., Elsevier. London, pp. 183-217.

Sharma, R.K., Wooten, J.B., Baliga, V.L., Lin, X.H., Chan, W.G., Hajaligol, M.R. 2004. Characterization of chars from pyrolysis of lignin. *Fuel*, **83**(11-12), 1469-1482.

Sluiter, A., Harmes, B., Ruiz, C., Scarlata, C., Sluiter, J., Templeton, D., Crocker, D. 2008. NREL Laboratory Analytical Procedure. in: *Determination of structural carbohydrates and lignin in biomass*, Vol. NREL/TP-510-42618.

Soltes, E.J., Elder, T.J. 1981. Pyrolysis. in: *Organic Chemicals from Biomass*, (Ed.) I.S. Goldstein, CRC Press. Boca Raton, FL, pp. 63.

Tjeerdsma, B.F., Boonstra, M., Pizzi, A., Tekely, P., Militz, H. 1998. Characterisation of thermally modified wood: molecular reasons for wood performance improvement. *Holz Als Roh-Und Werkstoff*, **56**(3), 149-153.

Tjeerdsma, B.F., Militz, H. 2005. Chemical changes in hydrothermal treated wood: FTIR analysis of combined hydrothermal and dry heat-treated wood. *Holz Als Roh-Und Werkstoff*, **63**(2), 102-111.

Wikberg, H., Maunu, S.L. 2004. Characterisation of thermally modified hard- and softwoods by C-13 CPMAS NMR. *Carbohydrate Polymers*, **58**(4), 461-466.

Yan, W., Hastings, J.T., Acharjee, T.C., Coronella, C.J., Vasquez, V.R. 2010. Mass and Energy Balances of Wet Torrefaction of Lignocellulosic Biomass. *Energy & Fuels*, **24**, 4738-4742.

Yang, H.P., Yan, R., Chen, H.P., Lee, D.H., Zheng, C.G. 2007. Characteristics of hemicellulose, cellulose and lignin pyrolysis. *Fuel*, **86**(12-13), 1781-1788.

Yeh, T.F., Chang, H.M., Kadla, J.F. 2004. Rapid prediction of solid wood lignin content using transmittance near-infrared spectroscopy. *Journal of Agricultural and Food Chemistry*, **52**(6), 1435-1439.

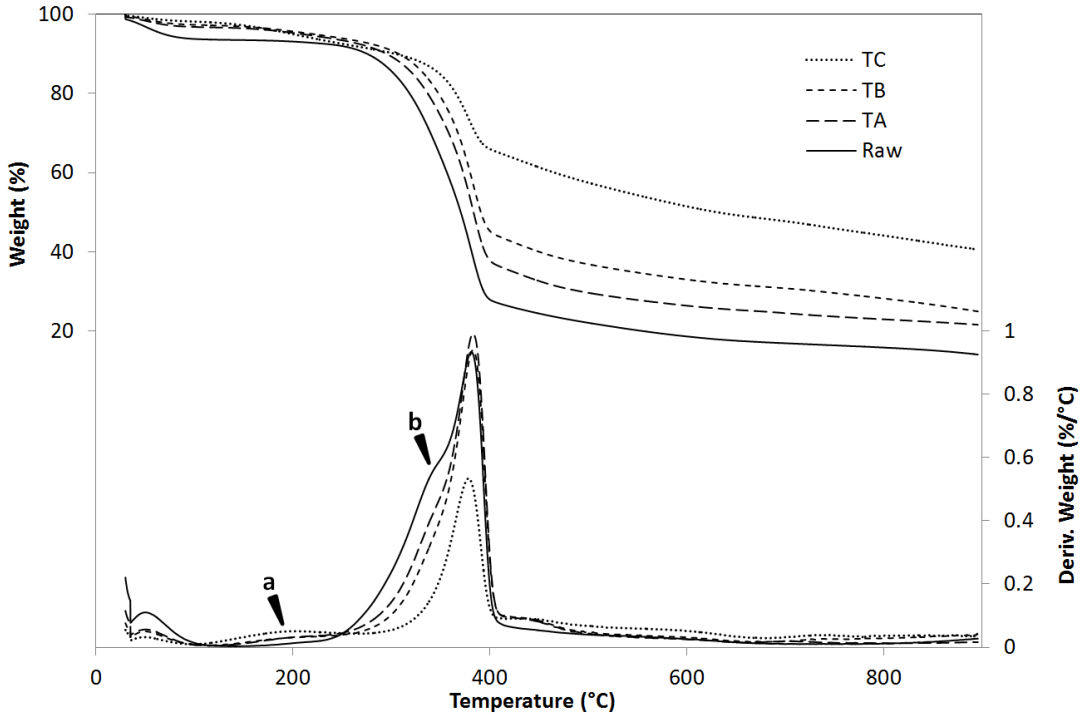

Figure 1. Thermogravimetry profile and its derivative for untorrefied (Raw) and torrefied biomass (TA, TB, and TC).

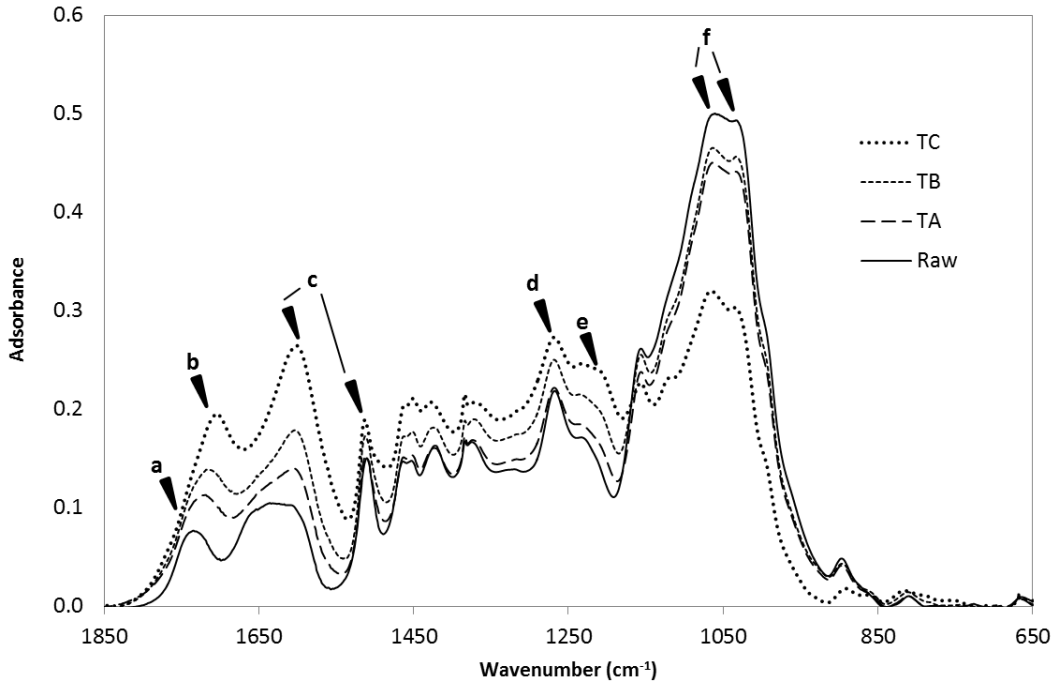

Figure 2. FTIR spectra between 650 and 1850 cm^{-1} range for untorrefied (Raw) and torrefied biomass (TA, TB, and TC).

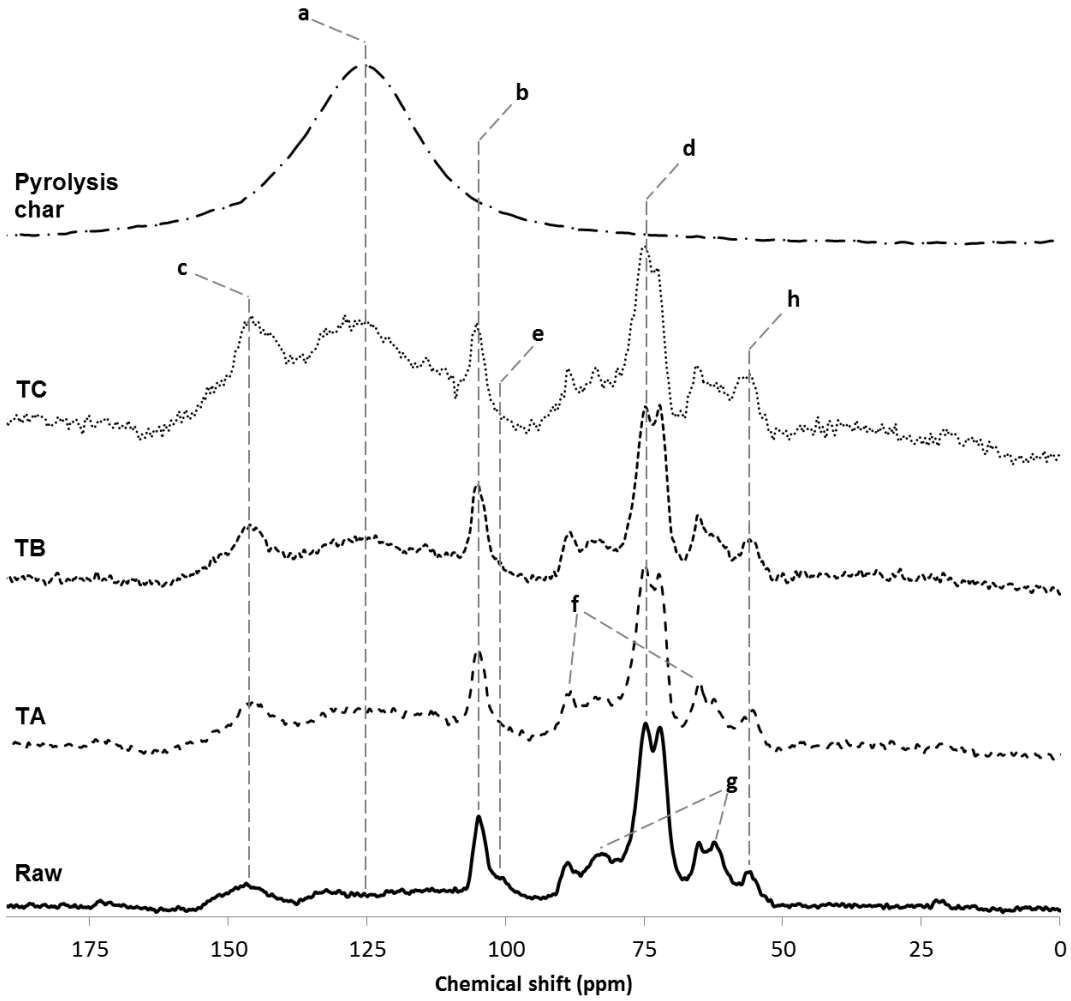

Figure 3. Solid-state ^{13}C CP/MAS NMR spectra for untorrefied (Raw) and torrefied biomass (TA, TB, and TC). The spectrum of pyrolysis char is included as a reference for signals from highly aromatic carbon structures.

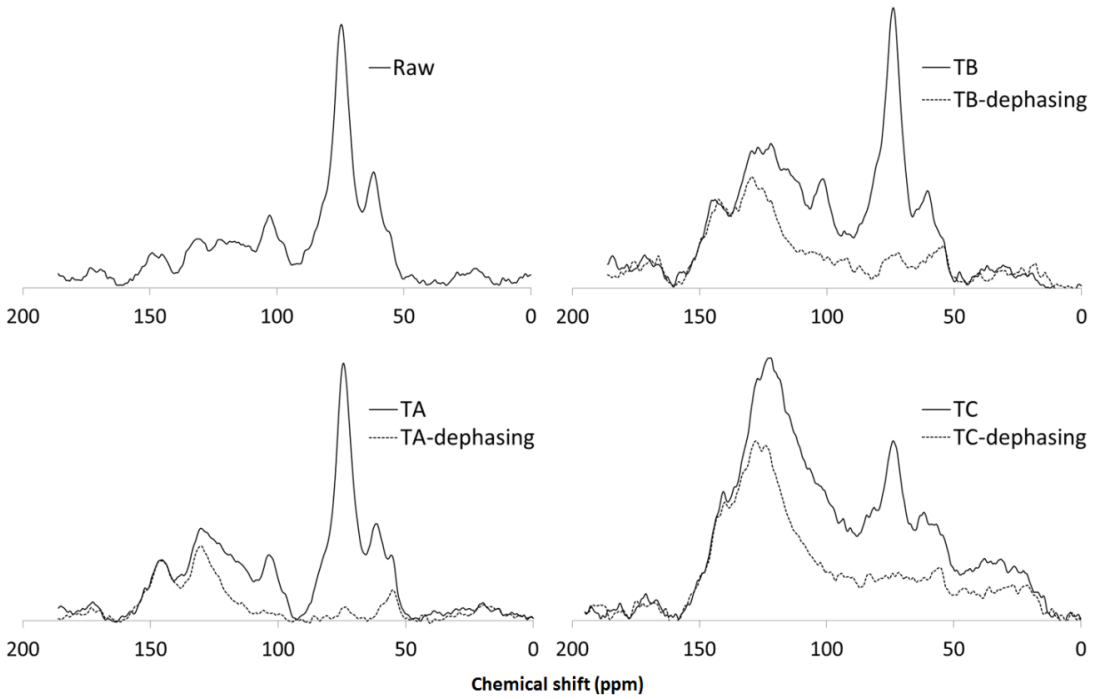

Figure 4. Solid-state ^{13}C DP/MAS NMR spectra (solid line) and DP/MAS NMR with dipolar dephasing (dotted line) for untorrefied (Raw) and torrefied biomass (TA, TB, and TC). DP/MAS NMR with dipolar dephasing for raw material was not shown, due to its low intensity of signal.

Table 1. Proximate, ultimate analyses and heating values of the untorrefied (Raw) and torrefied biomass (TA, TB, and TC) [a].

		Proximate analysis, %			Ultimate analysis, %				O/C Ratio	Heating Value (HHV)[c], MJ/kg
	MC[b]	VM[b]	FC[b]	Ash	C	H	N	O		
Raw	7.69	84.6	14.8	0.6	50.5	6.26	0.09	42.6	0.63	20.0 (18.2)
TA	6.32	78.6	20.8	0.6	55.0	5.94	0.11	38.3	0.52	22.7 (20.8)
TB	5.43	76.4	22.8	0.8	57.3	5.79	0.14	36.0	0.47	24.0 (22.1)
TC	4.03	59.9	38.6	1.4	65.8	4.87	0.28	27.6	0.31	26.3 (25.2)
Lignite[d]	36.1	41.5	43.1	15.4	61.9	4.29	0.98	16.4	0.20	24.3

[a] Proximate and ultimate analyses data were presented as a dry basis
[b] MC - moisture content (%, as received); VM - volatile matter; FC - fixed carbon
[c] Higher heating values : dry-basis (wet-basis)
[d] Values for North Dakota Beulah-Zap lignite (2011)

Table 2. Compositional analysis of the untorrefied (Raw) and torrefied biomass (TA, TB, and TC). The values were calculated based on 100 g of untorrefied biomass.

	Weight loss after torrefaction [a], g	Chemical composition, g			% Compositional change		
		Glucan [b]	Other carbs.[b]	Residue [c]	Glucan [b]	Other carbs.[b]	Residue [c]
Raw	0	36.1	18.7	30.1	-	-	-
TA	16.4	28.8	10.2	34.3	-20.2	-45.6	14.1
TB	24.4	24.2	6.9	36.4	-32.9	-63.2	20.9
TC	48.5	9.3	0.6	38.2	-74.3	-97.0	27.1

[a] Weight loss was estimated based on linear correlation with atomic O/C ratio from lab-scale experiments
[b] Glucan & other carbohydrates were calculated based on the monosaccharide amount obtained from HPLC
[c] Residue is the insoluble solid after two-step acid hydrolysis (Klason lignin method)

Table 3. Methoxyl (MeO) content analysis of the untorrefied (Raw) and torrefied biomass (TA, TB, and TC). The weight values were calculated based on 100 g of untorrefied biomass.

	Residue, g	MeO content, g	% relative decrease in MeO content	Unmodified lignin [a], g	Modified lignin + acid-insoluble carbohydrates, g
Raw	30.1	5.00	-	30.1	0
TA	34.3	3.93	21.4	23.6	10.7
TB	36.4	3.72	25.6	22.3	14.0
TC	38.2	2.45	51.0	14.7	23.5

[a] Unmodified lignin in a torrefied sample = initial amount of unmodified lignin in raw material × (MeO content in torrefied wood / MeO content in raw material)

Table 4. Quantitative spectral analysis for solid-state ^{13}C DP/MAS NMR of the untorrefied (Raw) and torrefied biomass (TA, TB, and TC). The values were calculated based on 100% carbon in each biomass.

	Carbonyls, %	Aromatics, %				Alkyls, %
		C-O	Protonated	Non-protonated	Total aromatic	
Raw	3.6	4.7	a [a]	b [a]	35.8	60.6
TA	2.8	6.1	18.7	19.9	44.6	52.5
TB	4.5	5.1	19.2	29.5	53.8	41.7
TC	2.2	3.0	21.0	35.6	59.6	38.2

[a] Non-protonated carbon fraction for Raw sample was not determined due to the low signal intensity of NMR spectrum with dipolar dephasing. The total amount of protonated and non-protonated aromatic carbon is 31.1% (a + b).

CHAPTER 3

Activated Carbon from Biochar: Influence of its physicochemical properties on the sorption characteristics of phenanthrene

1. Introduction

Thermochemical conversion of lignocellulosic biomass has been considered as a viable option to produce intermediate liquid streams for biofuels and biochemicals. During the conversion process, biochar is generated as a byproduct of pyrolysis; its optimization and application is essential to make the overall process economically feasible. Pyrolysis engineers have traditionally sought to minimize char production, as it has been considered as a low-value fraction, decreasing the yield of bio-oil. Recently, there is a growing interest in biochar due to the potential benefits of its application to soil as carbon sequestration and soil amendment (Chan et al., 2007; Gaunt and Lehmann, 2008; Novak et al., 2009; Woolf et al., 2010). It was also shown that biochar has promising sorption properties for various contaminants of water including polycyclic aromatic hydrocarbons (PAHs) and heavy metals (Cao et al., 2009; Chen and Chen, 2009; Kong et al., 2011; Sun et al., 2011; Uchimiya et al., 2011). Biochar made from renewable biomass has high surface area, ranging from 100 to 460 $m^2\ g^{-1}$ and present diverse surface sites such as carboxylic, phenolic, hydroxyl, and carbonyl groups (Novak et al., 2009). The physicochemical and porous properties of biochar are highly attractive for the development of effective and low-cost sorbents for removal of water contaminants.

Biochar can also be used as a precursor of value-added activated carbons. Recent studies have shown that steam activation of fast pyrolysis biochar greatly enhances the surface area and porous structure, and thus the sorption capacity for water contaminants (Lima et al., 2010). Chemical activation using KOH increased the surface area of biochar to values as large as 1500 m^2 g^{-1}, comparable to those for commercial activated carbons (Azargohar and Dalai, 2008). Optimization of the activation process may further improve porous structures and sorption capacity of activated biochar, which will help develop renewable alternatives to activated carbons made from coal. According to "Global Activated Carbon Market Forecast & Opportunities 2017", the demand for activated carbon is expected to increase more than 10% per year for the next five years to make it a $3 billion market by 2017 (Global Activated Carbon Market Forcast and Opportunities, 2012). The successful utilization of biomass to produce biofuels as well as activated carbon will not only help relieve environmental problems caused by coal mining, but also lower the production cost of effective sorbents that can be used in water treatment and wastewater reclamation.

In this study, we hypothesize that the porous structure and sorption characteristics of activated biochar are dependent upon the physicochemical properties of the precursor biochar as well as the activation methods. In particular, aromatic structures in biochar may play an important role in the formation of porous networks during the activation process. The physicochemical properties of biochar are strongly dependent upon the nature of feedstock and pyrolysis conditions (e.g., heating temperature and residence time). Thus, an investigation of the biochar properties and sorption capacity of the activated counterparts is essential to identify optimum pyrolysis conditions.

We employed conventional analytical methods as well as advanced solid-state NMR techniques to determine the physicochemical properties of biochar prepared under different conditions. Solid-state NMR was used as a proven and effective tool for structural analyses of inhomogeneous solid samples. For example, ^{13}C solid-state NMR has provided quantitative structural information related to the aromaticity and the size of aromatic clusters (Brewer et al., 2009; Park et al., 2013). In addition, ^{2}H NMR was used to examine the dynamics of deuterated contaminants (phenanthrene) adsorbed on activated biochar, which provides valuable information as to the pore size. The porous properties of activated carbons such as surface area and pore volume have typically been examined through N_2 and CO_2 adsorption. The probe molecules are, however, much smaller than the actual water contaminants. Thus, ^{2}H NMR spectra from the actual sorbate allow detailed examination of pore size as well as binding affinity.

The present systematic investigation will help in the development of value-added materials from various sources of biomass and identify optimum processing conditions to produce biochars and to maximize the sorption capacity of activated carbons from the tailored biochars.

2. Material and Methods

2.1 Sample production and activation

Debarked loblolly pine (*Pinus taeda*) chips were milled to pass through 20 ~ 40 mesh sieves and air-dried before further treatment. A porcelain boat containing 3 g of softwood

mill was loaded into a quartz-tube furnace (MTI Corporation, Richmond, CA); the tube was purged for 10 minutes with nitrogen (1 L min^{-1} flow rate). During the purging, the boat with samples was placed outside the heating element of the furnace, then it was loaded into the preheated furnace and treated for 15 min with continuous nitrogen flow (1 L min^{-1}) at different temperatures (300, 350, 500, and 700°C). Each treated sample was designated as "N-*treatment temperature*" (e.g., N-300 for the sample treated at 300°C). After the heat treatment, the boat was removed from the furnace, and cooled down to ambient temperature under nitrogen flow. After weight loss measurement, all samples were stored in a desiccator before further treatment or analyses.

NaOH activation method was used to improve the sorption properties of biochar. Thermally-treated biochar (3 g) was mixed with 40 mL of 4 M NaOH aqueous solution and incubated at room temperature for 2 h under intermittent shaking (15 min intervals). After NaOH impregnation, the excess solution was discarded with vacuum filtering and the chemically-treated solid was dried overnight in an oven at 105 °C. The dried sample was heated in a quartz-tube furnace to 800 °C with a heating rate of 3 °C min^{-1} under inert atmospheric conditions (2 L min^{-1} N_2 flow) for 2 hours. After activation, the samples were pulled out from the heating element and cooled down to ambient temperature under nitrogen flow. The activated samples were washed with 2 L of deionized (DI) water followed by 0.1 M HCl solution (200 mL) and washed again with DI water until the pH of filtrates was about 7.0. The washed activated carbon samples were dried in an oven set at 105 °C and stored in a desiccator for further analysis. Each activated sample was denoted as "N-*treatment temperature* AC" (e.g. N-300AC for activated carbon from N-300).

2.2 Characterization of biochar

Carbon, hydrogen, and nitrogen content in the thermally-treated and activated samples were analyzed by using a PerkinElmer 2400 Series II Elemental Analyzer (PerkinElmer, Waltham, MA). Oxygen content was calculated by subtraction of CHN and ash content from the total mass. Proximate analysis was conducted according to the ASTM standard D7582-10.

2.3 Solid-state ^{13}C NMR

Solid-state NMR spectra for the biochar samples were acquired with a Varian 3.2 mm MAS probe on a Varian Inova 500 spectrometer. For the DP/MAS (direct polarization/magic angle spinning) experiments, the sample was spun at a high frequency of 15 kHz. A dephasing time of 68 μs was used for dipolar dephasing experiments to determine non-protonated aromatic carbon fractions (Brewer et al., 2009; Brewer et al., 2011). For the quantitative DP/MAS experiments, 1,000 – 2,000 FIDs were collected with a long acquisition delay of 60 s. The 90° pulse-lengths for ^{1}H and ^{13}C were 3.0 μs and 2.7 μs, respectively. The two-pulse phase-modulated (TPPM) decoupling scheme was employed with a radio-frequency field strength of 80 kHz. Quantitative spectral analysis was performed by integrating the assigned area of DP/MAS spectra and fractionating into three major categories – carbonyl, aromatic, and alkyl carbon fractions (Brewer et al., 2009). Quantification of the non-protonated aromatic carbon fraction was carried out in the same manner using DP/MAS and dipolar dephasing NMR spectra.

Long-range ^{1}H-^{13}C dipolar dephasing NMR experiments were also carried out to probe the size of the aromatic clusters. The QCPMG detection scheme(Larsen et al., 1998) was incorporated into the dephasing experiment for signal enhancement.

2.4 Static ^{2}H NMR

Solid-state ^{2}H NMR spectra for stationary samples were acquired using Varian Inova 500 spectrometer equipped with a Varian 3.2 mm MAS probe. A quadrupole echo pulse sequence with a refocusing delay of 30 μs was used. The 90° pulse-lengths for ^{2}H was 6.0 μs.

2.5 Surface characterization

BET (Brunauer–Emmett–Teller) surface area and pore-size distribution were measured by using N_2 adsorption. The adsorption of N_2 at 77 K was determined with a Micromeritics Gemini VII 2390p apparatus and the adsorption data was analyzed using built-in calculation protocols. The BET surface area was calculated from the linear fit of the adsorption data. Micropore volumes were obtained by the t-plot method (Hu and Srinivasan, 1999), and the total pore volumes were estimated from the adsorbed amount of N_2 at a relative pressure of 0.99.

2.6 Adsorption test with a representative PAH - phenanthrene

To investigate adsorption property of the thermally-treated/activated samples with phenanthrene (Sigma-Aldrich, St. Louis, MO), a fixed amount of powdered biochar samples (sieved through 200 mesh screen) was mixed with a phenanthrene solution, then the

concentration of phenanthrene was measured by UV-Vis spectrophotometer. 6.5 mg of phenanthrene was dissolved in 500 ml of methanol (HPLC grade), and DI water was added to make a total volume of 1 L solution. 30 mL of the prepared phenanthrene solution was mixed with 1 mg of the biochar sample and incubated at 25°C for a fixed period of time. A commercial powdered activated carbon (NORIT® GAC 1240) was used in similar experiments as referent sorbent. After incubation, 1 mL of aliquot was centrifuged at 13,000 rpm for 5 min and the supernatant was analyzed by UV-Vis spectrophotometer at 251 nm wavelength to measure the concentration of phenanthrene. UV absorbance at 251 nm for phenanthrene solution with concentration between 0.05 ~ 6.5 mg L^{-1} was measured; the measured values showed a good linearity, R^2=0.999.

3. Results and Discussion

3.1 Characterization of biochar before and after activation

Proximate analysis: The result of proximate analysis for the heat-treated samples showed substantial changes in volatile matter and fixed carbon (Table 1). With the increase in temperature, the content of volatile matter is substantially decreased from 87.4 % in untreated feedstock to 10 % in N-700, while the amount of fixed carbon is increased. The thermal breakdown and release of volatile matter are expected to be mainly from the carbohydrate fractions that are less stable during the heat treatment (Yang et al., 2007). Correspondingly, the content of fixed carbon increased with the increasing severity of the treatment conditions.

After the activation process, the mass fraction of volatile matter also decreased with the increased fixed carbon fractions. The changes in the mass fraction were more prominent in the N-300 and N-350 biochar samples. During the activation process, the volatile fraction in the biochar may be fused to more condensed aromatic structures and/or burned off, which may help to develop porous structures. On the other hand, the changes in proximate analysis become less substantial for the N-500 and N-700. These results suggest that the biochar prepared under more severe pyrolysis conditions has more condensed structures resistant to thermal degradation during the activation process.

Ultimate analysis: Atomic O/C ratio from ultimate analysis data in Table 1 showed similar trends that those from proximate analyses. Large reductions in oxygen content and relatively higher carbon content were observed in the more severely treated biochar samples. This decrease in the oxygen content may arise from dehydration reactions, as well as the loss of volatile organic products and their release as gases (mostly of CO and CO_2). The decrease in O/C ratio after the activation process can also be explained by similar mechanisms. Previous studies reported that the relative content of acidic moieties on the surface decreases during activation processes (Chun et al., 2004; Li et al., 2009). The N-700 and N-700AC, however, showed a different trend in the atomic O/C ratio. This observation might be due to oxidation after the activation process, as reported that activated carbon treated at high temperature (1,100°C) for 1 hr has relatively high oxygen content, presumably due to the re-oxidation by exposure to the atmosphere (Figueiredo et al., 1999).

3.2 Solid-state ^{13}C NMR

Biochar: Solid-state NMR spectroscopy was employed to obtain quantitative structural information of the thermally-treated lignocellulosic biomass. Previous studies have shown that heat treatment of biomass induces condensed aromatic structures in biochar. The changes in the aromatic structures were investigated with solid-state ^{13}C DP/MAS and recoupled ^{1}H-^{13}C dipolar dephasing NMR experiments (Figure 1) (Brewer et al., 2009; Czimczik et al., 2002). It was clearly observed that the characteristic peaks of guaiacyl lignin in softwood, such as methoxyl groups at 56 ppm and C_3/C_4 at about 146–148 ppm(Holtman et al., 2006), were substantially decreased with the increasing heating temperature (Figure 1). On the other hand, the NMR peak at around 130 ppm from the sp^2 carbons became more dominant at higher temperature in the ^{13}C DP/MAS spectra, suggesting that aromatic condensation took place after the heat treatment of woody biomass.

The combined DP/MAS and dephasing spectra were analyzed to obtain more quantitative structural information such as aromaticity (% fraction of total aromatic carbons in Table 2) (Brewer et al., 2009; Brewer et al., 2011). The quantitative analysis of biochar samples indicated that with the increase in temperature, the amount of non-protonated aromatic carbons substantially increased, while the relative content of alkyl carbons significantly decreased. Total aromatic carbon fraction also increased, but after 500 °C, it slightly decreased (Table 2). The increases in the non-protonated aromatic carbon fraction suggest that the heat treatment induces a high degree of aromatic condensation, which may result in aromatic clusters of large sizes.

The size of the aromatic cluster was calculated from the quantitative NMR data in Table 2. Briefly, the number of carbons on the edge of aromatic cluster was estimated with the assumption that most dominant carbon species on the cluster edge are from the aromatic C-H and C-O. The estimated edge fraction, combined with the geometry of condensation, allowed us to calculate the minimum number of carbons in a cluster (detailed description can be found elsewhere (Brewer et al., 2009; Solum et al., 1989)). For the biochar produced under low pyrolysis temperatures < 350 °C, it was impractical to estimate the cluster size due to the low degree of condensation and relatively large fraction of the alkyl carbons. The formation of aromatic clusters was observed at higher pyrolysis temperatures > 500°C (N-500 and N-700) and the size of the cluster was notably increased from N-500 to N-700 biochar samples.

The aromatic condensation (size of the aromatic cluster) was probed by long-range dipolar-recoupled dephasing experiments (Mao and Schmidt-Rohr, 2003). In the dephasing experiment, the NMR signal decreases during the dephasing time due to ^{1}H-^{13}C dipolar interactions (Figure 2). The slower decay for the sample treated at a higher temperature indicates weaker dipolar interactions, and thus a larger average distance between the two nuclei. The relative content of the non-protonated carbons inside the cluster would increase in a larger cluster, leading to the slower signal decay because of the weaker dipolar interactions. Thus, the slower signal change at higher temperature clearly suggests that the size of the aromatic cluster increased during the heat treatment, leading to a higher degree of aromatic condensation, as predicted from the non-protonated carbon fractions and the number of carbons in the cluster (Table 2).

Activated Biochar: After the activation process, the NMR signals from the aliphatic carbons further were decreased, particularly for the N-300AC and N-350AC samples (Figure 1e-1h). The broader peak at around 130 ppm indicates that more complex aromatic structures might be developed during the activation process. The quantitative analyses of the NMR spectra showed that the chemical activation using NaOH increased aromatic carbon fractions as well as the non-protonated carbon content (i.e. size of the cluster), indicating that more condensed aromatic structures were developed during the activation. These changes in carbon structure were more substantial when the woody biomass was treated at lower temperature prior to the activation process. These results suggest that the post-heat treatment of biochars induces the development of more condensed aromatic carbon structures by burning off the volatile carbon fraction and thermal transformation of structures, making solid products with higher aromaticity than their precursor biochars.

As for N-500AC, the number of carbons in a cluster was increased more than 2-fold, from 11 to 27. This substantial increase imply that despite the high aromaticity (72.5 %), the carbon structure inside N-500 is amenable to further structural alteration, resulting in larger size of aromatic clusters. This larger cluster might be from condensation of non-aromatic carbon structures in N-500 or fusion of existing clusters. Compared to N-500AC, N-700AC showed a relatively lower increase in the number of carbons inside clusters, from 16 to 23. This might be due to that the N-700 has a more rigid structure and consequently less flexibility toward further structural changes, even with severe chemical and thermal treatment, such as NaOH-activation.

3.3 Surface area and pore volume

Biochar: The surface area and pore volume of the biochars were measured before and after activation (Table 1). For the biochar samples, the BET analysis of N-300 and N-350 yielded very low values, less than 10 m^2 g^{-1}. Biochars prepared at higher temperatures (N-500 and N-700) exhibited higher BET surface areas, 239 m^2 g^{-1} and 321 m^2 g^{-1}, respectively, which are about one-third of those typical of commercial activated carbons.

Activated Biochar: It has been shown that physical or chemical activation increases the surface area and pore volume of carbonaceous materials (Chen and Chen, 2009; Chun et al., 2004). In fact, the surface area and pore volume greatly increased after the activation (Table 1). In particular, the activated counterpart from biochar prepared at a low pyrolysis temperatures (N-300AC) exhibited a surface and pore volume higher than those of the reference, commercial activated carbons (NORIT). It is also notable that activated counterparts from the biochar produced at a higher pyrolysis temperature have lower surface area and pore volume. As for N-700AC, there is a substantial decrease in surface area after the activation process, from 321 to 57 m^2 g^{-1}. This might be due to the thermal condensation of carbon structures inside the biochar. Our structural analyses showed that the low temperature pyrolysis biochar has a lower aromaticity and smaller aromatic cluster (Table 2 and Figure 2). It was also shown that the N-300 biochar contains higher amount of alkyl carbons and volatile matter. The volatile carbon fractions almost completely disappeared after the activation process, as evident in the DP/MAS spectra of the activated N-300AC sample (Figure 1e), indicating that the thermal degradation produces highly porous structures. Condensed aromatic structures might be more resistant to thermal degradation,

and thus the pre-formed aromatic structures in biochar produced at a high pyrolysis temperature (> 500°C) may inhibit development of surface area and porous structures during the activation process.

3.4 Adsorption of phenanthrene on thermally-treated biomass

Biochar: The sorption ability of the biochar was tested for hydrophobic PAH (phenanthrene) (Figure 3). It was expected for the biochar with a higher aromaticity to be better sorbent for aromatic compounds such as the PAHs, due to more favorable hydrophobic and π-π interactions (Boving and Zhang, 2004; Chen et al., 2008; Moreno-Castilla, 2004). In our study, biochar produced at higher temperatures had a higher aromaticity as well as larger surface area. However, the sorption capacity of N-700 for phenanthrene was very close to that of N-300 with much lower aromaticity and smaller surface area. These sorption results suggest that the BET surface area alone might not govern the adsorption of phenanthrene. Aliphatic regions of the biochar, as well as other structural or chemical properties of adsorbents may also contribute to the binding of the hydrophobic contaminant.

The adsorption kinetics of the biochar displayed similar trends. After the relatively efficient initial adsorption, the adsorption process was significantly slowed down over the longer incubation times. These results suggest that the binding sites of the biochar are not readily available to the adsorbents, which requires a long time to be saturated.

Activated biochar: The chemical activation of the biochar greatly enhanced sorption ability of the PAH (Figure 3), particularly for the biochars prepared at lower pyrolysis temperatures (300 and 350°C). It is also noted that N-300AC almost immediately adsorbs the hydrophobic

contaminant, in a very short period of time (< 3min), which is ideal for water remediation. The activated biochar (N-300AC) also exhibited a good initial sorption efficiency (156 mg g^{-1}) after 30 min, which compares favorably against values for commercially available activated char prepared from coal (NORIT, 129.8 mg g^{-1}). However, when the lignocellulosic biomass was treated at a higher pyrolysis temperature followed by activation, no substantial changes in adsorption performance were observed.

To compare the adsorption kinetics of the generated samples, a pseudo-second order adsorption model was applied to the phenanthrene measured adsorption data (Figure 3). This model can be expressed as below;

$$t/q = 1/(k_2 \cdot q_e^2) - (t/q_e)$$

where k_2 is the equilibrium rate constant of pseudo-second order sorption (g mg^{-1} min^{-1}) and q_e is the amount of adsorbed sorbate at equilibrium (mg g^{-1}) (Ho and McKay, 1998; Ho et al., 1996). The linear plot of t/q vs. t was fitted with the measured data to obtain the model parameters. N-500AC showed about 11% increase in q_e for phenanthrene removal, compared to the N-500 sample, and N-700AC showed less than 6% of difference with the N-700 sample. To find any correlation between the properties of adsorbents and the adsorption kinetics, several plots were tested and some of them are presented in Figure 4 along with linear regressions. Based on these observations, the total aromaticity of the thermally-treated samples is not well-correlated to the adsorption kinetics for phenanthrene, in both non-activated and activated samples.

The sorption kinetics of the activated biochar seems to be governed largely by other structural characteristics of the surface such as BET surface area and pore volume. It may also be affected by the size of adsorbents. N-300AC was shown to have larger surface and pore volume, particularly pores larger than micropores, compared to other activated carbons (Table 1). The larger surface area may originate from the larger pores with diameters greater than 2 nm. The activated carbon with larger pores would be more efficient for removal of larger size contaminant, especially during the initial adsorption stage. If the size of target sorbate is large enough to slow down the access to micropores with diameters of less than 2 nm, then it will affect negatively the overall adsorption performance, as well as the correlation to the surface area and total pore volume. The larger pores may play an important role in the sorption for the large contaminant molecule. Valderrama and coworkers reported that the removal of organic molecules by activated carbon largely depends on the size of the organic compounds. It was shown that a large micropore (high surface area) is more efficient for the removal of small molecules, but for larger molecules such as PAHs, mesopores and macropores play more important roles in the adsorption (Valderrama et al., 2008).

Activated biochars prepared in this study are shown to have large surface area and pore volumes comparable to the commercial activated carbons. In particular, N-300AC has a large surface area and a much bigger fraction of pore volume from larger pores (Table 1). Although our NMR analyses showed that the activated carbon containing more mesopores has lower aromaticity, it exhibited better sorption capacity for the hydrophobic phenanthrene (3.6 × 7.0 Å). These results suggest that the larger pores consisting of smaller aromatic

clusters in N-300AC may be more effective for the phenanthrene adsorption than micropores with bigger clusters in the other activated biochars.

3.5 Solid-state ^2H NMR for phenanthrene-d_{10} -saturated samples

The surface area and pore volume of activated carbons have been typically measured by adsorption of N_2 and CO_2. The probe molecules are, however, much smaller than the actual contaminants and have different physical properties than the contaminants containing aromatic side chains. Thus, the surface area measured from the small molecule adsorption may not represent real binding sites for large contaminants with different physical properties.

Deuterium (^2H) is a spin I = 1 nucleus with an electric quadrupole moment that can interact with electric field gradients. The anisotropic interaction gives rise to a broad NMR spectrum spanning 100–200 kHz for stationary samples. The ^2H NMR line shape is strongly sensitive to the dynamics of the molecule (Eastman et al., 2011; Rice et al., 1981; Spiess, 1983; Vold, 1994). Thus, the line width of the ^2H NMR spectrum can be an indicator of the pore size and binding affinity. The static ^2H NMR spectra were acquired for the deuterated phenanthrene adsorbed on activated biochar (Figure 5). The broad NMR spectra spanning ~200 kHz for N-500AC and N-700AC are a characteristic static ^2H NMR spectrum from rigid molecules, suggesting that phenanthrene is tightly bound to the activated biochar. On the other hand, the deuterated sorbate on N-300AC exhibits much narrower lineshape with stronger signal centered at 0 Hz. The narrow ^2H NMR spectrum clearly indicates that the sorbate molecule undergoes more significant motions on the surface of N-300AC. The less tightly bound phenanthrene on the N-300AC appears contradictory to the higher sorption

efficiency of the N-300AC biochar, since the more dynamic sorbate molecule suggests weaker interactions between the sorbate and biochar.

The tighter binding on the N-500AC may be just because of the restricted motions of the sorbate molecules trapped in smaller pores with limited surface area. However, the ^{2}H NMR spectra were collected after 3 min adsorption where small amount of sorbate (26 mg g^{-1}) is adsorbed on the activated biochar (Figure 5). In addition, the ^{2}H NMR spectrum measured from the fully saturated sample was identical to those from the sample incubated for 3 min. These results indicate that the tight binding on the N-500AC arises from the stronger interaction between the biochar and the sorbate rather than from more limited space available for the sorbate. Our quantitative structural analyses showed that N-500AC has a higher aromaticity and a larger aromatic cluster based on the non-protonated carbon fraction than N-300AC (Table 2), suggesting that the hydrophobic phenanthrene is more tightly bound to N-500AC with stronger $\pi - \pi$ interactions. Thus, the better sorption capacity and the higher initial adsorption rate of N-300AC particularly at the short incubation time may arise not only from its larger surface area and pore volume (mesopore), which may accommodate more sorbate molecules, but also from the smaller entropy change. The binding of the free molecule to the surface is highly unfavorable in terms of entropy, and adsorption on the larger surface area (pore) may minimize the loss of entropy, compensating for the weaker interactions (enthalpy-entropy compensation). In addition, the larger pores in N-300AC may be more readily accessible to the contaminants than those in other activated carbons tested in this study. The tighter binding of the sorbate molecule on N-500AC and N-700AC may also

lead to the slow diffusion of sorbates and subsequently less adsorption efficiency of the activated biochars.

4. Conclusions

The NMR analysis and surface characterization exhibited more substantial changes in carbon structure and surface properties of the activated biochars, when they were pretreated at lower pyrolysis temperature. The results imply that the condensed carbon structure in severely-treated biochars might be not suitable to make activated carbons with larger surface area and pore volume. The activated carbon from N-300 biochar presented the faster initial sorption rate and the higher equilibrium concentration for phenanthrene adsorption, but the activated N-700 biochar exhibited stronger binding with the sorbate. These observations suggest the possibilities of designing appropriate adsorbents for specialized application needs.

References

Azargohar, R., Dalai, A.K. 2008. Steam and KOH activation of biochar: Experimental and modeling studies. *Microporous and Mesoporous Materials*, **110**(2-3), 413-421.

Boving, T.B., Zhang, W. 2004. Removal of aqueous-phase polynuclear aromatic hydrocarbons using aspen wood fibers. *Chemosphere*, **54**(7), 831-839.

Brewer, C.E., Schmidt-Rohr, K., Satrio, J.A., Brown, R.C. 2009. Characterization of Biochar from Fast Pyrolysis and Gasification Systems. *Environmental Progress & Sustainable Energy*, **28**(3), 386-396.

Brewer, C.E., Unger, R., Schmidt-Rohr, K., Brown, R.C. 2011. Criteria to Select Biochars for Field Studies based on Biochar Chemical Properties. *BioEnergy Research*, 1-12.

Cao, X., Ma, L., Gao, B., Harris, W. 2009. Dairy-manure derived biochar effectively sorbs lead and atrazine. *Environmental Science & Technology*, **43**(9), 3285-91.

Chan, K.Y., Van Zwieten, L., Meszaros, I., Downie, A., Joseph, S. 2007. Agronomic values of greenwaste biochar as a soil amendment. *Australian Journal of Soil Research*, **45**(8), 629-634.

Chen, B., Chen, Z. 2009. Sorption of naphthalene and 1-naphthol by biochars of orange peels with different pyrolytic temperatures. *Chemosphere*, **76**(1), 127-33.

Chen, W., Duan, L., Wang, L., Zhu, D. 2008. Adsorption of Hydroxyl- and Amino-Substituted Aromatics to Carbon Nanotubes. *Environmental Science & Technology*, **42**(18), 6862-6868.

Chun, Y., Sheng, G., Chiou, C.T., Xing, B. 2004. Compositions and sorptive properties of crop residue-derived chars. *Environmental Science & Technology*, **38**(17), 4649-55.

Czimczik, C.I., Preston, C.M., Schmidt, M.W.I., Werner, R.A., Schulze, E.D. 2002. Effects of charring on mass, organic carbon, and stable carbon isotope composition of wood. *Organic Geochemistry*, **33**(11), 1207-1223.

Eastman, M.A., Brothers, L.A., Nanny, M.A. 2011. (2)H NMR Study of Dynamics of Benzene-d(6) Interacting with Humic and Fulvic Acids. *Journal of Physical Chemistry A*, **115**(17), 4359-4372.

Figueiredo, J.L., Pereira, M.F.R., Freitas, M.M.A., Orfao, J.J.M. 1999. Modification of the surface chemistry of activated carbons. *Carbon*, **37**(9), 1379-1389.

Gaunt, J.L., Lehmann, J. 2008. Energy balance and emissions associated with biochar sequestration and pyrolysis bioenergy production. *Environmental Science & Technology*, **42**(11), 4152-4158.

Global Activated Carbon Market Forcast and Opportunities. 2012. www.reportlinker.com/p0937503/Global-Activated-Carbon-Market-Forecast-and-Opportunities.html.

Ho, Y.S., McKay, G. 1998. Sorption of dye from aqueous solution by peat. *Chemical Engineering Journal*, **70**(2), 115-124.

Ho, Y.S., Wase, D.A.J., Forster, C.F. 1996. Kinetic studies of competitive heavy metal adsorption by sphagnum moss peat. *Environmental Technology*, **17**(1), 71-77.

Holtman, K.M., Chang, H.M., Jameel, H., Kadla, J.F. 2006. Quantitative C-13 NMR characterization of milled wood lignins isolated by different milling techniques. *Journal of Wood Chemistry and Technology*, **26**(1), 21-34.

Hu, Z., Srinivasan, M.P. 1999. Preparation of high-surface-area activated carbons from coconut shell. *Microporous and Mesoporous Materials*, **27**(1), 11-18.

Kong, H., He, J., Gao, Y., Wu, H., Zhu, X. 2011. Cosorption of phenanthrene and mercury(II) from aqueous solution by soybean stalk-based biochar. *Journal of Agricultural and Food Chemistry*, **59**(22), 12116-23.

Larsen, F.H., Jakobsen, H.J., Ellis, P.D., Nielsen, N.C. 1998. QCPMG-MAS NMR of half-integer quadrupolar nuclei. *Journal of Magnetic Resonance*, **131**(1), 144-7.

Li, W., Peng, J., Zhang, L., Yang, K., Xia, H., Zhang, S., Guo, S.H. 2009. Preparation of activated carbon from coconut shell chars in pilot-scale microwave heating equipment at 60 kW. *Waste Management*, **29**(2), 756-60.

Lima, I.M., Boateng, A.A., Klasson, K.T. 2010. Physicochemical and adsorptive properties of fast-pyrolysis bio-chars and their steam activated counterparts. *Journal of Chemical Technology and Biotechnology*, **85**(11), 1515-1521.

Mao, J.D., Schmidt-Rohr, K. 2003. Recoupled long-range C-H dipolar dephasing in solid-state NMR, and its use for spectral selection of fused aromatic rings. *Journal of Magnetic Resonance*, **162**(1), 217-27.

Moreno-Castilla, C. 2004. Adsorption of organic molecules from aqueous solutions on carbon materials. *Carbon*, **42**(1), 83-94.

Novak, J.M., Busscher, W.J., Laird, D.L., Ahmedna, M., Watts, D.W., Niandou, M.A.S. 2009. Impact of Biochar Amendment on Fertility of a Southeastern Coastal Plain Soil. *Soil Science*, **174**(2), 105-112.

Park, J., Meng, J., Lim, K.H., Rojas, O.J., Park, S. 2013. Transformation of lignocellulosic biomass during torrefaction. *Journal of Analytical and Applied Pyrolysis*, **100**(0), 199-206.

Rice, D.M., Wittebort, R.J., Griffin, R.G., Meirovitch, E., Stimson, E.R., Meinwald, Y.C., Freed, J.H., Scheraga, H.A. 1981. Rotational Jumps of the Tyrosine Side-Chain in Crystalline Enkephalin - H-2 Nmr Line-Shapes for Aromatic Ring Motion in Solids. *Journal of the American Chemical Society*, **103**(26), 7707-7710.

Solum, M.S., Pugmire, R.J., Grant, D.M. 1989. C-13 Solid-State Nmr of Argonne Premium Coals. *Energy & Fuels*, **3**(2), 187-193.

Spiess, H.W. 1983. Molecular-Dynamics of Solid Polymers as Revealed by Deuteron Nmr. *Colloid and Polymer Science*, **261**(3), 193-209.

Sun, K., Ro, K., Guo, M., Novak, J., Mashayekhi, H., Xing, B. 2011. Sorption of bisphenol A, 17alpha-ethinyl estradiol and phenanthrene on thermally and hydrothermally produced biochars. *Bioresource Technology*, **102**(10), 5757-63.

Uchimiya, M., Klasson, K.T., Wartelle, L.H., Lima, I.M. 2011. Influence of soil properties on heavy metal sequestration by biochar amendment: 1. Copper sorption isotherms and the release of cations. *Chemosphere*, **82**(10), 1431-7.

Valderrama, C., Gamisans, X., de las Heras, X., Farran, A., Cortina, J.L. 2008. Sorption kinetics of polycyclic aromatic hydrocarbons removal using granular activated carbon: Intraparticle diffusion coefficients. *Journal of Hazardous Materials*, **157**(2-3), 386-396.

Vold, R.R. 1994. *Nuclear Magnetic Resonance Probes of Molecular Dynamics* Kluwer Academic Publishers, Norwell, MA.

Woolf, D., Amonette, J.E., Street-Perrott, F.A., Lehmann, J., Joseph, S. 2010. Sustainable biochar to mitigate global climate change. *Nature Communications*, **1**.

Yang, H.P., Yan, R., Chen, H.P., Lee, D.H., Zheng, C.G. 2007. Characteristics of hemicellulose, cellulose and lignin pyrolysis. *Fuel*, **86**(12-13), 1781-1788.

Table 1. Proximate analysis, atomic O/C ratio, and surface characteristics for the thermally-treated samples and their activated counterparts.

	Proximate analysis [a] (%)			Atomic O/C ratio [b]	BET surface area (m^2/g)	Pore volume (cm^3/g)	
	Volatile matter	Fixed carbon	Ash			Micropore [c]	Meso- & macropore [d]
Raw	87.4	11.0	1.55	0.632	0.38	n.d.[e]	n.d.
N-300	72.0	23.6	4.44	0.232	1.41	0.000	0.009
N-350	42.3	56.3	1.38	0.208	7.37	0.000	0.028
N-500	18.4	79.4	2.16	0.107	239	0.076	0.075
N-700	10.1	87.1	2.77	0.065	321	0.129	0.045
N-300AC	15.6	79.7	4.71	0.220	1250	0.289	0.783
N-350AC	20.7	77.4	1.87	0.165	702	0.241	0.246
N-500AC	12.5	86.5	1.01	0.093	346	0.128	0.162
N-700AC	14.5	83.8	1.73	0.107	57.0	0.013	0.041

[a] Dry-basis
[b] Calculated based on ultimate analysis
[c] *t*-plot micropore volume
[d] Calculated by subtracting *t*-plot micropore volume from total pore volume
[e] Not determined

Table 2. Quantitative spectral analysis for solid-state ^{13}C DP/MAS NMR of the thermally-treated samples and their activated counterparts. The values were calculated based on 100% carbon in each biomass.

	Carbonyls %	Aromatics, %				Alkyls, %	Min. # of C in a cluster [b]
		C-O	Protonated	Non-protonated	Total aromatic		
Raw	4.1	4.7	a [a]	b [a]	44.1	51.8	-
N-300	3.4	8.1	18.1	26.9	53.2	43.4	-
N-350	3.7	10.4	14.9	38.9	64.2	32.1	-
N-500	3.6	6.0	20.0	46.4	72.5	24.0	11
N-700	5.1	7.3	4.9	56.7	68.9	26.1	16
N-300AC	12.3	12.6	4.4	50.9	67.9	19.78	12
N-350AC	4.8	8.2	4.2	59.7	72.2	23.1	20
N-500AC	6.9	11.6	1.2	63.8	76.5	16.7	27
N-700AC	7.2	12.5	2.8	61.1	76.3	16.5	23

[a] Non-protonated carbon fraction for Raw sample was not determined due to the low signal intensity of NMR spectrum with dipolar dephasing. The total amount of protonated and non-protonated aromatic carbon is 39.4% (a + b).

[b] Estimated minimal number of carbons in an aromatic carbon cluster.

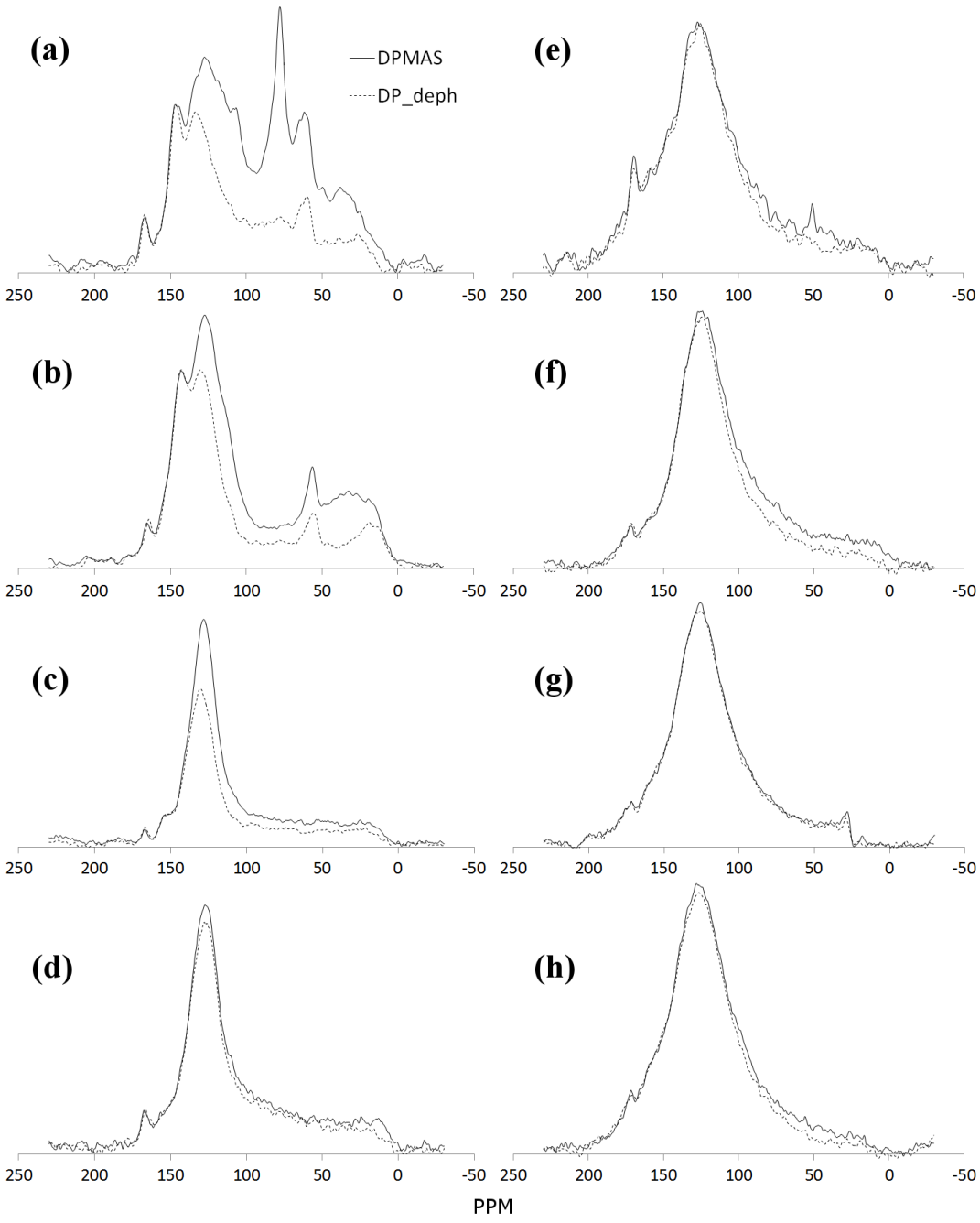

Figure 1. Solid-state ^{13}C DP/MAS NMR analysis for thermally-treated samples (a: N-300, b: N-350, c: N-500, d: N-700) and their activated counterparts (e: N-300AC, f: N-350AC, g: N-500AC, h: N-700AC); DP/MAS spectrum (solid line) and DP/MAS with dipolar dephasing spectrum (dotted-line).

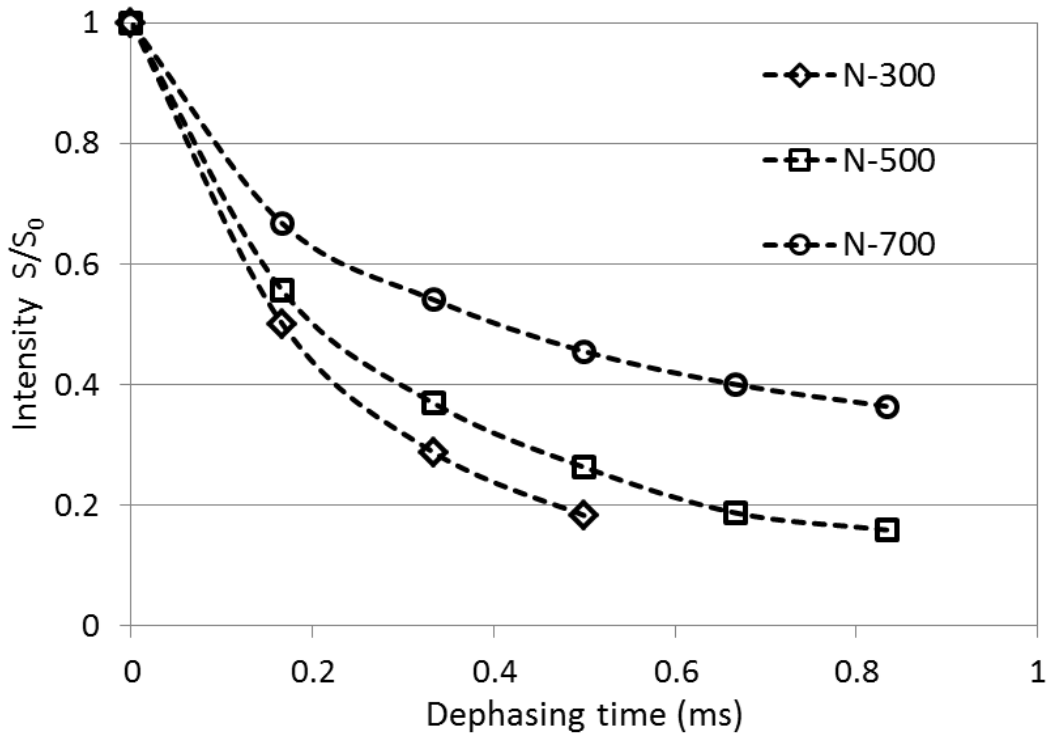

Figure 2. Quantitative ^{13}C NMR analysis with long-range dipolar-recoupled dephasing experiments. Total aromatic carbon fraction includes non-protonated aromatic carbon and protonated aromatic carbon fractions.

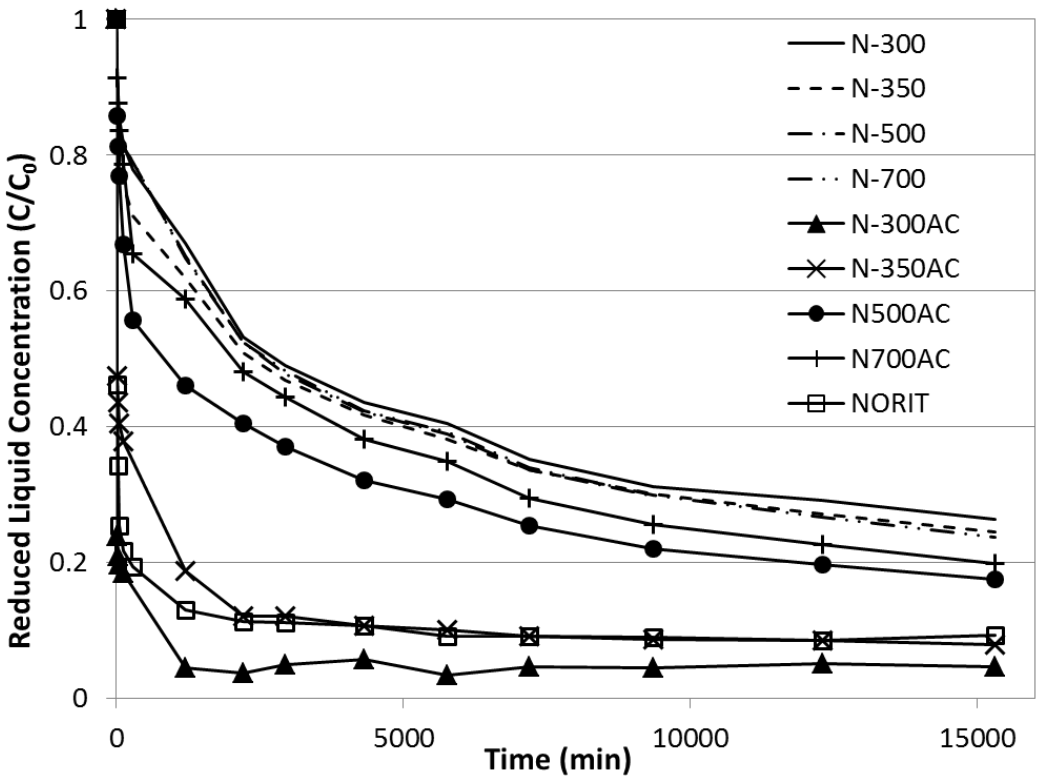

Figure 3. Adsorption of phenanthrene onto thermally-treated biomass samples - removal of pheanthrene after different incubation time.

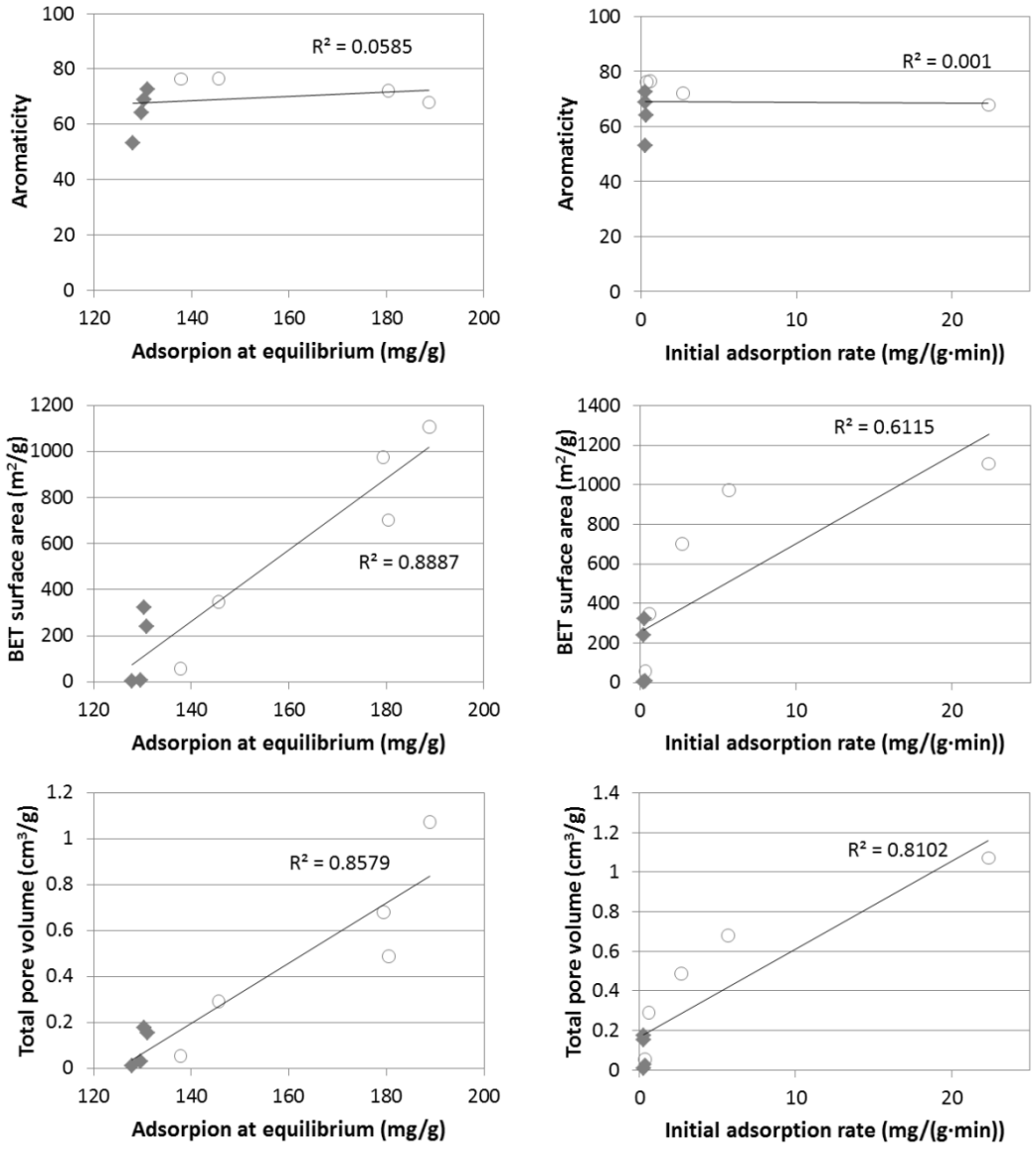

Figure 4. Correlation plots between aromaticity/surface properties and adsorption parameters obtained by pseudo-second order sorption model; biochar (solid diamonds) and activated carbons (blank circles).

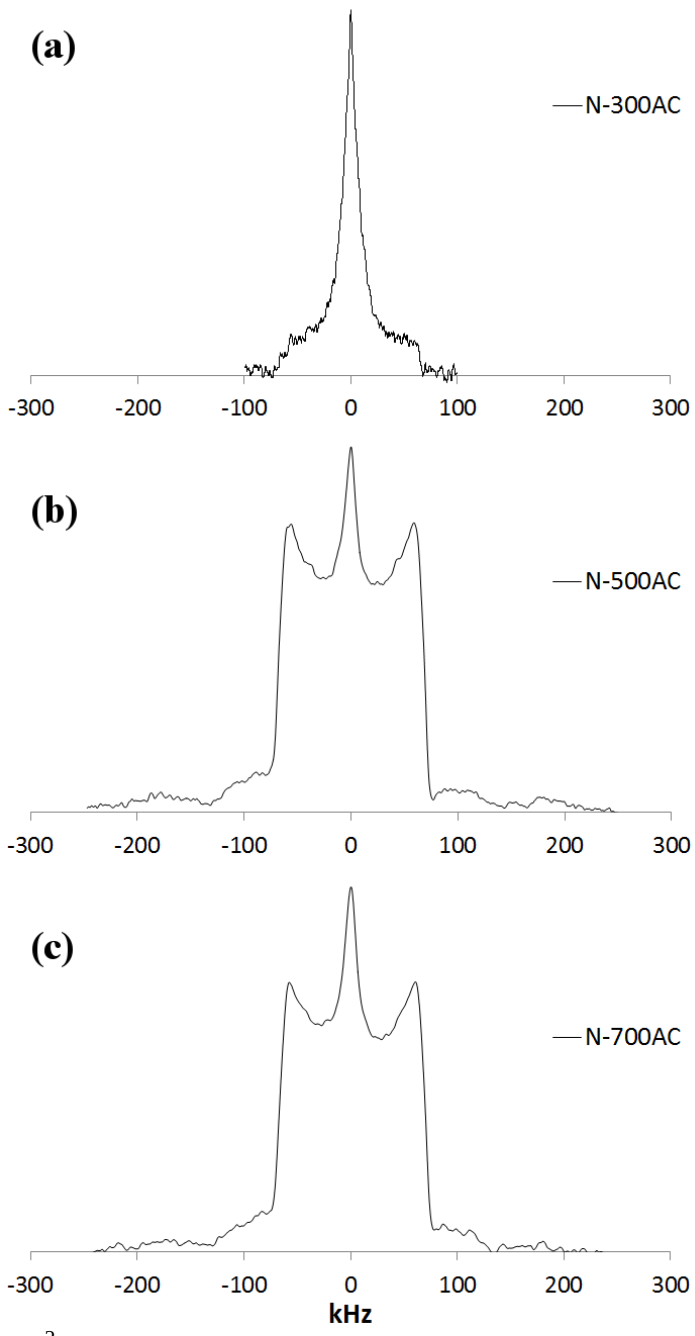

Figure 5. Solid-state ^{2}H NMR analysis for activated samples, saturated with phenanthrene-d_{10}; (a) N-300AC, (b) N-500AC, and (c) N-700AC.

CHAPTER 4

Effect of Atmospheric Oxygen during the Pyrolytic Treatment of Woody Biomass on the Changes in Aromatic Carbon Structure

1. Introduction

There have been continuous attempts to investigate the chemical and structural changes in thermally-treated lignocellulosic biomass, but the molecular level changes during the process have not been fully elucidated yet, due to many difficulties in obtaining detailed information about the changes in the solid products (Mészáros et al., 2007). The chemistry and structural characteristics of thermally-treated biomass, e.g. biochar, has close relations with biodegradability and interaction with water and soil nutrients, which is important for its applications such as soil amendment and carbon sequestration (Gaunt & Lehmann, 2008; Novak et al., 2009). Recently, there have been a few studies to elucidate correlations between chemical/structural characteristics of biochars and their end-use properties for such applications (Brewer et al., 2011; Novak et al., 2009; Spokas, 2010).

There are intrinsic limitations for characterization of thermally-treated biomass, due to its heterogeneity in both chemical and structural ways. Due to thermal-induced degradation, transformation and condensation of these constituents, however, most of the conventional methods are not feasible for the characterization of thermally-treated biomass. To overcome such problems and limitations, there have been several trials recently, such as

modifying conventional methods for biomass characterization and borrowing specialized techniques from other fields of study.

In a previous study, it was found that torrefaction of biomass induced thermal transformation and condensation of lignin, and also increased the aromaticity and non-protonated carbon fraction, as measured by quantitative ^{13}C NMR, which implies the evolution of larger aromatic carbon clusters with elevated treatment temperature (Park et al., 2013). Sun and coworkers investigated factors during pyrolysis processes and their impacts on carbon structures and pore properties in biochars (Sun et al., 2012). They set two different levels for pyrolysis variables that included temperature, heating rate, particle size, and feedstock type. By analyzing and comparing their chemistry and structural properties, it was observed that feedstock and temperature affect biochar properties to a greater extent than the other processing conditions. As for the application of biochars soil conditioning within short-time spans have been reported (Brewer et al., 2011). The chemical composition, surface area, and functional groups in biochar from six thermal processes (torrefaction, slow pyrolysis, fast pyrolysis, flash pyrolysis, kiln carbonization, and gasification) were determined under varying conditions. The same authors explained the effect of oxygen during thermal treatment on the structural and chemical properties of biochar, based on their observation for kiln-produced biochars, which showed combined chemical and structural properties of slow pyrolysis and gasification chars. Since carbon structures and surface chemistry need to be determined in order to evaluate and predict the efficiency of biochar in their applications (Uchimiya et al., 2011; Wu et al., 2012), a systematic investigation on the effect of oxygen during the thermal treatment of lignocellulosic biomass is necessary.

In this study, we characterized thermally-treated biomass following treatment under different temperature and atmospheric conditions, to observe the differences in chemical and structural properties of the tailored biochars. Several characterization techniques, including XPS, solid-state ^{13}C NMR, and simultaneous TGA/DSC analysis were employed to demonstrate how the presence of oxygen during the thermal treatment affect the weight changes and the heat flow of biochars. From these observations, we propose an explanation for the effect of oxidative atmosphere during thermal treatment of lignocelluolsic biomass on the structural alteration of thermally-treated woody biomass.

2. Materials and Methods

2.1 Thermal treatment of woody biomass

Debarked loblolly pine (*Pinus taeda*) chips were milled to make a particle size of 20–40 mesh and air-dried before further treatment. A porcelain boat containing 3 g of softwood mill was loaded into the quartz-tube furnace (MTI Corporation, Richmond, CA), and the tube was purged for 10 minutes at the flow rate of 1 L/min with two different gases: 100% nitrogen (inert atmosphere) and 7% oxygen + 93% nitrogen (oxidative atmosphere) by volume. During the purging, the boat with samples was placed outside of the heating element of the furnace, then it was loaded into the preheated furnace and treated for 15 min with continuous nitrogen or 7% oxygen flow at different temperatures (300, 350, 500, and 700 °C). In this study, samples were named according to their treatment conditions, generally referred to as N- and O-biochars; for example, O-300 indicates a sample treated at 300 °C

under oxidative condition. After 15 min of residence time at the target temperature, the boat was pulled out of the heating element and cooled down to ambient temperature under nitrogen flow. After measuring weight loss, all the samples were stored in a desiccator before further analyses.

2.2 Ultimate and proximate analysis

Carbon, hydrogen, and nitrogen content in the samples were analyzed by using PerkinElmer 2400 Series II Elemental Analyzer (PerkinElmer, Waltham, MA). Oxygen content was calculated by subtraction of CHN content from the total. Proximate analysis was conducted according to ASTM standard method (ASTM, 2010), using a thermogravimetric analysis unit, TA Q500 (TA Instruments, New Castle, DE, USA).

2.3 X-ray Photoelectron Spectroscopy.

XPS C1s spectra for the thermally-treated woody biomass were obtained using SPECS XPS system (SPECS Surface Nano Analysis GmbH, Berlin, Germany). High-resolution C1s spectrum was peak-deconvoluted into four carbon peaks which represent different carbon chemical environments, C-C, C=C, and C-H bondings at 284.6 eV, carbon singly bonded to oxygen at 286.2 eV, carbonyl carbon at 287.6 eV, and the carboxyl carbon at 289.1 eV, respectively (Cheng et al., 2008).

2.4 Solid-state NMR

The solid-state magic angle spinning (MAS) NMR spectra were acquired with a Varian 3.2 mm MAS probe, on a Varian Inova 500 spectrometer. For the direct-polarization (DP) MAS experiments, the sample was spun at a high frequency of 15 kHz. A dephasing time of 68 μs was used for dipolar dephasing experiments to determine the non-protonated aromatic carbon fraction (Brewer et al., 2009; Brewer et al., 2011). For the quantitative DP NMR experiments, 1,000 – 2,000 FIDs were collected with a long acquisition delay of 60 s. The 90° pulse-lengths for ^{1}H and ^{13}C were 3.0 μs and 2.7 μs, respectively. The two-pulse phase-modulated (TPPM) decoupling scheme was employed with a radio-frequency field strength of 80 kHz. Quantitative spectral analysis was performed by integrating the assigned area of DP/MAS NMR spectra and fractionating into three major categories – carbonyl, aromatic, and alkyl carbon fractions (Brewer et al., 2009). Quantification for corresponding non-protonated aromatic carbon fraction was carried out in the same manner using DP/MAS and dipolar dephasing NMR spectra.

2.5 Simultaneous TGA/DSC

Thermogravimetric analysis and corresponding heat flow during the thermal treatment under 100% N_2 (inert) and 7% O_2 + 93% N_2 (oxidative) atmospheric conditions were analyzed using TA Q600 (TA Instruments, New Castle, DE, USA). Raw biomass (Loblolly pine) was milled to pass through 200 mesh, and 20 mg of samples were used for the measurement. Samples were heated up to 350 °C with a heating rate of 20 °C/min, then

held for 5 min under isothermal condition, and cooled down for both atmospheric conditions. During the whole analysis, a continuous gas flow of 100 mL/min was maintained.

3. Results and Discussion

3.1 Basic Characterization

The proximate and ultimate analyses for the feedstock material and thermally-treated samples are presented in Table 1. Thermal breakdown and release of volatile matter is expected to be mainly from the carbohydrate fractions, especially hemicelluloses, the content of which decreased from 87to around 10 % after the thermal treatment at 700°C. Correspondingly, the content of fixed carbon increased with the increasing severity of the treatment conditions. Ultimate analysis data showed large reductions in oxygen and relatively high carbon content in thermally treated samples. This decrease of oxygen content can be explained by dehydration reaction, as well as the loss of volatile organic products and their release as gases (mostly of CO and CO_2). The amount of hydrogen also decreased along with the loss of volatile/gaseous products and water.

The weight loss after thermal treatment showed an increasing trend with the increased treatment temperature. Some of carbohydrate fractions were retained in the samples treated at 300 °C. After the treatment at 350 °C, no monomeric sugars were detected in the acid hydrolysate from the Klason lignin method. As the carbohydrates fraction decreased, the amount of acid-insoluble residue was increased substantially, comprising over 90% of composition in the treated biomass.

In the previous study, it was shown that the amount of the solid residues after acid hydrolysis, expressed as Klason lignin, increased with temperature, up to relatively mild torrefaction condition (330 °C for 2.5 min) (Park et al., 2013). This observation might indicate the evolution of condensed structures into thermally degraded/modified products that are resistant to the acid hydrolysis. In this study with extended temperature conditions, however, it was observed that the amount of residue decreased with increasing temperature under both atmospheric conditions. This might be due to the thermal degradation of lignin fraction and/or acid-insolubles at temperatures higher than 330 °C. When lignocellulosic biomass is treated under milder condition (lower temperature and shorter residence time), condensed products from carbohydrates and lignin fractions contribute to increasing the total amount of acid-insoluble solids. Above a certain threshold of temperature or time, however, this kind of thermal products is not generated any more, and more complete thermal degradation of the solids is achieved.

3.2 X-ray photoelectron spectroscopy.

It is hypothesized that the oxidation state of carbon structures on the surface of biochars is dependent on the thermal treatment conditions and carbon bonding structure on the sample surface, as revealed by XPS. XPS spectra of C1s in N- and O-biochars were deconvoluted and fractionated into different chemical environments of carbon atoms, providing information about the surface chemistry of biochars generated under the two different atmospheres (Table 2).

Under both atmospheric conditions, it was observed that the peak area for C=O at 287.9 eV decreased with the increased temperature. At low temperature range, this might be due to the degradation of carbohydrates and their thermal derivatives, especially hemicellulose that contains acetyl and othre carbonyl-containing groups. In addition, the thermal degradation of aldehyde groups in lignin and thermal products of lignin at higher temperatures also could contribute to the decrease of the C=O peak. The increase of C-O at 286.5 eV was observed, which could be from the phenolic groups in lignin fractions, as well as from the evolution of phenolic groups by the cleavage of β-O-4 linkages at elevated temperatures. In addition, lower areas for carbon-carbon and higher areas for carbon-oxygen binding structures were observed under oxidative atmosphere, which might be from the oxidation reaction between the surface of the thermally-treated samples and the atmospheric oxygen. The oxidized chemical environments under 7% oxygen seem to have affected the surface of the samples, as the XPS data for the finely-powdered O-350 samples (particle size < 74 μm) showed area values between those determined for N-350 and O-350 (data not shown), and the atomic O/C ratios of two biochars measured by ultimate analysis also presented close values between N- and O-samples.

3.3 Quantitative NMR spectroscopy.

Solid-state NMR spectroscopy was used to investigate structural characteristics of the thermally-treated woody biomass. The ^{13}C DP/MAS NMR technique has shown to be an effective tool to obtain quantitative structural information of biochar (Brewer et al., 2009; Czimczik et al., 2002; Kelemen et al., 2007). Quantitative analyses of the combined solid-

state NMR spectra are particularly useful for examining changes in the aromatic structures after the heat treatments. The solid-state NMR experiments were, therefore, carried out for the biochar prepared under different atmospheric environments to investigate the effect of oxygen during the heat treatment, and the corresponding spectra for all the biochars generated, as well as one from raw feedstock (loblolly pine) presented as a reference. For the samples treated at 300 °C for both atmospheres, the characteristic signals from carbohydrates in the range of alkyl carbons (< 95 ppm) were still present in the NMR spectra (Figure 1). Meanwhile, a wide peak at about 130 ppm for aryl carbons increased, indicating the relative increase of aromatic carbon fraction. Above 300 °C, the peak for aryl carbon kpet increasing for both atmosphere, and the signals for carbons in carbohydrate fraction became negligible at 350 °C. A noticeable spectral difference between the two atmospheric conditions was observed in N-350 and O-350 biochars. As already shown previously, there was little difference between the ultimate and proximate analyses for both biochars. In NMR spectra, however, lower peaks at around 145 ppm (aromatic C-O in guaiacyl lignin) and at 56 ppm (methoxyl groups) were observed in O-350 biochar, compared to those in N-350 samples, which implies a greater extent of thermal alteration of lignin under oxidative atmospheres. Above 350 °C, characteristic NMR peaks for lignin and carbohydrates were not observed, and one wide peak for aryl carbons at about 130 ppm became significant for both inert and oxidative atmospheres.

The structural carbon fractions were calculated from the measured NMR spectra (Table 3). The quantitative analyses for N- and O-biochar samples showed that the total aromatic carbon fraction (aromaticity) generally increased with increasing pyrolysis

temperature. Non-protonated carbon fractions also increased, while the relative content of alkyl carbons decreased in biochars obtained at higher temperatures. The changes in the carbon fractions suggest that the heat treatment led to the development of more condensed aromatic structures and the volatilization of the alkyl carbons. It is, however, notable that little change in the aromaticity was observed between N-500 and N-700 biochar samples, while the non-aromatic carbon fraction was substantially increased at the higher temperature. These changes might indicate that the thermally-decomposed carbons in N-700 biochar are mainly from less-condensed carbon structures with higher fraction of protonated carbons, as well as from other non-aromatic carbons. When considering aromatic carbon clusters, protonated carbons, which are usually dominant along the edge of clusters, will account for a lesser fraction with increasing size of the aromatic cluster. The less-condensed and smaller-sized aromatic carbons clusters will be decomposed more easily than highly-condensed carbon structures. Consequently, the residual solid after thermal treatment at higher temperature can have larger fraction of non-protonated carbon without substantial changes in total aromaticity.

In the presence of oxygen during the pyrolysis, the quantitative solid-state NMR analysis showed some differences, when compared to the values from N-biochars. For the same treatment temperature, thermally treated samples under oxidative atmosphere presented less alkyl carbon and protonated aromatic carbon than samples generated under inert conditions, indicating higher thermal reactivity during the thermal treatment in the presence of atmospheric oxygen. As a result, O-biochar samples consisted of more highly-condensed

aromatic carbon structures, i.e. larger fractions of total aromatic carbons and non-protonated aromatic carbons.

The changes in the fraction of non-protonated aromatic carbon for two atmospheric conditions were plotted as a function of atomic O/C ratio and weight loss after thermal treatment (Figure 2). It was observed that samples treated under oxidative atmosphere have higher fractions of non-protonated aromatic carbon, with the same value of atomic O/C ratio or weight loss in the plots. This trend is more obvious at lower temperature ranges, and the difference becomes smaller with increasing treatment temperature.

3.4 Estimated aromatic carbon cluster

The quantitative NMR analysis suggested that biochars produced under oxidative environment have a higher fraction of non-protonated aromatic carbon and thus larger aromatic carbon clusters. To estimate cluster sizes between samples, the fraction of carbons along the edges of the aromatic clusters was calculated from quantitative data, and the minimum number of carbons in an aromatic carbon cluster was estimated by a series of calculations (Brewer et al., 2009; Solum et al., 1989). Because the fraction of the aromatic edge carbons can be estimated from the fraction of the bridge carbons inside, the larger size of aromatic carbon cluster results in the decrease of the fraction of the aromatic edge carbons. By combining the information of carbon structures from solid-state ^{13}C NMR and the geometry of carbon condensation, the minimum number of carbons in an aromatic carbon cluster inside biochars can be estimated (Brewer et al., 2009).

The estimated minimum numbers of carbons inside the aromatic cluster are presented in Table 3. At temperatures lower than 350 °C, the lower degree of condensation and relatively larger fraction of alkyl carbons from residual carbohydrates yielded small the calculated values, not suitable to estimate the cluster structure. However, above 350 °C, biochars generated under inert and oxidative atmospheric conditions show clear differences in their sizes. Samples exposed to oxygen presented larger number of carbons in their clusters than samples exposed only to nitrogen. This implies that the addition of oxygen during thermal treatment at higher temperature promotes the condensation of aromatic carbon structures, resulting in larger sizes of the aromatic carbon cluster, which agrees with the quantitative NMR observations.

Meanwhile, the mechanism to make larger aromatic clusters under oxidative atmosphere is not clearly understood. It is hypothesized that thermal energy generated on the biomass surface during oxidation might cause the difference in carbon structure. The effect of treatment temperature on the development of aromatic carbon cluster is presented in this study, and it has also been reported that the heating rate and/or final temperature during thermal treatment of lignocellulosic biomass can change the characteristics of solid products (Sun et al., 2012). To investigate the actual difference in thermal reactions under the two different atmospheres, a thermo-analytical technique was employed, as described in the next section

3.5 Simultaneous TGA/DSC

The observations described above showed larger size of aromatic carbon cluster in thermally-treated wood biomass under oxidative atmospheric conditions. It was hypothesized that the heat energy from oxidation and combustion of organic matters could induce cluster size changes. In order to demonstrate this hypothesis, simultaneous TGA/DSC was used to investigate the heat flow during thermal treatment, under different atmospheric conditions. A temperature of 350 °C was selected for comparison purposes, due to the fact that the values for the weight loss for N-300 and O-300 were very close, *i.e.* 63.2 and 63.6 %, respectively. As for thermal profiling during the analysis, the ramp-rate was set to 20 °C/min since the actual thermal condition during the treatment could not be monitored accurately. After 5 min of isothermal phase, samples were cooled down. Such a procedure might not reproduce the actual thermal profile during the sample treatment, but the difference in heat-flow during the analysis under two atmospheric conditions was substantial.

A simultaneous TGA/DSC profile including weight difference and heat flow as a function of time is presented in Figure 3. As for the thermal degradation of sample mass, the final weight of residual solid was very close for both atmospheres after 30 min of thermal program, which corresponds with the weight loss of N-300 and O-300 samples. It is noted that the temperature of maximum weight loss for sample produced under oxidative atmosphere was a little lower than that under inert conditions, which were 339 and 345 °C, respectively. This might be due to the weight decrease from the thermal decomposition, which occurred simultaneously with oxidation and combustion reactions under oxidative atmosphere, which is faster than for the thermal decomposition by volatilization in inert

environments. These differences in the thermal reactions were also reflected in the heat flow during the analysis.

After 10 min and reaching a temperature of about 220 °C, the heat flow showing endothermic reactions, for both atmospheric conditions, were almost identical. This observation can be associated with the removal of water (Yang et al., 2007). After 10 min of analysis, however, the heat flow of the two conditions followed a different pattern. The inert atmospheric treatment condition exhibited endothermic flow, and the 7% O_2 treatment showed relatively higher exothermic flow. The former might be from the thermal decomposition of cellulose fraction, which coincides with observations in a study with three biomass components (Yang et al., 2007). The latter is likley due to the oxidation, as well as combustion reactions of organic matter with the limited amount of O_2 in the gas feed. Although the weight loss from these two different thermal reactions exhibited similar solid yields after the treatment, the patterns of heat flow were in clear contrast with each other. Considering the effect of higher temperature on the development of aromatic carbon cluster, it is expected that the additional thermal energy from the oxidation reactions under oxidative atmosphere might be responsible for the larger size of aromatic cluster in O-300 sample.

The difference in heat flow during thermal treatment of woody biomass was observed for two different atmospheres, but there are still other possible factors, which can contribute to the evolution of aromatic carbon clusters. In Table 3, the increase of the minimum number of carbons per aromatic cluster was more substantial between the two atmospheric conditions, than the changes between biochars generated at different temperatures. One possible explanation is that oxidation reactions can promote the evolution of aromatic

condensed carbon structures. During the oxidation by atmospheric oxygen, reactive moieties can be formed and play an important role in condensation reactions of carbon structures. XPS analysis exhibited higher oxidation states of carbons on the surface of biochars treated under 7% oxygen, and this might support other possible mechanisms on how the condensation reactions between aromatic organic matters are promoted, not only by the additional exothermal heat, but also by reactive moieties generated during oxidation reactions. To demonstrate this, more detailed studies about the surface chemistry of biochars and the mechanisms of oxidation and condensation during the thermal treatment of woody biomass are necessary.

4. Conclusions

Thermally-induced chemical and structural changes of lignocellulsic biomass under inert and oxidative gas conditions were studied by using a series of complementary methods. Proximate and ultimate analyses showed a consistent trend of increasing fraction of fixed carbon and decreasing atomic O/C ratio with treatment temperature, but did not present substantial differences between inert and oxidative atmospheric conditions. XPS analysis provided some evidences for oxidized carbon moieties in thermally-treated biochars with the presence of oxygen, while the oxidation reactions seemed to be dominant on the surface of biochars. A significant increase in non-protonated aromatic carbon up to 69 % for O-700 sample was detected by quantitative ^{13}C NMR analysis, when woody biomass was treated under oxidative atmosphere and at a higher temperature within a treatment temperature range

of 300–700 °C. These observations, e.g. increase in non-protonated carbon and aromaticity, imply the formation of large aromatic carbon clusters comprising more than 58 carbons inside for O-700 sample. From simultaneous TGA/DSC analysis, it was suggested that the structural difference in samples generated under inert and oxidative atmosphere conditions might be due to the exothermal energy from oxidation and combustion of organic matter in the presence of atmospheric O_2 during the thermal treatment.

References

ASTM. 2010. D7582-10: Standard Test Methods for Proximate Analysis of Coal and Coke by Macro Thermogravimetric Analysis.

Brewer, C.E., Schmidt-Rohr, K., Satrio, J.A., Brown, R.C. 2009. Characterization of Biochar from Fast Pyrolysis and Gasification Systems. *Environmental Progress & Sustainable Energy*, **28**(3), 386-396.

Brewer, C.E., Unger, R., Schmidt-Rohr, K., Brown, R.C. 2011. Criteria to Select Biochars for Field Studies based on Biochar Chemical Properties. *BioEnergy Research*, 1-12.

Cheng, C.H., Lehmann, J., Engelhard, M.H. 2008. Natural oxidation of black carbon in soils: Changes in molecular form and surface charge along a climosequence. *Geochimica Et Cosmochimica Acta*, **72**(6), 1598-1610.

Czimczik, C.I., Preston, C.M., Schmidt, M.W.I., Werner, R.A., Schulze, E.D. 2002. Effects of charring on mass, organic carbon, and stable carbon isotope composition of wood. *Organic Geochemistry*, **33**(11), 1207-1223.

Gaunt, J.L., Lehmann, J. 2008. Energy balance and emissions associated with biochar sequestration and pyrolysis bioenergy production. *Environmental Science & Technology*, **42**(11), 4152-4158.

Kelemen, S.R., Afeworki, M., Gorbaty, M.L., Sansone, M., Kwiatek, P.J., Walters, C.C., Freund, H., Siskin, M., Bence, A.E., Curry, D.J., Solum, M., Pugmire, R.J., Vandenbroucke, M., Leblond, M., Behar, F. 2007. Direct characterization of kerogen

by x-ray and solid-state C-13 nuclear magnetic resonance methods. *Energy & Fuels*, **21**(3), 1548-1561.

Mészáros, E., Jakab, E., Várhegyi, G., Bourke, J., Manley-Harris, M., Nunoura, T., Antal, M.J. 2007. Do all carbonized charcoals have the same chemical structure? 1. Implications of thermogravimetry - Mass spectrometry measurements. *Industrial & Engineering Chemistry Research*, **46**(18), 5943-5953.

Novak, J.M., Busscher, W.J., Laird, D.L., Ahmedna, M., Watts, D.W., Niandou, M.A.S. 2009. Impact of Biochar Amendment on Fertility of a Southeastern Coastal Plain Soil. *Soil Science*, **174**(2), 105-112.

Park, J., Meng, J., Lim, K.H., Rojas, O.J., Park, S. 2013. Transformation of lignocellulosic biomass during torrefaction. *Journal of Analytical and Applied Pyrolysis*, **100**(0), 199-206.

Solum, M.S., Pugmire, R.J., Grant, D.M. 1989. C-13 Solid-State Nmr of Argonne Premium Coals. *Energy & Fuels*, **3**(2), 187-193.

Spokas, K.A. 2010. Review of the stability of biochar in soils: predictability of O:C molar ratios. *Carbon Management*, **1**(2), 289-303.

Sun, H., Hockaday, W.C., Masiello, C.A., Zygourakis, K. 2012. Multiple Controls on the Chemical and Physical Structure of Biochars. *Industrial & Engineering Chemistry Research*, **51**(9), 3587-3597.

Uchimiya, M., Klasson, K.T., Wartelle, L.H., Lima, I.M. 2011. Influence of soil properties on heavy metal sequestration by biochar amendment: 1. Copper sorption isotherms and the release of cations. *Chemosphere*, **82**(10), 1431-7.

Wu, W.X., Yang, M., Feng, Q.B., McGrouther, K., Wang, H.L., Lu, H.H., Chen, Y.X. 2012. Chemical characterization of rice straw-derived biochar for soil amendment. *Biomass & Bioenergy*, **47**, 268-276.

Yang, H.P., Yan, R., Chen, H.P., Lee, D.H., Zheng, C.G. 2007. Characteristics of hemicellulose, cellulose and lignin pyrolysis. *Fuel*, **86**(12-13), 1781-1788.

Table 1. Proximate and ultimate analyses [a]

	Weight loss (%)	Proximate analysis, %			Ultimate analysis, %				O/C Ratio
		Volatile matter	Fixed carbon	Ash	C	H	N	O	
Raw	0	87.4	11.0	1.5	49.5	7.24	0.08	41.7	0.632
N-300	57.7	72.1	26.5	4.4	68.9	5.16	0.16	21.3	0.232
N-350	63.2	40.0	57.9	1.4	73.4	4.67	0.19	20.4	0.208
N-500	73.6	20.4	77.8	2.2	82.9	2.93	0.20	11.8	0.107
N-700	82.0	11.1	86.6	2.8	88.1	1.28	0.18	7.68	0.065
O-300	35.8	72.0	23.6	1.4	59.4	5.51	0.12	33.6	0.424
O-350	63.6	42.3	56.3	2.2	73.9	3.90	0.18	19.9	0.202
O-500	78.8	18.4	79.4	1.8	83.4	2.76	0.22	11.8	0.106
O-700	86.4	10.1	87.1	2.3	88.7	1.07	0.19	7.81	0.066

[a] All measurements were performed as a dry basis

Table 2. Deconvoluted peak area (%) of C1s in XPS spectra.

	Deconvoluted Peak Area (%)			
	C-C, C=C	C-O	C=O	COO-
N-300	78.25	10.61	8.76	2.38
N-350	80.72	9.10	7.41	2.77
N-500	76.67	15.74	3.06	4.53
N-700	80.10	14.06	2.53	3.32
O-300	76.43	12.55	7.23	3.78
O-350	79.32	10.57	6.79	3.31
O-500	75.35	16.94	2.83	4.88
O-700	74.63	16.44	3.19	5.74

Table 3. Quantitative spectral analysis for solid-state ^{13}C DP/MAS NMR and estimated minimum number of carbons in an aromatic cluster.

	Carbonyls, %	Aromatics, %				Alkyls, %	Carbons in an cluster [b]
		C-O	Protonated	Non-protonated	Total aromatic (Aromaticity)		
Raw	4.13	4.7	a [a]	b [a]	44.1	51.8	-
N-300	3.78	8.73	21.25	23.45	53.44	42.78	-
N-350	3.40	8.79	23.02	31.25	63.06	33.53	-
N-500	3.19	8.39	22.54	44.39	75.32	21.50	> 11
N-700	5.53	9.09	7.35	58.15	74.59	19.88	> 16
O-300	5.68	8.80	18.18	30.05	57.03	37.30	-
O-350	4.35	7.67	17.47	45.09	70.23	25.42	> 12
O-500	5.87	6.70	10.62	61.08	78.40	15.73	> 28
O-700	5.33	9.88	7.39	69.10	86.37	8.30	> 58

[a] Non-protonated carbon fraction for Raw sample was not determined due to the low signal intensity of NMR spectrum with dipolar dephasing. The total amount of protonated and non-protonated aromatic carbon is 31.1% (a + b)

[b] Estimated minimum number of carbons in an aromatic cluster; '-' means the estimation was not applicable.

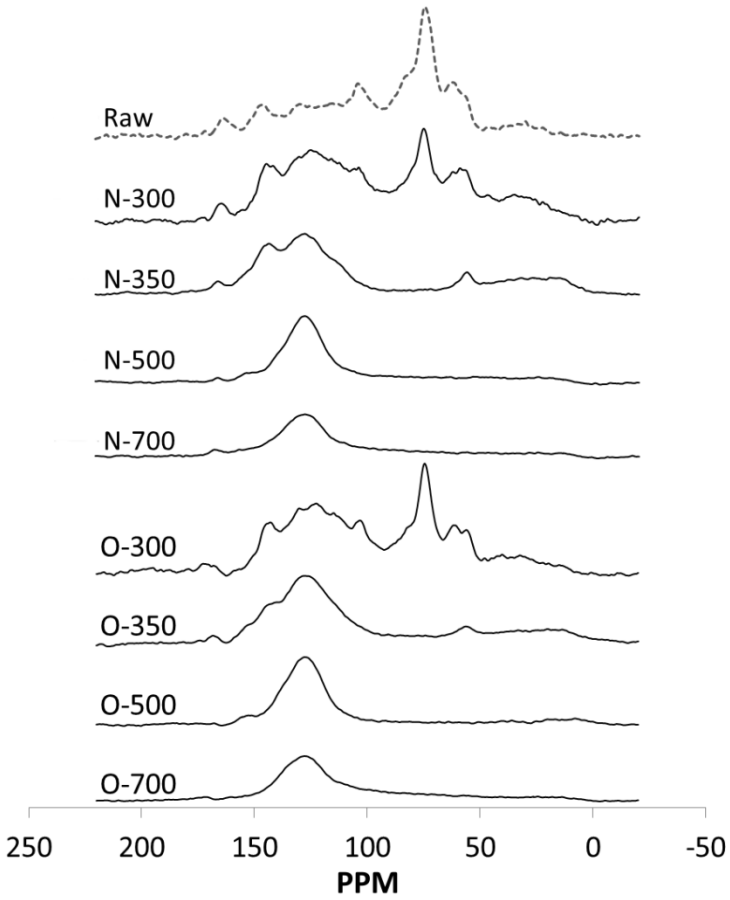

Figure 1. Solid-state ^{13}C DP/MAS NMR analysis for thermally-treated samples under two different atmospheric conditions – N-samples under 100% N_2 and O-sample with 7 % O_2 + 97% N_2.

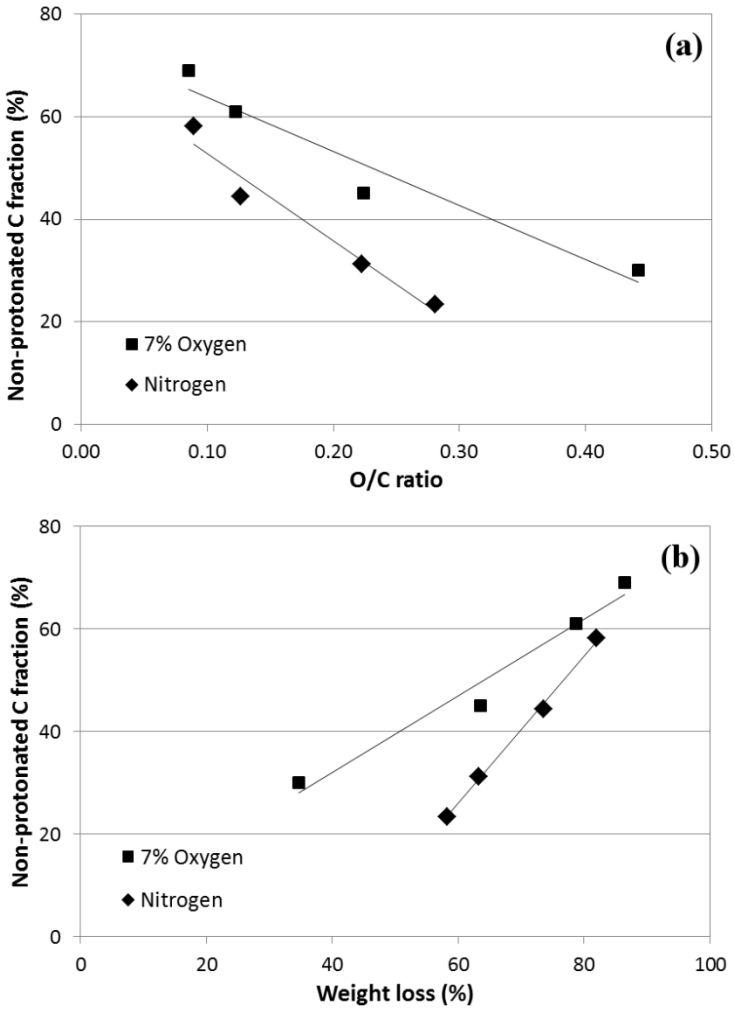

Figure 2. Changes in the fraction of non-protonated aromatic carbon fraction, as a function of (a) atomic O/C ratio and (b) % weight loss after treatment, for two different atmospheric conditions – inert (nitrogen; filled diamond) and oxidative (7 % oxygen; filled square).

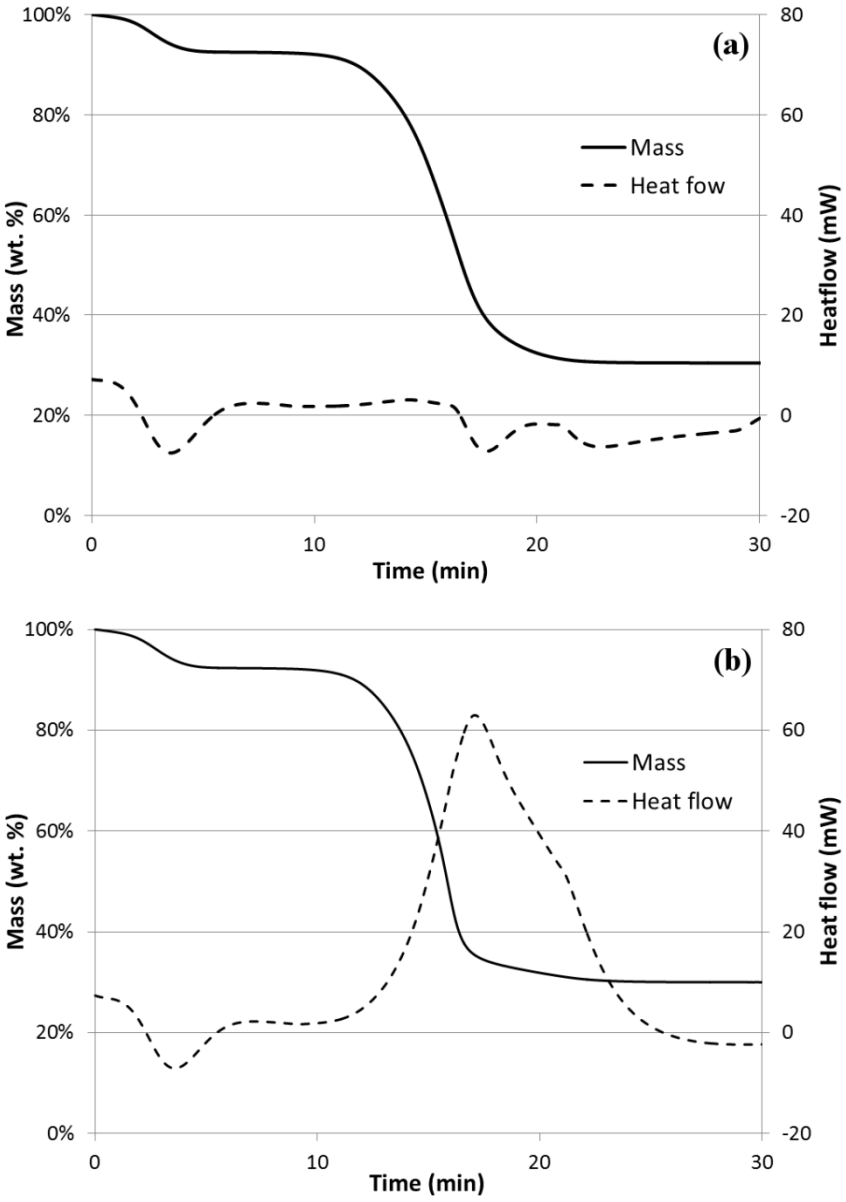

Figure 3. Simultaneous TGA/DSC graph for biomass sample treated at 350 °C under (a) inert (100 % N_2) and (b) oxidative (7 % O_2 + 93% N_2) atmospheric conditions.

CHAPTER 5

Removal of Paracetamol in Aqueous Solution by Activated Carbons from Softwood Biochar in Fixed-Bed Columns

1. Introduction

Pharmaceuticals and personal care products (PPCPs) are chemicals which we can be exposed to in daily activities, including therapeutic drugs or consumer products such as cosmetics and fragrances. These chemicals can be frequently detected in aquatic environments, including surface waters and wastewater, even including drinking water (Benotti et al., 2009; Donn, 2008; Jones et al., 2005). Despite of existing studies about no acute human health risk from the presence of low concentration of many PPCPs (Christensen, 1998; Schulman et al., 2002), the widespread occurrence of these dissolved chemicals in water sources is of concern due to their possible long-them adverse effects, when consumed chronically by humans and aquatic species (Jones et al., 2005). In addition, although concentrations of individual chemicals might be low, it is not clear that what can be happened on human health, when chronically exposed to a mixture of various PPCPs and other chemicals in aquatic environment (Jones et al., 2004). In this study, paracetamol (acetaminophen) was selected as a representative PPCP, which is one of the most common over-the-counter pharmaceuticals in general for its analgesic and antipyretic properties. It has been reported that paracetamol is frequently found in varying aqueous environments. (Ternes, 2006)

Filtration with activated carbon (AC) is well-known process for removing various organic contaminants from aqueous phase, and many studies reported that removal of heavy metals, dyes, and endocrine-disrupting compounds (EDCs), as well as pharmaceuticals and other organic pollutants using the filtration method (Garg et al., 2003; Kobya, 2004; Mestre et al., 2007; Rossner et al., 2009; Yu et al., 2008). Most of the studies about removal of PPCPs were using commercially available ACs, and mainly focused on the analytical chemistry about the adsorption of target chemicals (Mestre et al., 2007). Hence, from the practical point of view, finding low-cost and effective adsorbents, as well as investigating the efficient utilization of adsorbent are necessary.

Biochar is a solid product after thermal treatment of lignocellulsic biomass, usually referring the residues after pyrolytic process. This solid product were generally considered as a byproduct after the thermal conversion of biomass into liquid and gaseous fuel, and used as a low-ranked solid fuel for combustion. Recently, there has been increasing interest about using biochars for more value-added applications, such as adsorbents for environmental remediation, soil amendment, and carbon sequestration. In the previous study about investigating the correlation between chemical/structural properties and adsorption kinetics of an aromatic chemical – phenanthrene onto biochars and their activated counterparts, it was found that the AC from thermally-treated woody biomass at lower temperature (300 and 350 °C) exhibited high values of initial sorption rate and adsorption capacity at equilibrium, which was comparable or even better than commercial ACs. (Park, 2013) And, a collaborating work about adsorption of selected endocrine-disrupting compounds (EDCs) and pharmaceutical active compounds (PhACs) onto an AC from thermally-treated loblolly

pine at 300 °C showed higher adsorption affinity and capacity, compared to a commercialized powdered AC (Jung, 2013).

Hence, using the cost-effective activated carbons we generated from thermally-treated loblolly pine, continuous flow adsorption experiments were performed in this study. By analyzing the characteristics of the breakthrough curves in fixed-bed column experiments, it is possible to obtain valuable information about the efficiency of adsorbents under varying operation conditions, such as the concentration of target chemicals in influent stream, the flow rate into the fixed-bed column, and the effect of packed amount of the adsorbent. These observations can provide important parameters, which will be necessary when designing scaled-up adsorption system in practical applications, including low-cost water treatment technology for removal of PPCPs.

2. Materials and Methods

2. 1 *Activated carbon production*

The activated biochar which showed a good adsorption efficiency in previous studies (Jung, 2013; Park, 2013) was prepared via thermal treatment under inert atmosphere, followed by NaOH activation, as described elsewhere (Park, 2013). Briefly, debarked loblolly pine (*Pinus taeda*) chips were milled to powder (20 ~ 40 mesh), then thermally-treated in the quartz-tube furnace (MTI Corporation, Richmond, CA) at 300 °C for 15 min under 100% N_2 atmosphere. After the heat treatment, the biochar was impregnated with NaOH aqueous solution and dried, followed by activation process in the quartz-tube furnace

at the temperature up to 800 °C. The activated biochar was thoroughly washed and dried, then sieved to pass through 20~40 mesh for packing fixed-bed columns., and labeled as 'N300AC'. As for commercial ACs, NORIT® GAC 1240 and activated coconut shell charcoal (CSC), purchased from Sigma-Aldrich (Sigma-Aldrich Co., St. Louis, MO, USA), were sieved (20~40 mesh) and used for comparison.

2. 2 *Surface characterization*

BET (Brunauer–Emmett–Teller) surface area and pore characteristics were measured by using N_2 adsorption at 77 K with a Micromeritics Gemini VII 2390p apparatus (Micromeritics Instrument Co., Norcross, GA, USA) and the adsorption data was analyzed using its included software package. The BET surface area (S_{BET}) was calculated from the linear fit of the adsorption data. Micropore volumes were obtained by the *t*-plot method and the total pore volumes were estimated from the adsorbed amount of N_2 at a relative pressure of 0.99. The measured values are presented in Table 1.

2. 3 *Fixed-bed column adsorption*

A glass tube with 10 mm inner diameter and 150 mm height was used for making packed column with ACs. A known amount of AC was packed into the glass tube, and the remaining space was filled with glass beads (1 mm diameter). The column performance was investigated with different concentration of paracetamol in influent stream, amount of packing adsorbents, and flow rate (Table 1). For comparison of column performance between the tailored AC and commercial ACs, same weight of packed adsorbents (150 mg)

and bed-height (150 mg of loblolly pine AC, 312 mg of NORIT, and 381 mg of CSC were packed to make 11.8 mm of bed-height) were tested with a fixed concentration (100 mg/L) and a flow rate (4 mL/min). The inlet flow was controlled by a peristaltic pump, and the concentration of parasetamol in effluent was measured using a RI detector (Shodex RI-101, Shoko Scientific Co., LTD., Yokohama, Japan) at 30 °C.

3. Results and Discussion

3.1 *Adsorption kinetic models for fixed-bed columns*

To design a fixed-bed column for adsorption process, it is necessary to predict the concentration vs. time profile or breakthrough curve for the effluent. The maximum adsorption capacity for the column is also required. Thomas model is one of the most widely used methods for this purpose. The equation for the Thomas model is like below;

$$\frac{C_e}{C_o} = \frac{1}{1 + \exp(k_T \cdot \left(\frac{q_T \cdot m}{v} - C_0 \cdot t\right))}$$

where C_e is effluent concentration and C_0 is the influent concentration in mg L^{-1}, k_{TH} for the Thomas rate constant (ml mg^{-1} min^{-1}), q_0 for the amount of paracetamol adsorbed on ACs at equilibrium (mg g^{-1}), *m* for the mass of the adsorbent (g), *v* for flow rate (mL min^{-1}), and *t* is time in min. (Reynolds, 1995). This model assumes Langmuir kinetics of adsorption-desorption and no axial dispersion is derived, so the Thomas model is suitable for adsorption

processes where the external and internal diffusions will not be the limiting step (Aksu & Gonen, 2004).

Along with the Thomas model, an empirical model is also employed, which was proposed by Yan and coauthors (Yan et al., 2001). This model could overcome the draw-backs of Thomas model, such as the prediction of effluent concentration at $t = 0$. The equation for Yan model is like below;

$$\frac{C_e}{C_0} = 1 - \frac{1}{1 + \left(\frac{Q^2 t}{k_Y q_Y m}\right)^{(k_Y C_0/Q)}}$$

where k_Y is kinetic rate constant for Yan model (L mg^{-1} min^{-1}) and qY is maximum adsorption capacity (mg g^{-1}). The predicted parameters from the two adsorption models were in Table 2.

3.2 *Comparison in kinetics with commercial ACs*

The adsorption performance of fixed-bed column packed with the tailored AC, N300AC was tested, in comparison with two commercially available ACs, NORIT and CSC. The comparison was performed with the same weight basis (150 mg of packed amount). Figure 1 presents the breakthrough curves from 3 ACs with same weight of 150 mg. It was observed that two commercial ACs could not adsorb the given concentration of paracetamol efficiently, and about 60% of dissolved paracetamol was flowing out instantly from the beginning of the experiment. This might be due to low initial adsorption rate and slower

intraparticle diffusion of adsorbate in NORIT and CSC. For detailed comparison between the samples, adsorption models for fixed-bed column were employed.

As presented in Table 2, Thomas model rate constant for N300AC is higher than those for two commercial ACs, and the solid phase concentration at equilibrium is also higher for N300AC. As for Yan model, the trend in rate constant and adsorption capacity is close to that from Thomas model. Relatively low goodness of fit for NORIT in Thomas model might be due to intraparticle diffusion during the adsorption experiments in the fixed-bed column.

3.2 *Effect of the influent concentration of paracetamol*

The effect of initial concentration on the breakthrough curves was investigated by the adsorption models. Three different inlet concentrations of paracetamol – 50, 100, and 200 mg/L – were tested, and the measured curves and the calculated model fittings are presented in Figure 2. The initial concentrations of target adsorbates are important factors, because the adsorption capacity of a certain amount of AC is limited. Therefore, the higher influent concentration means the less treatment capacity of a column (Al-Ghouti et al., 2007). The breakthrough curve for the higher initial concentration showed faster saturation and steeper slope in our experiment. This means that the changes in concentration of influent affect the saturation rate and breakthrough time, resulting in the decrease of the time required to reach its effective adsorption. After adsorption model fitting, Yan model seems to exhibit a better goodness of fit, compared to Thomas model. The increasing initial concentration leads to higher adsorption capacity in both models, but it seems that there are some over-estimation

for the adsorption capacity, especially the values from the Thomas model. When Ce/C0 is greater than 0.8, the experimental data did not fit well with the model, which has been reported (Al-Ghouti et al., 2007).

3.3 *Effect of the flow rate*

Due to the importance of contact time in fixed-bed column study, flow rate and bed height are the major parameters which can affect the adsorption behavior of the column. The high flow rates reduces the time that adsorbates in solutions can contact with the adsorbents, resulting in less time for adsorption to occur and consequently earlier breakthough. On the other hand, too low flow rates will result in longer processing time, which is undesirable in practical applications for large-scale operation (Chu, 2004).

To investigate the effect of flow rate on the adsorption, the flow rate was changed from 2 to 6 mL/min, while the influent concentration was fixed at 100 mg/L. The corresponding breakthrough curves are given in Fig. 3. It was observed that when the flow rate increases, much steeper breakthrough curves were obtained, implying faster saturation of the fixed-bed column with paracetamol. As for the flow rates of 4 and 6 mL/min, the concentration of paracetamol in the effluent stream started to increase rapidly at the beginning of column operation. At the flow rate of 2 mL/min, it reached the breakthrough point (C_e/C_0=0.05) after 39 min of adsorption flow. Beyond the breakthrough point, the column with 2 mL/min flow rate also exhibit steep increase in the curve, but the steepness of the curve is relatively lower than those from the higher flow rates.

The adsorption capacity from the two different models showed substantial discrepancy between each other. The values from the Thomas model exhibit 2 ~ 3 folds higher than the values from the Yan model, so here we used the Yan model for comparison. Although the breakthpoint time is creased when the flow rate increases, the adsorption capacity between the three flow rates did not showed substantial difference. This adsorption behavior can be explained by that the contact time of paracetarol with N300AC in the fixed-bed column is sufficient enough to ensure the stable adsorption. If the contact time is insufficient, then the decreasing trends of the breakpoint time and the total adsorbed amount might be observed with the elevated flow rates (Aksu & Gonen, 2004).

3.4 *Effect of the bed-height (packed weight)*

The effect of the bed-height of the packed ACs was shown in Figure 4. It was found that the breakpoint time and the saturation time is increased when the bed-height increases. The larger weight and bed-height of packed AC provides a greater number of adsorption sites (Singh et al., 2012) and a longer contact time (Yahaya, 2011) for the binding between AC and paracetamol, resulting in an increased time to reach breakthrough of the fixed-bed columns. The estimated model parameters (Table 2) showed smaller adsorption capacity with the least bed-depth of 3.8 mm, which might be to insufficient contact between paracetamol and packed AC. The Thomas model predicted increased in adsorption capacity when the bed-height increases, but the Yan model showed a little decreased in q_0.

4. Conclusions

The Thomas model, based on Langmuir kinetics, and the empirical Yan model were applied to experimental data obtained from dynamic adsorption studies performed on fixed-bed column of activated carbons, to predict the breakthrough curves and to determine the column kinetic parameters. The full description of breakthrough curves could be accomplished by the two employed models, and the goodness of fit statistics of the fitted results showed good agreements with measured values. These estimated parameters can provide useful information for designing and predicting the performance of fixed-bed columns. It was also presented in this study that N300AC, an activated carbon from a biochar treated at a relatively lower temperature, exhibit a considerable potential for the removal of paracetamol, a model PPCP, over a wide range of operation conditions, including varying initial concentrations, flow rates and bed-heights. The effects of operation parameters on the adsorption performance also showed how the parameters can be manipulated to adjust the dynamic adsorption kinetics inside the prepared columns to fulfill specific requirements for certain applications. By adjusting the operating conditions of the packed column, such as the flow rate and the influent concentration, rapid and efficient paracetamol uptake can be achieved.

References

Aksu, Z., Gonen, F. 2004. Biosorption of phenol by immobilized activated sludge in a continuous packed bed: prediction of breakthrough curves. *Process Biochem*, **39**(5), 599-613.

Al-Ghouti, M.A., Khraisheh, M.A.M., Ahmad, M.N., Allen, S.J. 2007. Microcolumn studies of dye adsorption onto manganese oxides modified diatomite. *J Hazard Mater*, **146**(1-2), 316-327.

Benotti, M.J., Trenholm, R.A., Vanderford, B.J., Holady, J.C., Stanford, B.D., Snyder, S.A. 2009. Pharmaceuticals and Endocrine Disrupting Compounds in US Drinking Water. *Environ Sci Technol*, **43**(3), 597-603.

Christensen, F.M. 1998. Pharmaceuticals in the environment - A human risk? *Regul Toxicol Pharm*, **28**(3), 212-221.

Chu, K.H. 2004. Improved fixed bed models for metal biosorption. *Chem Eng J*, **97**(2-3), 233-239.

Donn, J.M., M.; Pritchard, J. 2008. Pharmaceuticals lurking in U.S. drinking water, Associated Press.

Garg, V.K., Gupta, R., Yadav, A.B., Kumar, R. 2003. Dye removal from aqueous solution by adsorption on treated sawdust. *Bioresource Technol*, **89**(2), 121-124.

Jones, O.A., Lester, J.N., Voulvoulis, N. 2005. Pharmaceuticals: a threat to drinking water? *Trends Biotechnol*, **23**(4), 163-167.

Jones, O.A.H., Voulvoulis, N., Lester, J.N. 2004. Potential ecological and human health risks associated with the presence of pharmaceutically active compounds in the aquatic environment. *Crit Rev Toxicol*, **34**(4), 335-350.

Jung, C.P., Junyeong; Lim, Kwang Hun; Park, Sunkyu; Heo, Jiyong; Her, Nam-Guk; Oh, Jeill; Yoon, Yeomin. 2013. Adsorption of Selected Endocrine Disrupting Compounds and Pharmaceuticals on Activated Biochars. *Environ Sci Technol*, ***(submitted)***.

Kobya, M. 2004. Adsorption, kinetic and equilibrium studies of Cr(VI) by hazelnut shell activated carbon. *Adsorpt Sci Technol*, **22**(1), 51-64.

Mestre, A.S., Pires, J., Nogueira, J.M.F., Carvalho, A.P. 2007. Activated carbons for the adsorption of ibuprofen. *Carbon*, **45**(10), 1979-1988.

Park, J.H., Ivan; Gan, Zhehong; Rojas, Orlando J.; Lim, Kwang Hun ; Park, Sunkyu. 2013. Activated carbon from biochar: Influence of physicochemical properties of biochar on the characteristics of its activated counterparts. *Environ Sci Technol*, ***(submitted)***.

Reynolds, T.D.R., Paul. 1995. *Unit Operations and Processes in Environmental Engineering*. *2nd ed*. PWS Publishing, Boston.

Rossner, A., Snyder, S.A., Knappe, D.R.U. 2009. Removal of emerging contaminants of concern by alternative adsorbents. *Water Res*, **43**(15), 3787-3796.

Schulman, L.J., Sargent, E.V., Naumann, B.D., Faria, E.C., Dolan, D.G., Wargo, J.P. 2002. A human health risk assessment of pharmaceuticals in the aquatic environment. *Hum Ecol Risk Assess*, **8**(4), 657-680.

Singh, A., Kumar, D., Gaur, J.P. 2012. Continuous metal removal from solution and industrial effluents using Spirogyra biomass-packed column reactor. *Water Res,* **46**(3), 779-788.

Ternes, T. 2006. Assessment of Technologies for the Removal of Pharmaceuticals and Personal Care Products in Sewage and Drinking Water Facilities to Improve the Indirect Potable Water Reuse.

Yahaya, N.K.E.M.A., Ismail; Latiffa, Muhamad Faizal Pakir Mohamed; Bellob, Olugbenga Solomon; Ahmadb, Mohd Azmier. 2011. Fixed-bed Column Study for Cu (II) Removal from Aqueous Solutions using Rice Husk based Activated Carbon. *International Journal of Engineering & Technology*, **11**(1).

Yan, G.Y., Viraraghavan, T., Chen, M. 2001. A new model for heavy metal removal in a biosorption column. *Adsorpt Sci Technol,* **19**(1), 25-43.

Yu, Z.R., Peldszus, S., Huck, P.M. 2008. Adsorption characteristics of selected pharmaceuticals and an endocrine disrupting compound - Naproxen, carbamazepine and nonylphenol - on activated carbon. *Water Res*, **42**(12), 2873-2882.

Table 1. Surface characteristics of activated carbons for fixed-bed columns.

	BET surface area (m^2/g)	Total pore volume (cm^3/g)	Average pore size (Å)
N300AC	1248.47	1.07	38.5
NORIT	973.58	0.68	27.9
CSC	1059.33	0.56	21.1

Table 2. Experimental conditions for the adsorption experiments and the predicted parameters from Thomas and Yan models fitted to the breakthrough curves from the adsorption of paracetamol on activated carbons.

	m (mg)	Bed Height (mm)	C_0 (mg/L)	*v* (mL/ min)	Thomas model			Yan model		
					k_T	q_T	R^2	k_Y	q_Y	R^2
N300AC	50	3.8	100	4	0.06066	942.5	0.910	4.021	526	0.976
	150	11.8	50	4	0.01658	3670	0.985	8.967	1435	0.997
	150	11.8	100	2	0.01752	2147	0.990	5.42	733	0.999
	150	11.8	100	4	0.03323	1545	0.980	7.058	697.3	0.994
	150	11.8	100	6	0.04667	1616	0.975	10.77	728.7	0.995
	150	11.8	200	4	0.07093	810.4	0.975	7.549	354.8	0.999
	300	24.2	100	4	0.02088	1929	0.982	11.31	634.7	0.999
NORIT	150	5.8	100	4	0.01510	512.7	0.916	3.164	422.2	0.912
CSC	150	4.7	100	4	0.01434	917.3	0.951	3.475	612.7	0.893

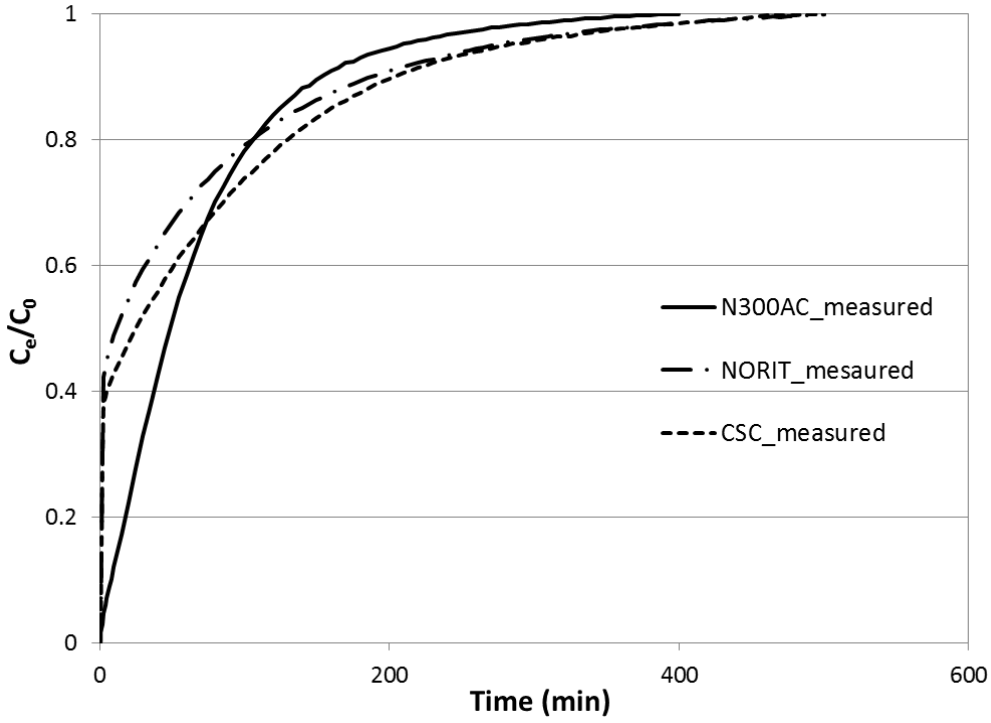

Figure 1. Breakthrough curves for three activated carbons – 150 mg of packed bed of N300AC, NORIT, and CSC, with initial concentration of 100 mg/L paracetamol and 4 mL/min flow rate.

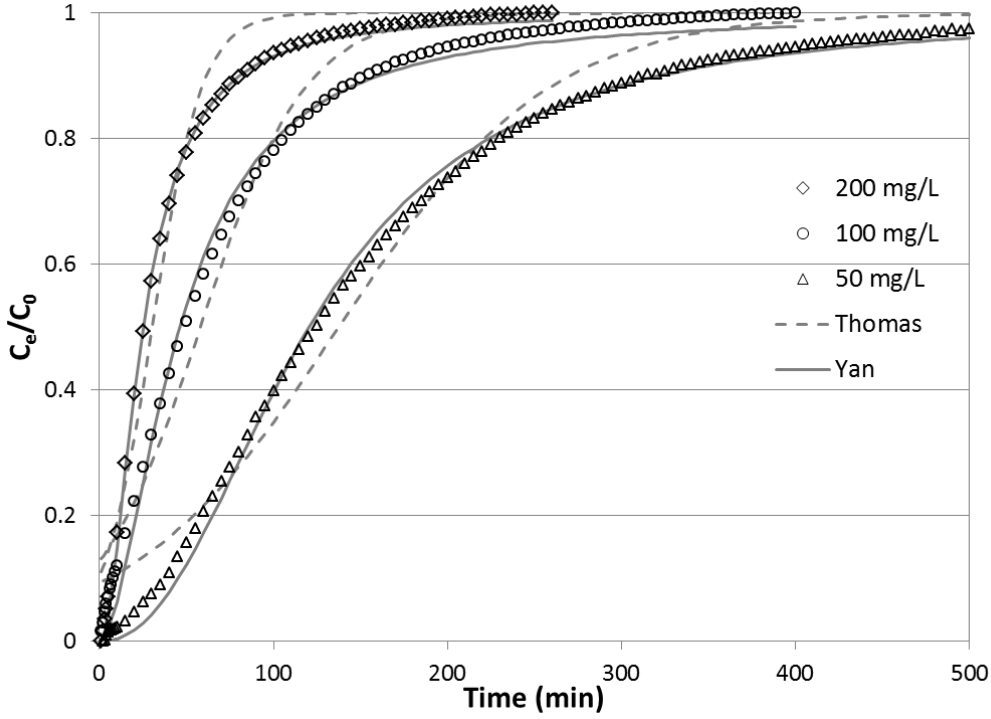

Figure 2. Breakthrough curves for N300AC with different initial concentrations of paracetamol – 50, 100, and 200 mg/L.

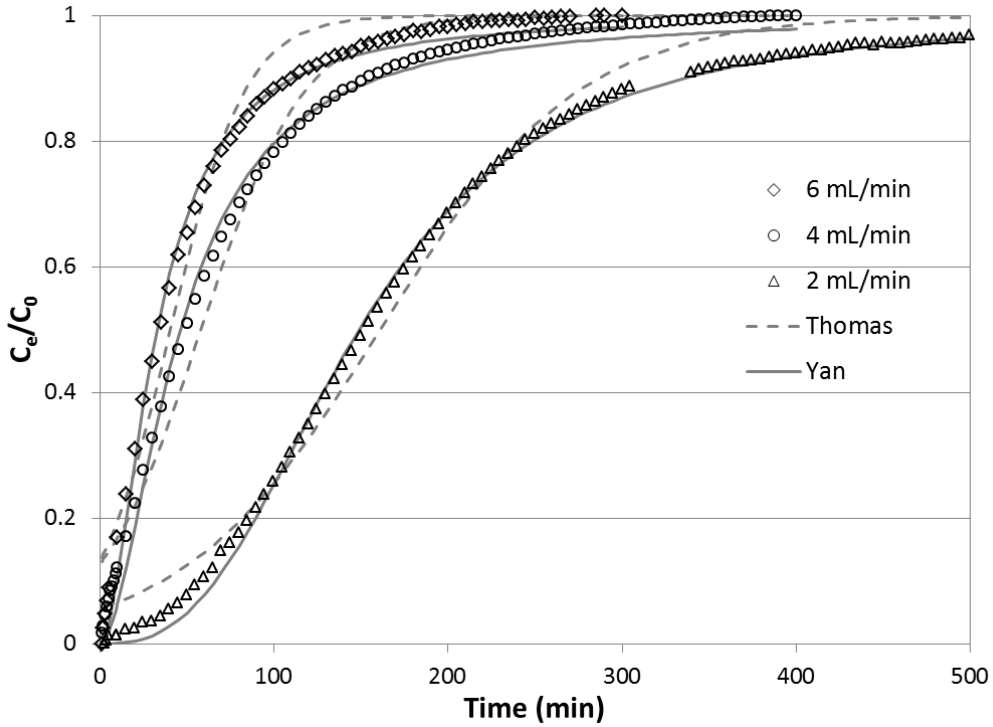

Figure 3. Breakthrough curves for N300AC with different flow rates – 2, 4, and 6 mL/min.

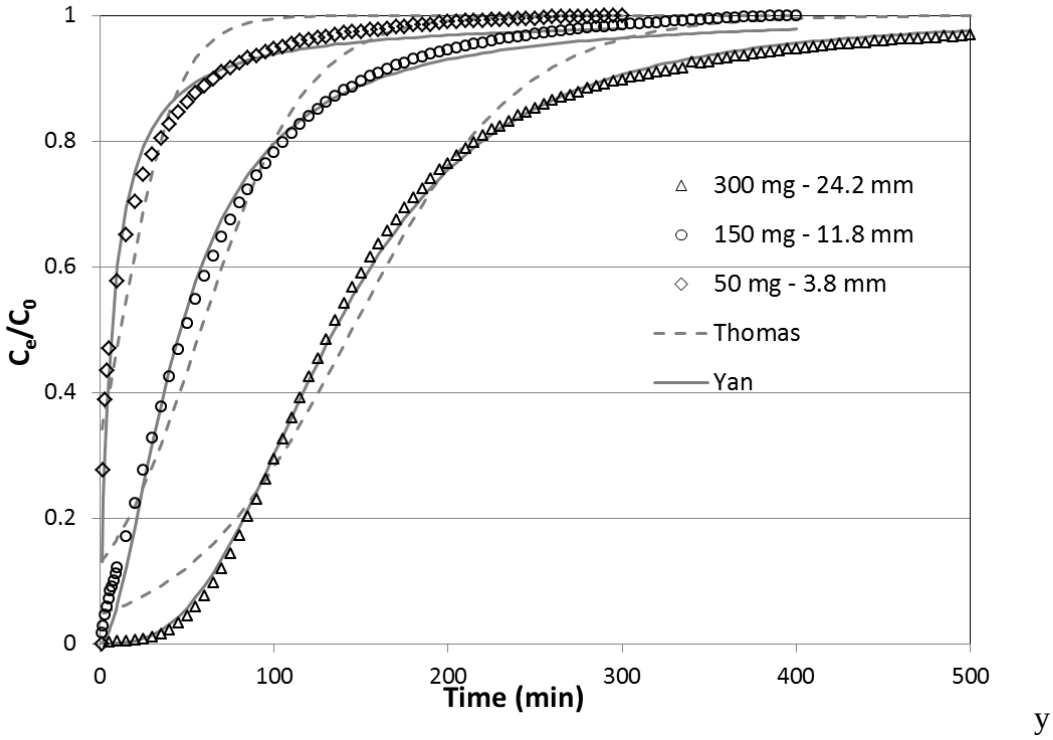

y

Figure 4. Breakthrough curves for N300AC with different packed weight (bed-height in mm) – 50 (3.8), 150 (11.8), and 300 (24.2) mg.

CHAPTER 6

Suggested Future Works

The presented studies proposed the correlation between the parameter during thermal treatment, such as treatment temperature and oxidative atmospheric condition, and the evolution of aromatic carbon structures inside biochars. In addition, the promising potential of activated biochar as biosorbents was also presented. Based on these results, several suggestions for future researches have been considered, in both fundamental and applicative directions.

The effect of additional process parameters of thermal treatments on the structural properties of biochars from woody biomass

Biochar produced in previous studies were generated by introducing feedstock into pre-heated reactor directly, so the effect of heating rate on the structural and chemical properties of biochar was not elucidated sufficiently. It has been reported that the heating rate during thermal treatment of lignocellulosic biomass affects the reactions and the properties of biochars. Okumura and coworkers reported that the elevated heating rate of gasification increased the thermal reactivity of char formation, and produced biochars with coarse surface and internal textures (Okumura, Hanaoka and Sakanishi, 2009). They proposed that this might be due to rapid volatilization of organic materials inside the feedstock. The authors

employed Raman spectroscopy to investigate the structural changes with different heating rate showed no effects on uniformity (increase in amorphous structure) of carbonaceous structure. The effect of heating rate, as well as temperature on the physicochemical and morphological properties of biochar were also observed, and it was shown that BET surface area and pore volume were decreased when the heating rate increased (Angin, 2013). The existing studies were generally approached the effect of the heating rate from the chemical, morphological, or thermogravimetric viewpoints. Many studies reported the heating rate affect the char reactivity (Okumura, Hanaoka and Sakanishi, 2009; Cetin, Gupta and Moghtaderi, 2005; Zanzi, Sjöström and Björnbom, 2002), which can induce the changes in structural alteration during thermal treatment. The investigation about the effect of heating rate can provide more detailed information about the correlation between the process parameters of thermal treatment and the structural properties of biochar, which might help the elucidation about the mechanisms for the evolution on aromatic carbon structure.

The effect of different activation process

Our previous study has reported that the NaOH activation process for biochar from loblolly pine was effective to enhance the surface characteristics, such as BET surface area and pore volume, especially when biochar was generated at relatively lower temperature. In addition, it was presented that these alterations in surface properties are considered to have some correlations with condensed carbon structure inside the thermally-treated woody biomass. And, the corresponding increases of the adsorption performance of the activated biochars in a static system with phenanthrene, as well as in a dynamic system with fixed-bed

column for removal of paracetamol were quite substantial, even in comparison with commercial ACs.

There are different activation methods exist, including physical and chemical ways. Beside NaOH activation, physical (stream, CO_2) and chemical (KOH, H_3PO_4) activation processes have been used for activation of carbonaceous materials, and several studies also presented the differences in the properties of activated carbons from varying conditions of activation. By analyzing the evolution of gaseous products during the activation processes, Lillo-Rodenas and coworkers presented that during the chemical activation processes, NaOH started to reaction with organic matters inside the biochar at about 570 °C, whereas KOH reacted with carbons at the temperature less than 400 °C (Lillo-Rodenas, Cazorla-Amoros and Linares-Solano, 2003). Steam activation was also compared to the other chemical activation processes, and showed some differences in surface properties (Azargohar and Dalai, 2008). Girgis and coworker also successfully presented the changes in the surface properties and corresponding removal of dye compounds by activated carbons from lignocellulosic biomasses, which were generated using steam and phosphoric acid (Girgis, Soliman and Fathy, 2011).

Based on these observations, it might be possible to find further ways to enhance the value of activated biochars as biosorbents. Several groups reported that KOH and NaOH showed different reactivity with ordered or disordered carbon structures inside carbonaceous materials, such as carbon nanotubes and carbon fibres (Macia-Agullo et al., 2007; Raymundo-Pinero et al., 2005). Therefore, it is expected that different chemical agents during the thermal process of biochar also can affect the structural and surface properties of

activated counterparts. This research can provide more details about the mechanisms of activation processes and their effects on the properties of biochar feedstock. In addition, it might expand the possibilities of to manipulate the characteristics of biochar-based adsorbents for various application needs.

The extended experiments for the fixed-bed adsorptions

In Chapter 5, it was presented that the effective removal of paracetamol from aqueous phase using a fixed-bed column of N300AC was quite promising, for use of the tailored AC as biosorbents from low-valued byproducts. Meanwhile, the employment of dynamic adsorption modeling provided valuable parameters, which will be necessary for the process operations, the scaling-up of the adsorption system, and the designing columns for applications. Another applicative approach for the adsorbent will be about the regeneration of used columns. There are several different ways to investigate the desorption ability of adsorbents, such as using low concentration (0.1 M) of HCl (Singh, Kumar and Gaur, 2012) or washing at elevated temperature (Zeinali, Ghoreyshi and Najafpour, 2010). After desorption of contaminants, cyclic operations for removal of target contaminants can be assessed for the possibility of using regenered columns.

Expanding the range of target contaminants can be a promising topic for the application of activated biochar as adsorbents. Removal of paracetamol from aqueous phase using an activated biochar - N300AC showed competitive results, compared to commercial activation carbons. Based on a preliminary data about the batch-system adsorption for paracetamol and phenanthrene in Figure 1, it was observed that activated carbons exhibit faster and more

adsorption for an aromatic and hydrophobic chemical – phenanthrene, than for a hydrophilic and polar chemical – paracetamol. So, it is expected that the fixed-bed column of activated biochar might be more effective for removal of aromatic contaminants, as presented in the study of Chapter 2. As for this study, considerably longer time for adsorption experiments is required, due to relatively low water solubility of hydrophobic chemicals, such as polycyclic aromatic hydrocarbons (PAHs). Moreover, a proper detection equipment to measure the low concentrated target chemicals in aqueous phase, such as an online flow-cell UV-Vis spectrophotometer, will be necessary. With the suitable additional set-up, it can be possible to evaluate the various adsorbents in dynamic sorption system.

Moreover, exploring the possibility for activated chars from specific thermal treatment can be another applicative topic about biochar as a cost-effective adsorbent. During the presented investigations about thermally-treated woody biomass, we generated biochars under laboratory conditions with the bench-scale tube furnace, then the additional activation process was employed to produce activated counterparts. By following this way for sample preparation, it was possible to obtain chemical, structural, morphological characteristics, as well as adsorption properties of biochar and activated carbons, and consequently, these observations can be correlated with treatment conditions, such as temperature, atmospheres, and activation. These results can provide us rough estimations, not the detailed information about the adsorption properties which is necessary to assess their feasibility as adsorbents from low-valued solid products. Fortunately, we have a pyrolysis and a gasification reactors which can produce chars, which will be close to real solid products from actual processes. Although our previous studies presented that biochars generated at higher temperature

exhibit lower efficiency and slow kinetics in adsorption experiments even after the activation, both biochars (treated at 500 and 700 °C) and their activated counterparts also removed a substantial amount of phenanthrene in batch-system sorption experiment after a few days, as shown in Figure 2. Therefore, it is expected that biochars generated at higher temperature and the activated carbons from them might be feasible for the application as adsorbents, in where the removal of contaminants with low concentration is necessary.

References

Angin, D., 2013. Effect of pyrolysis temperature and heating rate on biochar obtained from pyrolysis of safflower seed press cake, Bioresour. Technol. 128, 593-597.

Azargohar, R., Dalai, A.K., 2008. Steam and KOH activation of biochar: Experimental and modeling studies, Microporous and Mesoporous Materials. 110, 413-421.

Cetin, E., Gupta, R., Moghtaderi, B., 2005. Effect of pyrolysis pressure and heating rate on radiata pine char structure and apparent gasification reactivity, Fuel. 84, 1328-1334.

Girgis, B.S., Soliman, A.M., Fathy, N.A., 2011. Development of micro-mesoporous carbons from several seed hulls under varying conditions of activation, Microporous and Mesoporous Materials. 142, 518-525.

Lillo-Rodenas, M.A., Cazorla-Amoros, D., Linares-Solano, A., 2003. Understanding chemical reactions between carbons and NaOH and KOH: An insight into the chemical activation mechanism, Carbon. 41, 267-275.

Macia-Agullo, J.A., Moore, B.C., Cazorla-Amoros, D., Linares-Solano, A., 2007. Influence of carbon fibres crystallinities on their chemical activation by KOH and NaOH, Microporous and Mesoporous Materials. 101, 397-405.

Okumura, Y., Hanaoka, T., Sakanishi, K., 2009. Effect of pyrolysis conditions on gasification reactivity of woody biomass-derived char, Proceedings of the Combustion Institute. 32, 2013-2020.

Raymundo-Pinero, E., Azais, P., Cacciaguerra, T., Cazorla-Amoros, D., Linares-Solano, A., Beguin, F., 2005. KOH and NaOH activation mechanisms of multiwalled carbon nanotubes with different structural organisation, Carbon. 43, 786-795.

Singh, A., Kumar, D., Gaur, J.P., 2012. Continuous metal removal from solution and industrial effluents using Spirogyra biomass-packed column reactor, Water Res. 46, 779-788.

Zanzi, R., Sjöström, K., Björnbom, E., 2002. Rapid pyrolysis of agricultural residues at high temperature, Biomass Bioenergy. 23, 357-366.

Zeinali, F., Ghoreyshi, A.A., Najafpour, G.D., 2010. Adsorption of Dichloromethane from Aqueous Phase Using Granular Activated Carbon: Isotherm and Breakthrough Curve Measurements, Middle-East Journal of Scientific Research. 5, 191-198.

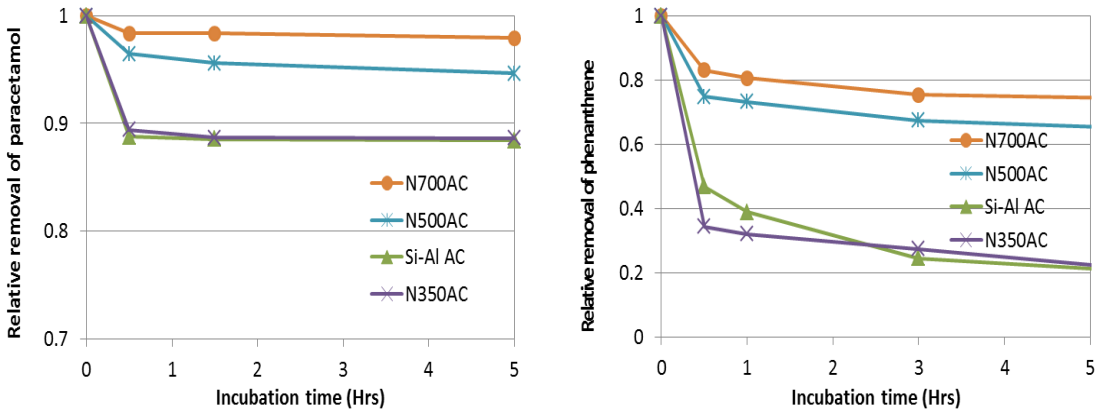

Figure 1. Removal of paracetamol and phenanthrene by activated biochars (N350AC, N500AC, and N700AC) and a commercial activated carbon (Si-Al AC).

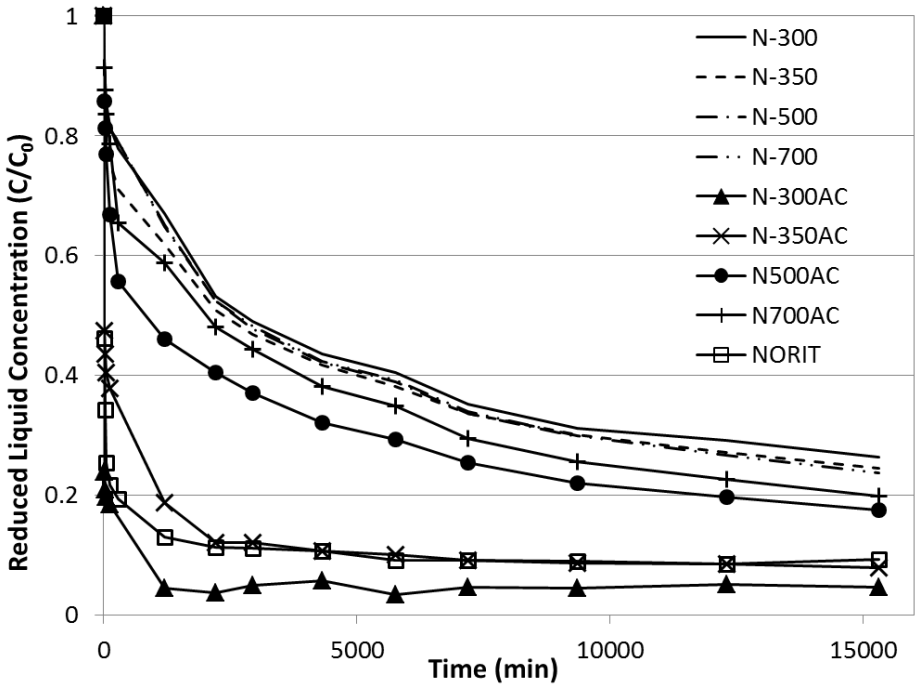

Figure 2. Removal of phenanthrene in aqueous phase by non-activation/activated biochars and a commercial activated carbon (NORIT) in a batch-system adsorption.